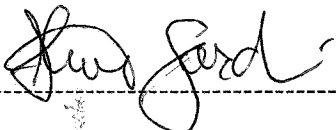


# Center for Extended Magnetohydrodynamic Modeling

**A proposal referencing program announcement LAB04-09  
Scientific Discovery through Advanced Computing  
Advanced Simulation of Fusion Plasmas  
Office of Fusion Energy Science  
U.S. Department of Energy  
19 March 2004**

**Lead Principal Investigator:**

Stephen C. Jardin  
Principal Research Physicist  
Princeton Plasma Physics Laboratory  
609 243-2635 (voice) -2662 (fax)  
email: [jardin@pppl.gov](mailto:jardin@pppl.gov)



**Laboratory Official:**

Rich Hawryluk  
Deputy Director  
Princeton Plasma Physics Laboratory  
609 243-3306 (voice) -2749 (fax)  
email: [rhawryluk@pppl.gov](mailto:rhawryluk@pppl.gov)



	<b>Scientific Application</b>	<b>SAPP</b>	<b>total</b>
<b>Requested Funding:</b> FY 2004:	\$1,000,000	\$200,000	\$1,200,000
FY 2005:	\$1,000,000	\$200,000	\$1,200,000
FY 2006:	\$1,000,000	\$200,000	\$1,200,000

**Co-PIs and Senior Personnel:**

**PPPL:** Guoyong Fu, Wonchull Park,  
Ravi Samtaney, Scott Klasky

**MIT:** Linda Sugiyama, Jesus Ramos

**New York U.:** Hank Strauss

**U. Wisc:** Jim Callen, Chris Hegna, Carl Sovinec

**Utah State U.:** Eric Held

**SAIC:** Dalton Schnack

**TecX:** Scott Kruger

**U. Colorado:** Dan Barnes, Scott Parker

**U. Utah:** Christopher Johnson, Allen Sanderson

Note: Institutional contacts are underlined

# Center for Extended Magnetohydrodynamic Modeling

## *Abstract*

The proposed work aims at developing the world's most powerful simulation codes for studying the macroscopic dynamics of MHD-like phenomena in fusion plasmas, and using them on the most advanced computers to address critical issues facing burning plasma experiments such as ITER. Our 8-institution Center has existed since June 2001. It has already pioneered simulations that have shed new insight in 10 different application areas (see Section 2.1). We have developed excellent working relationships with the SciDAC applied math and computer science centers TOPS, TSTT, and APDEC; these collaborations have substantially improved the algorithms and efficiency of our leading tokamak global codes, NIMROD and M3D, and have facilitated the development of an exploratory code utilizing adaptive mesh refinement. The physical problems we propose to focus on are: sawteeth, tearing modes, resistive wall modes, fast ion modes, disruptions, edge localized modes, and pellet fueling. To develop realistic simulation models for these key phenomena we propose to: 1) Critically examine and compare several extended-MHD models (kinetic, hybrid, and two-fluid closures), and develop criteria for when each is appropriate; 2) undertake key code development activities (efficiently implementing the extended-MHD terms in NIMROD, major upgrade of the finite-element representation and time advance algorithm underlying the M3D code); 3) develop a unique common visualization system; 4) build upon our excellent relations with the math centers listed above, and initiate new collaborations with the Logistical Network and PERC centers; and 5) begin some integration activities that will prototype those required for the Fusion Simulation Project.

Shown on the right is a frame from a NIMROD produced movie showing the detailed modeling of a high-beta disruption in the DIII-D tokamak. See section 2.1.2 for more details. [ courtesy of Allen Sanderson]

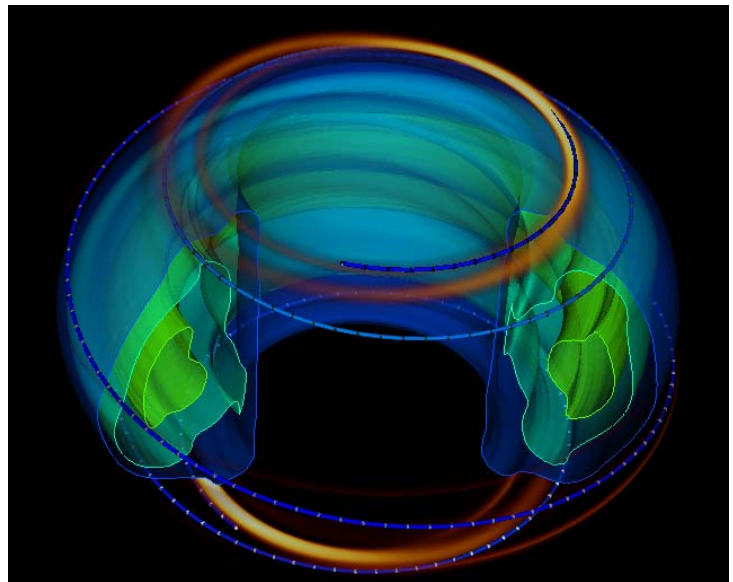


## Table of Contents

1.0 Background and significance . . . . .	Page 1
1.1 The CEMM computer codes . . . . .	Page 2
1.2 The proposed work . . . . .	Page 2
1.3 History of the CEMM . . . . .	Page 2
2.0 Preliminary studies	
2.1 Application results . . . . .	Page 3
2.1.1 <i>Physics of the current hole</i> ; 2.1.2 <i>The dynamics of high beta disruptions</i> ; 2.1.3 <i>Suppression of the Richtmyer-Meshkov instability by a magnetic field</i> ; 2.1.4 <i>Magnetic island thermalization at realistic parameters</i> ; 2.1.5 <i>Diamagnetic stabilization of instabilities in stellarators</i> ; 2.1.6 <i>Pellet fueling of a tokamak</i> ; 2.1.7 <i>Energetic particle driven modes in spherical tokamaks</i> ; 2.1.8 <i>Effects of strong toroidal shear on MHD modes</i> ; 2.1.9 <i>MHD and energy transport in SSPX</i> ; 2.1.10 <i>MHD behavior in CDX-U</i> ;	
2.2 Algorithmic development and code performance . . . . .	Page 6
2.2.1 <i>Linear Solvers and TOPS</i> ; 2.2.2 <i>Adaptive mesh refinement and APDEC</i> ; 2.2.3 <i>High order elements and advanced meshing and the TSTT</i> ; 2.2.4 <i>Parallel scaling and performance</i> ; 2.2.5 <i>Model studies in support of algorithm development</i> ; 2.2.6 <i>Code validation and verification</i> ;	
2.3 Summary of Phase I accomplishments . . . . .	Page 8
3.0 Research design and methods	
3.1 Applications . . . . .	Page 9
3.1.1 <i>Full nonlinear sawtooth oscillation modeling</i> ; 3.1.2 <i>Tearing and neoclassical tearing modes in high beta plasmas</i> ; 3.1.3 <i>Nonlinear evolution and control of resistive wall modes</i> ; 3.1.4 <i>Fast-ion driven instabilities</i> ; 3.1.5 <i>Edge MHD-type instabilities</i> ; 3.1.6 <i>Disruptions and vertical displacement events</i> ; 3.1.7 <i>Pellet fueling of a burning plasma</i> ;	
3.2 Two fluid and kinetic model development . . . . .	Page 14
3.2.1 <i>Background and goals</i> ; 3.2.2 <i>Extended fluid models of magnetized plasmas</i> ; 3.2.3 <i>Local closure relations in the general case</i> ; 3.2.4 <i>Drift ordering approximations</i> ; 3.2.5 <i>Parallel integral closures</i> ; 3.2.6 <i>Parallel local closures</i> ; 3.2.7 <i>Hybrid closures</i> ; 3.2.8 <i>Approach to the development and validation of extended MHD models</i> ;	
3.3 Code development . . . . .	Page 18
3.3.1 <i>Numerical considerations for two-fluid models</i> ; 3.3.2 <i>Algorithmic development for dispersive modes</i> ; 3.3.3 <i>Linear solver development for implicit two-fluid algorithms in NIMROD</i> ; 3.3.4 <i>Higher-order-of-continuity elements implicit approach in M3D</i> ; 3.3.5 <i>Straight field line coordinates</i> ;	
3.4 Integration activities . . . . .	Page 21
3.5 Visualization and data management . . . . .	Page 22
3.6 Planning, management, and collaboration with other SciDAC projects . . . . .	Page 23
3.7 Timetable and milestones . . . . .	Page 24
3.8 Computing resource requirements . . . . .	Page 25
3.9 Summary of proposed work . . . . .	Page 25
4.0 Subcontract or Consortium Arrangements . . . . .	Page 25
<b>Appendices:</b>	
Literature Cited . . . . .	Page A-1
Budget and Budget Explanation . . . . .	Page A-7
Biographical Sketches . . . . .	Page A-8
Description of Facilities and Resources . . . . .	Page A-12
Descriptions of NIMROD, M3D, and AMRMHD . . . . .	Page A-13
Glossary of Acronyms. . . . .	Page A-15
Letters from non-funded Collaborators. . . . .	Page A-19
Preprint “A finite element with first-derivative continuity for Fusion MHD Applications”. . . . .	Page A-23
Preprint “MHD Simulations with Resistive Wall and Magnetic Separatrix”. . . . .	Page A-47

## I. Background and Significance

It is hard to overstate the importance of macroscopic dynamics in tokamak fusion research. The operational space of tokamaks is largely set by non-linear global stability thresholds. These include the instabilities that set current limits, pressure limits, density limits, and limits on the cross-sectional shaping. High performance burning plasma tokamak discharges must necessarily operate near these stability boundaries, but can not exceed them. It is therefore essential that we develop a quantitative understanding of the detailed mechanisms that set these operational limits and how they scale with size and plasma parameters from the present generation of tokamaks to those of the ITER class.

The high-energy alpha particles present in a burning plasma will have significant effects on the global dynamics. These particles, created in the DT fusion reaction with a birth energy of 3.52 MeV, are expected to have a stabilizing effect on the internal kink mode, which can lead to large central disturbances (or giant sawteeth). The alpha particles can also resonantly excite shear Alfvén waves, such as toroidal Alfvén eigenmodes (TAE) or Energetic Particle Modes (EPM, e.g., fishbones). These alpha-driven modes can lead to anomalous alpha particle loss, degradation of alpha particle heating, or more seriously, damage in the reactor wall. Therefore, alpha particle physics is a key and essential component for understanding the macroscopic dynamics of a burning plasma experiment such as ITER.

It is not only the ability to *predict* stability thresholds that we are after, but also the ability to *control* them. It has now been demonstrated in a number of tokamaks that it is possible to apply feedback techniques to effectively enlarge the tokamak operating space and to mitigate the destructive consequences of off-normal events (i.e., disruptions). Stability feedback systems under consideration for ITER-class devices involve external current drive and heating, pellet injection, and the application of magnetic fields. The design of these feedback and mitigation systems for the next generation of devices relies on our ability to understand and to simulate them.

The equations we use to describe macroscopic dynamics in high-temperature magnetized plasma (with or without a high-energy alpha particle component) are called the extended-MagnetoHydroDynamic equations, or extended-MHD. These are obtained by combining the low-frequency Maxwell Equations with low-order velocity moments of the Boltzmann equation for the electrons and the ions. These equations are closed by one of the techniques described in Section 3.3 of this document. The resulting set of 3D plus time partial differential equations are a generalization of the resistive MHD equations to include certain essential kinetic effects that distinguish the dynamics of high temperature magnetized plasma from that of a conducting liquid.

The overarching goal of our proposal is to further advance our computational tools so that they will be of predictive value in studying the global nonlinear dynamics of a next-generation burning plasma experiment. In doing so, these tools and results will be an invaluable asset to the ITER design and operational teams in making that experimental device as productive and successful as possible. To this end, we need to further develop our advanced extended-MHD models so that they are appropriate to burning plasma conditions, and to benchmark these improved models as much as possible in existing devices. We will implement the most effective numerical techniques for our models on the latest generation of advanced computer hardware as efficiently as possible, so that high-resolution, high-fidelity simulations can be performed using realistic parameters in a practical amount of time.

### **1.1 The CEMM computer codes**

The center is built around the two workhorse extended-MHD codes, NIMROD [1,2] and M3D [3], and also involves an exploratory component that has produced an adaptive mesh refinement MHD code, now known as the Princeton/LBL AMRMHD [4] code. These codes are described more in the Appendix. The two primary codes, while in many ways similar, have significant differences in the underlying numerical representations and in their implementation of extended-MHD models. Having two code-lines, each with their advocates within the group, introduces a competitive “edge” to our collaboration that we find to be stimulating and motivating. We consider it essential that the two code-lines continue as they each have unique capabilities and the benchmarking of the codes with one another has proven invaluable in debugging and in gaining confidence in new and unexpected results. Having reliable means for comparison and testing will become even more essential in the proposed work, as it expands further into new physics territory and nonlinear prediction. The AMRMHD code is being applied to several applications that are distinguished by their multiple length scales: the Richtmyer-Meshkov instability, magnetic reconnection, and pellet fueling. These demanding applications are allowing us to evaluate the AMR technique and to determine its place in a comprehensive integrated model of a fusion plasma.

### **1.2 The proposed work**

The new level of funding that we are requesting will allow us to build on the infrastructure we have already developed and to take our activities to the next level by undertaking more ambitious (i.e., burning-plasma) applications and by funding associated efforts in extended-MHD model and code development and validation, physics integration, data management, and visualization. We feel these new activities are needed to put the extended-MHD modeling effort on more solid ground theoretically, computationally, and applications-wise. Through this proposed work scope, this Center will remain the worldwide leader in 3D modeling of the global dynamics of fusion experiments and will play a big role in shoring up the scientific foundations for ITER and other burning plasma devices. The work will be performed thru the partial funding of 10 leading computational physics researchers in the field, 1 algorithmic computer scientist, 3 junior researchers (or postdocs), at least 2 students, 2 data management and visualization specialists and an analytic theorist who is a recognized expert in the extended-MHD equations. The proposed work, including milestones, is described in much greater detail in Section III. Note that if the proposal is only partially funded, we will have no choice but to eliminate one or more of the new junior staff positions and to proportionally cut back on the proposed work scope and milestones.

### **1.3 History of the Center of Extended Magnetohydrodynamic Modeling (CEMM)**

The Center was founded in the summer of 2001. During these last 3 years, the CEMM group has transformed itself from a collection of separate groups to an actual Center of intellectual and computational activity in extended MHD. We have had 2-3 meetings per year, documented on the “workshops” page of our website <http://w3.pppl.gov/CEMM>. When these meetings are held as satellite attachments to the APS or Sherwood meetings, they normally draw 30-40 participants, many more than what are actually funded by our Center. The Center members engage in much more frequent communication through conference calls and extensive email discussions. We have learned much from one another and also from our other SciDAC collaborators, and have benefited from yearly meetings with our Program Advisory Committee (PAC). Even the modest funding that we received in the last round has had a large effect in allowing us to pursue the common goals of the Center: pioneering new applications, understanding new physical phenomena, development of improved extended-MHD physics models, code benchmarking, and advanced algorithmic and visualization development. As one measure of success, we note with pride that CEMM applications were featured as two of the three fusion “Advances in Computational Science” in the newly released NERSC 2003 annual report. [5]

## II. Preliminary Studies

We highlight here some of our progress in the form of new application results and code development accomplishments during the first grant period.

### 2.1 Application results

#### 2.1.1 *Physics of the “current hole” (and the importance of extended-MHD effects):* [6,7]

One of the greatest successes of fusion MHD in the last few years was to provide an explanation of the “current hole” phenomena. It was observed in large experimental facilities in Europe and Japan that the current density in the center of a tokamak can be made to go to zero, but cannot be made to reverse sign, regardless of what current-drive sources are applied to it. We have used the M3D code to explain this curious phenomenon by showing that as the current density begins to reverse, strong flows develop that cause a form of magnetic reconnection to occur that has the effect of clamping the current density near zero, as shown in the midplane current density plots in Figure (1). This is important since these configurations with near-zero central current density have very good energy confinement and other properties that may form the basis for a more attractive fusion reactor. The study of this phenomenon has been extended to high-beta, where two-fluid effects were shown to be essential in providing an effective poloidal rotation of a meta-stable state that would otherwise halt the reconnection. [8]

#### 2.1.2 *The Dynamics of high-beta disruptions:* [9]

We have used the NIMROD code to calculate details of a disruptive termination of the DIII-D tokamak (Fig. 2) when it is slowly heated to a pressure exceeding the ideal-MHD stability limit. The calculation of the “thermal quench” included a moving plasma/vacuum interface and an accurate treatment of the rapid heat loss along magnetic field lines that connect with the surrounding vessel as a result of the instability. We find that the plasma thermal energy is deposited in a localized beam, in good agreement with experimental measurements. A related calculation with M3D has been used to determine the induced currents in the vessel during the subsequent “current quench” phase of the disruption.

#### 2.1.3 *Suppression of the Richtmyer-Meshkov Instability by a Magnetic Field:* [10]

We have been the first to demonstrate, using our Chombo-based Adaptive Mesh Refinement (AMR) MHD simulation code, that the presence of a magnetic field will suppress the growth of the Richtmyer-Meshkov instability when a shock wave interacts with a contact discontinuity separating ionized gases of different densities. The top and bottom images in Figure (3) contrast the interface without (3a) and with (3b) the magnetic field. In the presence of the field, the vorticity generated at the interface is transported away by the fast and slow MHD shocks, removing the drive of the instability

#### 2.1.4 *Magnetic Island Thermalization at Realistic Parameters ( local and non-local kinetic closure):*

[2,11] Development of the high-order finite element representation in NIMROD has enabled the use of realistic ratios (up to  $10^{11}$ ) for the parallel ( $\chi_{\parallel}$ ) to perpendicular ( $\chi_{\perp}$ ) thermal conductivity for the first time in a fully 3D global calculation. Figure (4) (dotted line) illustrates a benchmark result on the width of a helical magnetic structure (called a “magnetic island”)  $w_d$  required to influence the temperature profile. This verified the theoretical prediction for cylindrical geometry that the required anisotropy ratio for flattening the temperature profile within the island will scale as  $\chi_{\parallel}/\chi_{\perp} \sim w_d^{-4}$ , and extended this result to toroidal geometry for the first time. Also shown (solid line) is the result with a non-local kinetic expression for the parallel electron heat flow. Comparison with the local, heuristic closure shows more robust flattening of temperature at smaller island widths. Such quantitative calculations of electron temperature flattening are crucial to predicting the growth of neoclassical tearing modes from seed islands.

### 2.1.5 *Diamagnetic stabilization of MHD modes and enhanced reconnection in Stellarators:* [12,13]

Our work has shown that extending the MHD description to the two-fluid model is essential in predicting the stabilization of an important class of localized instabilities in stellarators. Figure (5) contrasts two M3D simulations of the quasi-axisymmetric NSTX stellarator at high beta (pressure). The figure on the left shows stochastic field line traces for a pure resistive MHD simulation. The one on the right, which is seen to have good surfaces, included the two-fluid terms. The more complete plasma model generates self-consistent large-scale (diamagnetic) plasma flows that stabilize the localized resistive ballooning and interchange instabilities. The two-fluid nonlinear effects can also strongly accelerate magnetic reconnection and island growth. This effect, which increases strongly with beta, suggests that there is a natural “soft” beta limit in stellarators, where magnetic islands grow larger as beta increases, until plasma confinement is seriously degraded and beta saturates despite additional heating. The two-fluid terms have been shown to have effects similar to the 'parallel momentum damping' of the neoclassical stresses. These terms should be considered in evaluating neoclassical island theories, which depend on background rotation and electrostatic potential. These questions remain to be investigated in detail. (see Sec. 3.1.2)

### 2.1.6 *Pellet fueling of a tokamak:* [4]

We have used our AMR code to provide a realistic and efficient calculation of pellet fueling of a high-temperature tokamak (Fig. 6). In this process, a very small pellet of frozen hydrogen is injected at high velocities into the large plasma torus. The pellet causes a rapid, local pressure increase which drives a localized instability that tends to redistribute the pellet mass. Initial results from this demanding simulation are in qualitative agreement with experimental results. The AMR feature led to a calculation over 30 times as efficient as a uniform mesh equivalent.

### 2.1.7 *Energetic particle driven modes in Spherical Tokamaks:* [14]

Recent NSTX experiments show rich beam-driven Alfvén instabilities in neutral beam-heated plasmas. The M3D code, with a kinetic energetic particle component included, was applied to simulate the beam ion-driven Alfvén instabilities in NSTX. In the linear regime with an isotropic beam ion distribution, the M3D simulation results show unstable Toroidal Alfvén Eigenmodes (TAE) with frequencies consistent with experimental observations in NSTX. For a more realistic anisotropic distribution, the dominant linear  $n=2$  mode has a significantly lower frequency as compared to TAE's frequency. In the nonlinear regime, the M3D simulations show that the  $n=2$  mode's frequency chirps down as it moves out radially (See Fig. 7).

### 2.1.8 *Effects of Strong Toroidal Shear on MHD Modes:* [14]

New stabilizing effects have been demonstrated by including the effects of rapid rotation in the calculation of Spherical Torus (ST) stability. The sheared toroidal flow can have a strong stabilizing effect nonlinearly and, as shown in Figure (8), can cause saturation of otherwise unstable modes if the rotation profile is maintained. These M3D simulations may account for the exceptional stability recently observed in high-pressure discharges in the National Spherical Torus Experiment (NSTX).

### 2.1.9 *MHD and energy transport in SSPX:* [15,16]

Through numerical simulation of the SSPX spheromak at LLNL, we have shown that a synergy between transient MHD effects and temperature-dependent transport coefficients leads to conditions that reach approximately 100 eV. Using recent developments for collisional heat transport, Ohmic heating, and temperature-dependent resistivity with parameters and the current waveform used in SSPX, NIMROD simulations form large closed flux surfaces, allowing the simulated core plasma temperature to increase in good agreement with laboratory Thompson-scattering data (Fig. 9). The symmetry-restoring magnetic



reconnection occurs in the edge plasma, which cools and loses conductivity after the initial drive phase is complete. The close agreement throughout the nonlinear evolution from 3D chaotic magnetic topology to symmetric flux surfaces speaks to the accuracy of both the MHD and energy transport modeling.

### 2.1.10 MHD behavior in CDX-U [17]

Time-step and spatial resolution requirements presently preclude us from modeling all but the fastest MHD events using the actual parameters in today's largest tokamak fusion experiments. However, we have begun an experimental verification program using data from one of the smaller, less computationally demanding experiments: CDX-U (PPPL). The CDX-U small tokamak exhibits periodic central reconnections (sawtooth oscillations) that can be qualitatively reproduced with the simulation codes. Matching the repetition period and crash time is presenting an excellent test for the extended MHD model, as well as a testbed to benchmark the nonlinear predictions of M3D and NIMROD with one another. Having the two codes compute the same case turned out to be especially important in this application as we found that some higher- $n$  unstable modes, which we originally thought to be numerical artifacts, were in fact valid solutions of the resistive MHD equations and were obtained by both codes.

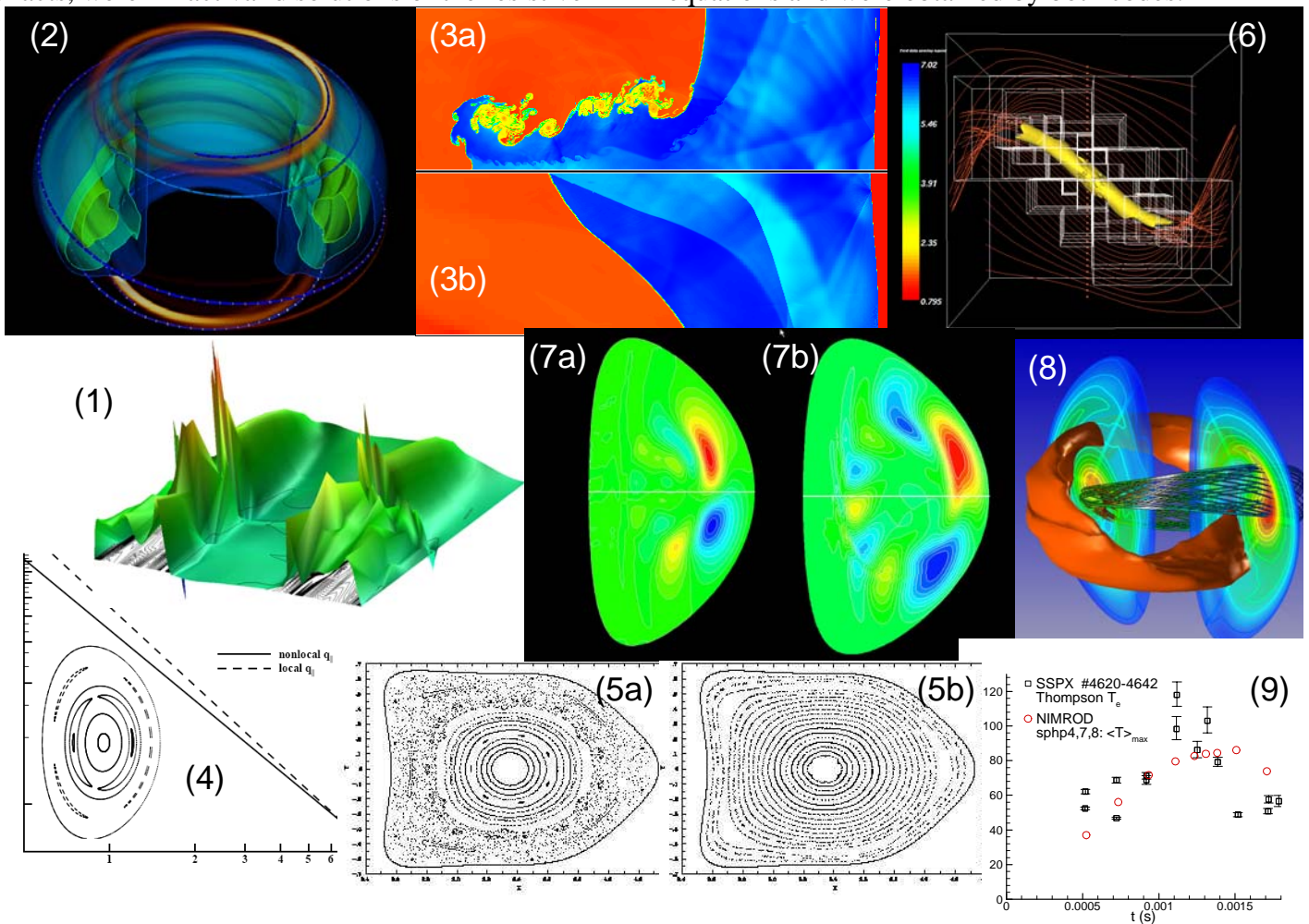


Figure 1-9: Illustrations of 9 of the applications accomplished during the first funding period.



## 2.2 Algorithmic Development and Code Performance

### 2.2.1 Linear Solvers and TOPS:

Both M3D and NIMROD solution times are dominated by the sparse matrix solves. NIMROD had previously used the conjugate gradient method together with a global line-Jacobi preconditioning technique. Working with the TOPS center, it was found that modern parallel sparse direct solvers are more effective on the very ill-conditioned matrices, and implementing SuperLU provided a factor of 4-5 improvement in computational time for nonlinear applications—even much more for linear calculations. In M3D, a reformulation of the equations suggested by the TOPS center allowed the sparse matrices to become symmetric. This permitted use of the new PETSc ICCG solver rather than GMRES, which led to about a factor of 2 decrease in computational requirements. The TOPS center has also supplied routines that support interfacing high-order finite elements with the AZTEC parallel solver library and interfacing with efficient algebraic multi-grid methods from HYPRE. The HYPRE routines will be especially effective for the larger matrices we will encounter for the work proposed in Sec. III.

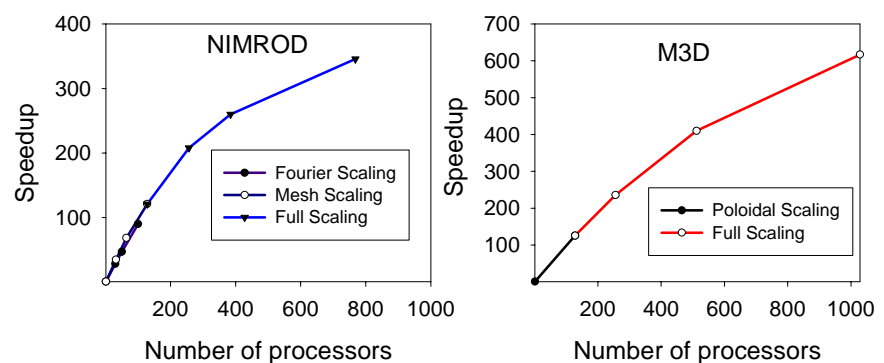
### 2.2.2 Adaptive Mesh Refinement and APDEC:

We have worked jointly with the APDEC center in developing the new Princeton/LBL AMRMHD code and in applying it to several demanding applications with multiple space scales. This involved jointly developing a generalized upwind 8-wave MHD solver[18-23] that is fully second order accurate and has corner coupling to minimize dispersion caused by wave propagation oblique to the grid lines. This work has already led to several publications [4,10] described above. This highly successful effort was funded jointly by the APDEC center and the Scientific Application Partnership Program (SAPP) and we expect this funding arrangement to continue into this next funding cycle.

### 2.2.3 High Order Elements and Advanced Meshing and the TSTT.

Through extensive discussions between CEMM members and the Trellis team at RPI and with TSTT researchers at ANL, we have carried out systematic tests of different classes of high-order finite elements on fusion extended-MHD relevant problems. These studies have confirmed the benefit of high-order elements [1] and also led to the discovery of an alternative element with  $C^1$  continuity [24] that is now being proposed to be implemented in M3D. We have also collaborated with the TSTT to investigate using the CUBIT mesh generation program as a means to provide general geometry modeling for the NIMROD preprocessor.

**Figure 2.2.4 Both NIMROD and M3D exhibit strong scaling that begins to deteriorate at about 500-1000 p for typical problem sizes. NIMROD runs had  $64 \times 128$  bi-quartic elements, 6 toroidal harmonics (held fixed). M3D runs had 5000 linear poloidal elements, 512 toroidal zones (held fixed).**



### 2.2.4 Parallel Scaling and performance

The extended-MHD codes are typical of many “real world” codes that model global multiple timescale physics in that their solution time is dominated by sparse matrix equations that are notoriously difficult to scale to very large processor number. However, by utilizing domain decomposition in several dimensions, we have been able to obtain adequate scaling for up to 1000 or more processors for realistic problem sizes. The results of typical strong scaling studies on the NERSC IBM SP3 (Seaborg) are shown

in Fig. 2.2.4. Note that this is for strong scaling with the number of spatial zones held fixed. Weak scaling studies, of course, show much better scaling behavior with number of processors.

### 2.2.5 Model studies in support of algorithm development

Implicit methods can eliminate the fast time-scales of a stiff system. This can be thought of as an alternative to applying an analytic ordering.. The numerical computation determines the balances that would otherwise need to be removed analytically using higher-order relations of a small-parameter expansion. In many cases (but not all), this leads to a simpler, more general, and more flexible numerical implementation, since any important higher-order contributions are necessarily present in the primitive equations.

The trade-off is the effort required to construct an accurate and numerically stable implicit algorithm, and this can only be done with a firm theoretical understanding of all behavior represented in the primitive equations. In this spirit, CEMM has undertaken a review of the dispersive normal modes in extended-MHD systems of equations, the results of which are summarized in Table 2.2.1.

**Table 2.2.1 Dispersive Modes in Extended-MHD Models**

Mode	Origin	Wave Equation	Dispersion	Comments
Whistler	$\mathbf{J} \times \mathbf{B}$ Ohm	$\frac{\partial^2 \mathbf{B}}{\partial t^2} = -\left(\frac{V_A^2}{\Omega}\right)^2 (\mathbf{b} \cdot \nabla)^2 \nabla^2 \mathbf{B}$	$\omega^2 = V_A^2 k^2 \left[1 + \frac{1}{\beta} (\rho_i k_{\parallel})^2\right]$	<ul style="list-style-type: none"> <li>finite <math>k_{\parallel}</math></li> <li>electron response</li> </ul>
KAW	$\nabla_{\parallel} p_e$ Ohm	$\frac{\partial^2 \mathbf{B}}{\partial t^2} = \left(\frac{V_A V_{th*}}{\Omega}\right)^2 (\mathbf{b} \cdot \nabla)^2 \nabla \times [\mathbf{b} \mathbf{b} \cdot \nabla \times \mathbf{B}]$	$\omega^2 = V_A^2 k_{\parallel}^2 \left[1 + (\rho_s k_{\perp})^2\right]$	<ul style="list-style-type: none"> <li>finite <math>k_{\parallel}, k_{\perp}</math></li> <li>ion and <math>e^-</math> response</li> </ul>
Parallel ion GV	$\eta_4$ term in $\nabla \cdot \Pi^{GV}$	$\rho \frac{\partial^2 \mathbf{V}_{\perp}}{\partial t^2} = -\eta_4^2 \nabla_{\parallel}^4 \mathbf{V}_{\perp}$	$\omega_{R\pm} = V_A k_{\parallel} \left[\pm 1 \pm \frac{1+\beta}{2\sqrt{\beta}} (\rho_i k_{\parallel})\right]$	<ul style="list-style-type: none"> <li>finite <math>k_{\parallel}</math></li> <li>ion response</li> </ul>
Perp. ion GV	$\eta_3$ term in $\nabla \cdot \Pi^{GV}$	$\rho \frac{\partial^2 \mathbf{V}_{\perp}}{\partial t^2} = -\eta_3^2 \nabla_{\perp}^4 \mathbf{V}_{\perp}$	$\omega^2 = V_A^2 k_{\perp}^2 \left[1 + \frac{\gamma\beta}{2} + \frac{\beta}{16} (\rho_i k_{\perp})^2\right]$	<ul style="list-style-type: none"> <li>finite <math>k_{\perp}</math></li> <li>ion response</li> </ul>

**Notation:**  $\rho_i = V_{thi} / \Omega$  is the ion gyro-radius;  $V_{th*} = \sqrt{T_e / m_i}$ ;  $\rho_s = V_{th*} / \Omega$ ;  $\eta_4 = nT_i / 2\Omega$ ;  $\eta_3 = 2\eta_4$

Each mode given in the table can be obtained in the proper limit of the general dispersion relations for magnetized plasmas [25]; however, the gyroviscous responses are seldom considered. They appear in the lowest-order FLR corrections to solutions of the MHD equations [26] and include a dispersive mode that propagates perpendicular to the magnetic field. These limiting forms of the higher order terms in the extended-MHD equations form the basis for the new implicit algorithms discussed in Sec. 3.3.

### 2.2.6 Code Validation and Verification

The Center recognizes the critical importance of a thorough validation and verification regime. We have approached this by performing cross-code comparisons and by comparing with experimental data. The cross-code comparisons involved several linear problems in ideal MHD, resistive MHD, and hybrid energetic-particle MHD that are described on our web site. We are now engaged in a nonlinear cross-code comparison, briefly described in Sec. 2.1.10, that is proving much more difficult (and rewarding) than what we had first anticipated. The beginnings of the joint visualization package has allowed us to make detailed comparisons of the differences of the predictions of M3D and NIMROD on the same

application, which have in turn forced us to examine the numerical representations used in each of the codes in greater detail. This non-linear cross-code comparison will be one of the major focuses of the next CEMM meeting, to be held on April 25<sup>th</sup>, 2004. The codes have been and will continue to be compared with experimental results whenever this is feasible. Essentially all of the tokamak applications described in Sec. 2.1 involved some degree of experimental comparison. Through the institutions represented in the center, we have access to data and good working relationships with NSTX, DIII-D, CMOD, CDX-U, as well as JET and other foreign devices through international collaboration agreements.

### **2.3 Summary of Phase-I activities**

Even though our center was funded at only half of the requested amount of \$1,000 k/year for 3 years starting in the summer of 2001, we have accomplished most of the milestones listed in our 15 March 2001 proposal, and gone beyond several of them. The principal applications have been highlighted in Sec. 2.1 above. These led to 3 IAEA papers in FY 2002, 4 Invited APS talks, 4 IAEA papers being submitted this year, and 13 refereed publications. In order to accomplish these activities, the following code development activities took place:

We developed a much more general mesh module for the M3D code that facilitates parallel scaling and is suitable for stellarators. The drift-ordered two-fluid equations have now been incorporated in M3D and have been applied to tokamaks, STs, and stellarators. A fully parallel hybrid energetic particle module has been developed and applied to TAE and fishbone modes in tokamaks and STs. The boundary conditions have been generalized to allow a separatrix, a vacuum region and a conducting wall. [27]

We have redesigned the linear solvers in the NIMROD code to allow non-Hermitian matrix solves. A semi-analytic CEL based closure for electrons has been developed and used in several large calculations. A parallel hybrid energetic particle module has been developed and used to perform test problems. We also developed a boundary condition for NIMROD that allows a separatrix, a vacuum region, and a conducting wall. We have made significant progress in developing an implicit treatment of some of the critical two-fluid terms (discussed more in Sec. 3.3) and equilibrium flow. [see [http://www.cptc.wisc.edu/sovinec\\_research/meetings/sovinec\\_aps03poster.pdf](http://www.cptc.wisc.edu/sovinec_research/meetings/sovinec_aps03poster.pdf)]

The extension of the MHD model beyond resistive MHD (see Sec. 3.2) has been shown to be critical in the applications discussed in Sections. 2.1.1, 2.1.2, 2.1.5, 2.1.7 and 2.1.10, as well as in many others. The new terms that appear in the two-fluid model have now been shown to stabilize high mode number MHD instabilities and they have also been shown to strongly accelerate magnetic reconnection [28-30] and island growth, particularly in stellarators. Including the energetic particle component in a hybrid description has also been shown to be an effective method of simulating energetic particle driven instabilities. These successes provide increased motivation to further refine and test the extended-MHD models and to apply them to new and more challenging applications as discussed in this proposal.

The accomplishments listed above, the extensive non-linear M3D/NIMROD benchmark now underway and described briefly in Sec. 2.1.10 and the joint visualization activity described in Sec. 3.5 show that our group has a history of working together and accomplishing what it proposes. This should give some confidence that the work described in the present proposal will be carried out if it is fully funded.

### III. Research Design and Methods

#### 3.1 Applications:

We list here some of the new applications that will be pursued for the present proposal. These applications were selected because of: (1) their importance for a burning plasma, [31] (2) our perceived ability to make progress on them, and (3) the need for each of them to make use of advanced computing resources. Most of these applications will be performed with several physics models (see Sec. 3.2) in order to clarify the dominant physical effects. At the end of each description, we list the specific questions that are outstanding in that area, and which we will be addressing.

##### 3.1.1 Full nonlinear sawtooth oscillation modeling in fusion –grade plasmas

The *sawtooth instability* occurs when the current peaks in a tokamak, creating a region in the center where the safety factor is less than unity,  $q < 1$ . While this instability is confined to the center of the plasma in low pressure, low current, large aspect ratio discharges, under certain conditions it can create magnetic islands at the outer resonant surfaces and sometimes set off a sequence of events that leads to a major disruption. Under some circumstances the reconnection following the sawtooth is observed to be complete (Kadomtsev-like), but in other conditions it is incomplete. Sawtooth behavior is complex and remains incompletely explained.

The challenge is to develop a better predictive model of the sawtooth for all plasma conditions. Extended MHD offers additional processes that influence sawteeth -- linear mode and nonlinear ion diamagnetic drift stabilization, nonlinear ‘kinetic Alfvén wave’ and ‘whistler wave’ enhancement of the reconnection rate, and neoclassical effects -- all of which will affect the sawtooth behavior in burning plasmas.

When an energetic particle component is present, sawtooth oscillations can be delayed leading to “giant sawteeth”. This has been observed in both Ion Cyclotron Resonance heating (ICRF) and Neutral Beam Injection (NBI) discharges [32]. Recent experiments [32-34] have demonstrated that the sawteeth suppression results from energetic ions stabilizing the internal kink mode as predicted by theory [34, 35]. This fast particle stabilization arises from conservation of the third adiabatic invariant for trapped fast particles [36] when their toroidal precession time scale is much shorter than that of internal kink mode.

The study of this instability with the extended-MHD codes will be the most self-consistent and comprehensive yet undertaken. It will include full geometry effects, both trapped and passing particle kinetic response with finite orbit width, and non-perturbative effects of alpha particles on the mode structure. This study will determine how effective the fusion alpha particle stabilization is for typical ITER parameters and profiles and this will in turn determine the possible extension of sawteeth period.

We will explore the alpha particle effects on the whole process of sawteeth oscillations. Another important question to answer is what is the additional alpha particle transport induced by sawteeth. These questions can be studied self-consistently by our hybrid extended-MHD model. (Sec. 3.2.7) However, we realize that this nonlinear aspect is very challenging due to two reasons. First, we expect that there will be order of unity change in the alpha particle distribution due to sawteeth so that the standard  $\delta f$  method may not be effective in reducing the particle simulation noise for the whole simulation. Second, the simulation of a whole sawteeth period for burning plasma parameters is computationally demanding even using a simple MHD model. We can begin immediately with scaling studies at reduced parameters, but the improved numerical methods, described in Section 3.3 will be needed in order to simulate sawteeth oscillations with alpha particle effects for realistic parameters of ITER. The outstanding questions are:

- What will be the period and inversion radius of the sawtooth oscillation in an ITER-class burning plasma, as a function of plasma current and pressure?
- What physics underlies complete and incomplete reconnection during the sawtooth?
- Under what conditions will the sawtooth instability trigger the onset of a metastable island (neoclassical tearing mode) or lead to a disruption?
- How does this picture change in the presence of energetic particles?

### 3.1.2 Tearing mode and neoclassical tearing mode excitation in high-beta plasmas:

The *neoclassical tearing mode* (NTM) occurs when a magnetic island develops in a tokamak causing the pressure to flatten, which subsequently causes the neoclassical “bootstrap current” to decrease, in turn causing the island to continue growing. Experimentally, the NTM is thought to limit the obtainable pressure in many long pulse tokamak discharges. [37-40] For these studies, an anisotropic thermal conduction model and a neoclassical closure for the ion and electron viscous stress tensors are essential.

The conventional theoretical analysis suggests that a seed island is necessary for the bootstrap current to affect the nonlinear evolution, but the physics underlying the generation of small seed islands is poorly understood both experimentally and theoretically. Experimentally, NTMs have been correlated to other magnetic perturbations including the internal kink, magnetic field errors, edge localized mode (ELM), and other tearing modes; however, “spontaneous NTMs” are also frequently observed. For the cases of MHD coupling to produce seed islands, the island rotation plays an important role [41]. Experimentally, magnetic islands rotate, and this rotation is observed in the extended-MHD codes when “two-fluid” or neoclassical pressure effects are included. [55] At present however, there is not confidence that the correct rotation velocities are predicted by the present models.

A strong emphasis will be placed on extending the realism of the closure model in the two-fluid equations and on comparing with relevant experimental results and analytic theories. Thus, much of the work in this application is closely tied to the developments of better extended MHD models as is discussed in Sec. 3.2.

Where NTMs cannot be avoided, active stabilization is required. Electron-cyclotron current drive has been experimentally demonstrated to stabilize tearing modes. We propose initially implementing existing models of RF driven current in M3D and NIMROD to investigate the feedback stabilization of NTMs, and later to collaborate with the RF SciDAC team in a more comprehensive integrated simulation as described in Sec. 3.4. The questions we seek to answer in this area are:

- Which extended-MHD models give adequate agreement with existing experiments for the formation, growth, and rotation velocity of the observed islands?
- What type of disturbance can cause the neoclassical tearing mode to form in an ITER-class tokamak?
- Under what conditions do “spontaneous NTMs” form?
- What will be the saturated island size as a function of plasma current and beta?
- What level of external current drive power is required to fully stabilize the NTM?

### 3.1.3 Nonlinear evolution and control of resistive wall modes, including toroidal flows

Resistive Wall Modes (RWMs) are external kink modes that would be unstable were it not for the presence of a nearby conductor (or wall). They grow on the resistive time of the wall, but can be stabilized by a combination of plasma flow and magnetic feedback. The application of the extended-MHD codes NIMROD and M3D to this problem requires non-ideal boundary conditions, which have

been implemented during the last proposal period. RWMs require a dissipation mechanism, such as Landau damping. There are several issues that will be addressed in the present proposal:

RWMs can be stabilized by a toroidal flow velocity which is a few percent of the Alfvén speed. Flows of this magnitude are not expected to occur in large RF-heated plasmas such as ITER. Nonetheless it is an important process and must be considered in interpreting experiments in DIII-D, NSTX and other tokamaks. Magnetic error fields are known to cause *toroidal flow damping*, but the detailed mechanism of how they do so is not well understood. It could be torque produced by islands, a nonlinear process, or it may be the result of parallel viscosity or some other process. Simulations will be carried out to try to elucidate and compare various mechanisms. The simulations must be closely coupled to closure development discussed in Sec. 3.2; in particular, the parallel viscosity will require development of a new local closure, and the rotation processes are closely coupled to the two-fluid effects.

Near the MHD external kink mode stability boundaries, *error fields can be resonantly amplified* by stable RWMs. This has been observed to cause toroidal flow damping and destabilization of the RWMs [42]. Although the amplification is a linear process, the flow damping can be nonlinear. We have obtained preliminary results on resonant destabilization of RWMs by magnetic error fields. The example in Fig. 3.1.3 shows a nonlinear predominantly  $m, n = 2, 1$  velocity perturbation, and the associated toroidal field function, which were excited by an external magnetic field perturbation, and which led to a disruption.

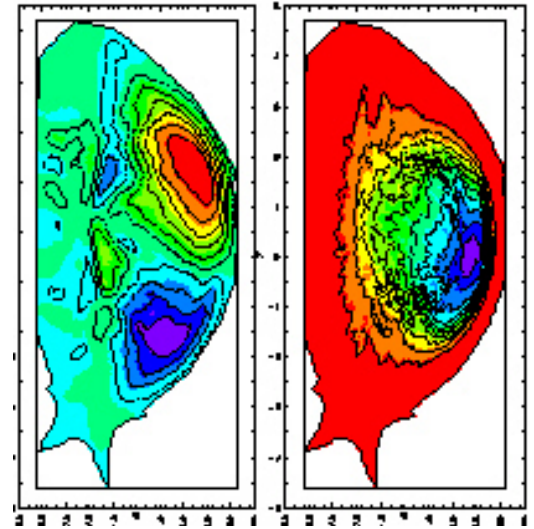


**Figure 3.1.3: Nonlinear electrostatic potential (left) and perturbed toroidal magnetic field (right) in a nonlinear RWM**

There are several *active feedback* experiments now proceeding or planned on present devices. These are presently being analyzed by several linear codes, including NMA, MARS and VALEN. The application of the 3D nonlinear extended-MHD codes to this problem would be a large step forward in realism, as it would include mode coupling, an improved plasma model, and self-consistent treatment of rotation. The outstanding questions are:

- What are the dominant toroidal flow and RWM damping mechanisms in present experiments, and how do these scale to ITER?
- What is an allowable error field in ITER as it relates to MHD stability limits?
- How much beyond the ideal-wall beta limit can an ITER-class plasma operate with a properly designed feedback system?

#### 3.1.4 Effects of fast ions:

The fusion alpha particles will not only stabilize MHD modes as described in 3.1.1, they will also drive MHD modes unstable (such as fishbone, TAE and EPM). These instabilities can in turn cause anomalous loss of alpha particles. We propose here to investigate the nonlinear consequences of alpha-driven Alfvén instabilities in burning plasmas such as ITER.

Although the emphasis of this work will be nonlinear effects, in the process we will also provide an accurate determination of linear stability thresholds in fusion plasmas. Most of the previous linear work has either used global perturbative calculations with full geometry or local non-perturbative calculations with simple geometry. In contrast, our extended-MHD hybrid model is both non-perturbative and global

with full geometric effects. The energetic ions are described by gyrokinetic equations and their effects enter the momentum equation via the stress tensor. The important "radiative damping" due to kinetic Alfvén waves will be treated globally by including the FLR effects of thermal ions to second order in the stress tensor (see Sec. 3.2.6). This work will determine self-consistently the stability thresholds and linear mode spectrum of alpha-driven TAE/EPM.

Most of the previous analytical and numerical work considered the nonlinear saturation of a single mode or a few low- $n$  modes. This work will study the nonlinear behavior of multiple high- $n$  modes driven simultaneously by alpha particles. From linear theory, the linear growth rate of alpha-driven shear Alfvén modes (i.e., TAE/EPM) peaks at  $k_{\theta}\rho_{\alpha} \sim 1$ . Thus, higher- $n$  modes are expected for an ITER-class device due to its larger size and stronger magnetic field as compared to present day tokamaks. Recent linear stability calculations with HINST and NOVA-K showed that TAEs with toroidal mode number  $n \sim 10$  are unstable in ITER.[43] Furthermore, it can be shown that the number of unstable modes is proportional to  $(a/\rho_{\alpha})^2$ . Thus, we can expect many unstable high- $n$  TAEs driven by alpha particles in a fusion reactor. Here, we will investigate for the first time the self-consistent alpha particle transport in the presence of multiple high- $n$  Alfvén modes in a burning plasma.

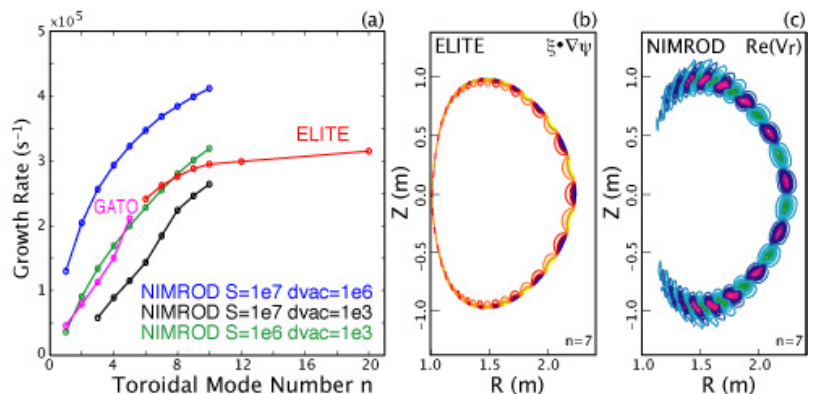
To resolve the high- $n$  mode structures most efficiently, we plan to implement a field-aligned mesh in the M3D code to take advantage of long parallel wavelengths. (see 3.3.5). For  $n \sim 10$  modes in ITER, we need about 200 radial mesh points, 600 poloidal grid points at the edge and 64 toroidal planes. This corresponds to about  $10^7$  numerical cells (for linear elements in M3D) and  $10^8$  particles. A typical run at this resolution would take about 30 hours using 1000 processors on Seaborg (for 10000 time steps). The higher order  $C^1$  elements, being implemented as part of this proposal, should reduce the run time, or increase the allowable resolution. The outstanding questions in this are:

- How does the presence of fast ions alter the nonlinear MHD behavior of the sawtooth, the NTM, and the other MHD modes?
- What new instabilities are introduced in an ITER-class plasma by the fast ions, and what are the non-linear consequences in terms of anomalous alpha particle transport?
- Under what conditions will a large fraction of alpha particles be lost?

### 3.1.5 Edge MHD-type instabilities

All tokamaks that operate in a high-performance H-mode similar to the ITER baseline exhibit Edge Localized Modes, or ELMs. Substantial progress has been made on understanding these during the last few years, and it is now clear that they are periodic MHD events that have both pressure and current drive [44, 45]. The H-mode edge pedestal in density and temperature leads to an edge pressure gradient and the associated edge bootstrap current which in turn drive these modes. We have made excellent recent progress in benchmarking NIMROD against the linear codes GATO and ELITE [46], as shown in the Figure 3.1.5(a-c). (The model in ELITE breaks down at low- $n$ , and GATO has practical limitations above  $n \sim 5$ .) The models used in ELITE and GATO enforce ideal MHD, assume that the separatrix is a sharp boundary, and compute vacuum fields with a Green's function.

**Figure 3.1.5.**(a) Comparison of ELM growth rate as a function of toroidal mode number for NIMROD (with different value of core and vacuum resistivity), GATO and ELITE; (b) ELITE eigenfunction for  $n = 7$  (only plasma perturbation is plotted); (c) Real part of the NIMROD eigenfunction for  $n = 7$ , showing both plasma and vacuum perturbations.





We now plan to go beyond the linear benchmarking to attempt to model the entire nonlinear ELM cycle. The computational challenge here will be to compute efficiently with the large number of toroidal modes that will be required for a fully non-linear computation. This work may lead to future opportunities for integration activities with edge physics models. Among the physics questions to be addressed by this work are:

- What type of ELM behavior do we expect in an ITER-class plasma as a function of current and beta?
- What external mechanisms, such as pellet injection, RF current drive, or boundary modulation, are effective in increasing the ELM period and reducing the magnitude?
- Can the nonlinear results be used to improve the heuristic models that are implemented in global transport models? [47]
- Can non-linear, dynamical models of ELM evolution be effectively coupled with other detailed models of edge dynamics and transport?

### 3.1.6 Disruptions and Vertical Displacement Events (VDEs):

The highest performance tokamak discharges are often terminated by a major disruption or a VDE. Disruptions result from various internal MHD instabilities that destroy magnetic surfaces, which in turn causes rapid loss of thermal energy (thermal quench) and then loss of current (current quench) as the cooled plasma becomes highly resistive. VDEs are disruptions that occur after the plasma has lost vertical control and drifted upward or downward. The current that flows from the plasma into the wall during the current quench is called *halo current*. The degree of toroidal asymmetry of the halo current is measured by the *toroidal peaking factor* [48]. This has been obtained from numerous experiments and incorporated in an international database. ITER scientists (in particular K. Lackner and S. Ortolani) have requested that this data be confirmed and projected to ITER by 3D extended-MHD numerical simulations, as it has a big consequence in the structural design of the vacuum vessel and in-vessel components.

MHD simulations have been used to identify the mechanism of a common type of disruption in the TFTR high-power DT discharges as a localized moderate-n ballooning mode nonlinearly destabilized by an internal kink.[49] NIMROD studies have reproduced many features of a beta-limit disruption in DIII-D [9]. Further studies with more resolution and improved physics models will be done to produce accurate criterion for such instabilities, which may shed light on ways to control them. The long term goal is to provide an understanding of all disruptions that occur experimentally and ultimately to provide insights leading to disruption-free regimes in tokamaks. Disruption mitigation techniques such as massive impurity injection will also be evaluated, extending previous killer pellet injection simulations done with TSC [50]. The questions we seek to answer in this area are:

- Under what circumstances will a chain of nonlinear events occur in an ITER-class plasma that result in a major disruption?
- What is the thermal quench time for each type of disruptive sequence, and where is the energy deposited?
- What are the mechanical forces on the ITER vacuum vessel for different types of disruptions, and how are these forces distributed spatially and temporally?
- Can we design a “killer pellet” or massive gas influx

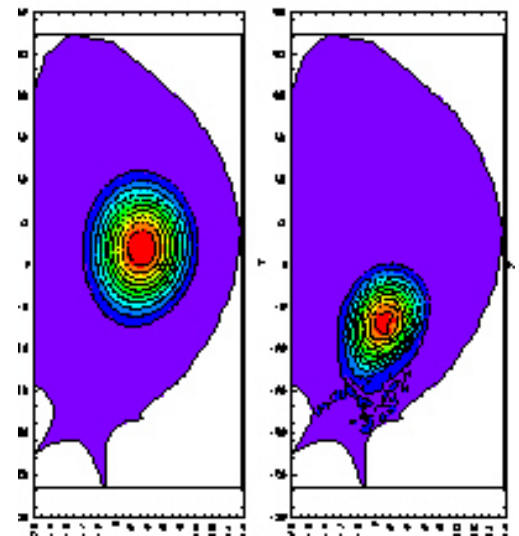


**Figure 2.1.6:** An example VDE is shown in which the toroidal magnetic field  $I=RB_{\theta}$  moves down into the wall. The poloidal halo current is tangent to the contours of  $I$ .

that, if initiated on an appropriate precursor signal, can significantly mitigate the effects of the disruption?

### *3.1.7 Pellet Injection fueling of a Burning Plasma (SAPP funding)*

As described in the application results Sec. 2.1.6, we have initial results for pellet fueling into a tokamak using the generalized upwind adaptive mesh refinement code AMRMHD, developed jointly by Princeton and LBL. We expect to make sufficient progress in the further development of this code in the areas of the treatment of stiff anisotropic physics and high-fidelity treatment of the global plasma geometry. This will allow more accurate simulations. The questions we seek to answer are:

- Can we reproduce the mass deposition differences between inside launch and outside launch as measured on the JET experiment?
- What mass deposition profile will we get for ITER as a function of pellet mass, injection velocity, and injection angle?
- Can we reproduce experiments performed on JET where Edge Localized Modes (ELMS) are induced by pellet injection, and project this to ITER (see 3.1.5)

## **3.2 Two Fluid and Kinetic Model Development**

### *3.2.1 Background and Goals*

The commonly used “resistive MHD” model is a single-fluid model that does not include finite Larmor radius (FLR) effects [51, 52] and is based on the assumption that the particle collision length is short compared to macroscopic scale lengths. To describe a magnetized fusion plasma, one must go beyond this description and apply an “extended MHD” model that allows independent electron and ion motions derived from the moments of the underlying kinetic equations [52-54]. This procedure produces a hierarchy of equations for successively higher velocity moments of the distribution function. The set is truncated at some order by an independent expression (closure relation) for the highest order velocity moments. The lowest order (in ion gyro-radius) corrections to resistive MHD are generally taken to be the ion and electron parallel stress tensors and heat fluxes, the Hall and electron pressure gradient terms in Ohm’s law, and the ion gyro-viscous stress. In toroidal plasmas the neo-classical contributions (due to toroidal particle trapping) to the parallel stress tensor dominates, and generally the electron heat flux dominates the total heat flux. However, the preferred form of the corrections for different parameter regimes is still the subject of research within the fusion theory community.

As part of CEMM, we propose to undertake research in theoretical and computational plasma physics that seeks to answer the following questions that are relevant to practical computation of macroscopic dynamics of fusion plasmas:

- What forms of the extended fluid equations are appropriate for different phenomena and different operating conditions?
- What are the limitations of the drift models? When must a more general (and complex) formulation be used?
- Under what circumstances can one or more of the extended fluid corrections (Hall term, electron pressure gradient, gyro-viscosity, neo-classical effects, etc.) be omitted in a global calculation?
- What is the most appropriate form, considering both physical accuracy and computational efficiency, of the neo-classical corrections to the ion and electron stresses and heat fluxes?
- To what extent must kinetic integral or hybrid calculations be used to close the fluid equations?
- What challenges do the advanced closures present for the design of numerical algorithms ?

This work will be closely coupled with the code development tasks described in Sec. 3.3.

### 3.2.2 Extended Fluid Models of Magnetized Plasmas

The lowest order finite-Larmor radius (FLR) corrections to the resistive MHD equations take the form of modifications to the electron and ion stress tensors and to Ohm's law. By considering different orderings of the characteristic frequency and velocities with respect to the small ratio of the ion gyroradius to other characteristic lengths  $\delta = \rho_i/L$ , and the order of accuracy with respect to  $\delta$  as well as the related  $\rho_s/L$  and  $d_i/L$  (where  $\rho_s$  is the ion sound gyroradius and  $d_i$  the ion inertial skin depth), it is possible to enumerate five different extended MHD models. These are summarized in Table 3.2.1.

The ion stress tensor is decomposed as  $\Pi_i = \Pi_{\parallel i} + \Pi_i^{gv}$ . The parallel component,  $\Pi_{\parallel}$ , includes the neoclassical part  $\Pi^{nc}$ , which describes collisional transport in a toroidal plasma. This becomes important when the collision frequency is less than the bounce frequency of the trapped particles. (Note that the Braginskii expression is proportional to collision length and is physically unrealistic in fusion plasmas). The cross component is taken to be the gyro-viscous stress,  $\Pi^{gv}$ , as given by Braginskii; unlike the other components of  $\Pi$ , it is not dissipative. The last three columns in Table 3.2.1 indicate dispersive ( $\omega \sim k^2$ ) normal modes that are introduced by the additional terms in the models. Each of these modes requires special attention when designing algorithms for extended MHD, as discussed in Sections 2.2.5 and 3.3.

**Table 3.2.1: Extended Fluid Models for Fusion Plasmas<sup>7</sup>**

Model	Momentum	Ohm's law	Whistlers <sup>1</sup>	KAW <sup>2</sup>	GV <sup>3</sup>	Slow dynamics <sup>4</sup>
General	$mn \frac{d\mathbf{V}}{dt} = -\nabla(p_e + p_i)$ $+ \mathbf{J} \times \mathbf{B} - \nabla \cdot (\Pi_{\parallel e} + \Pi_{\parallel i}) - \nabla \cdot \Pi_i^{gv}$	$\mathbf{E} = -\mathbf{V} \times \mathbf{B} + \eta \mathbf{J}$ $+ \frac{1}{ne} (\mathbf{J} \times \mathbf{B} - \nabla p_e - \nabla \cdot \Pi_{\parallel e})$	Yes	Yes	Yes	Either
Generalized Hall MHD <sup>5</sup>	$mn \frac{d\mathbf{V}}{dt} = -\nabla(p_e + p_i)$ $+ \mathbf{J} \times \mathbf{B} - \nabla \cdot (\Pi_{\parallel e} + \Pi_{\parallel i})$	$\mathbf{E} = -\mathbf{V} \times \mathbf{B} + \eta \mathbf{J}$ $+ \frac{1}{ne} (\mathbf{J} \times \mathbf{B} - \nabla p_e - \nabla \cdot \Pi_{\parallel e})$	Yes	Yes	No	No
Neoclassical-MHD	$mn \frac{d\mathbf{V}}{dt} = -\nabla(p_e + p_i)$ $+ \mathbf{J} \times \mathbf{B} - \nabla \cdot (\Pi_{\parallel e} + \Pi_{\parallel i}) - \nabla \cdot \Pi_i^{gv}$	$\mathbf{E} = -\mathbf{V} \times \mathbf{B} + \eta \mathbf{J} - \frac{1}{ne} \nabla \cdot \Pi_{\parallel e}$	No	No	Yes	Yes
Generalized resistive MHD <sup>5</sup>	$mn \frac{d\mathbf{V}}{dt} = -\nabla p + \mathbf{J} \times \mathbf{B} - \nabla \cdot \Pi_{\parallel}$	$\mathbf{E} = -\mathbf{V} \times \mathbf{B} + \eta \mathbf{J}$	No	No	No	No
Generalized drift <sup>6</sup>	$mn \frac{d\mathbf{V}}{dt} = -mn \mathbf{V}_{di} \cdot \nabla \mathbf{V}_{\perp} + \nu_{gv}$ $+ nm \mu \nabla_{\perp}^2 \mathbf{V} - \nabla \cdot (\Pi_{\parallel e} + \Pi_{\parallel i})$ $- \nabla(p_e + p_i) + \mathbf{J} \times \mathbf{B}$	$\mathbf{E} = -\mathbf{V} \times \mathbf{B} + \eta \mathbf{J}^*$ $- \frac{1}{ne} [\nabla_{\parallel} p_e + \nabla \cdot \Pi_{\parallel e}]$	No	Yes	Yes	Yes

<sup>1</sup>Whistler waves are dispersive waves arising from the  $\mathbf{J} \times \mathbf{B}$  term in Ohm's law.; <sup>2</sup>Kinetic Alfvén waves are dispersive waves arising from the  $\nabla_{\parallel} p_e$  term in Ohm's law.; <sup>3</sup>These are dispersive waves arising from the gyro-viscosity.; <sup>4</sup> this implies consistency in the ordering  $V/V_{thi} \sim \delta$  and  $\Omega/\Omega_{ci} \sim \delta^2$  where  $V_{thi}$  is the ion thermal speed and  $\Omega_{ci}$  is the ion gyrofrequency. <sup>5</sup>The term "generalized MHD" is used to indicate that the parallel stress or pressure anisotropy is retained, so the validity of the model is not restricted to short collision lengths. The conventional Hall-MHD and resistive-MHD models are recovered by assuming isotropic pressures. <sup>6</sup>In the Generalized drift model, the dependent velocity variable is  $\mathbf{V} = \mathbf{V}_i - \mathbf{V}_{di}$ , where  $\mathbf{V}_{di} = \mathbf{J}_{\perp} / ne - \mathbf{B} \times \nabla p_e / ne B^2$ . See Ref. [55] for a definition of the remaining terms. <sup>7</sup> Electron inertia consistently neglected for simplicity.

Closure relations express the components of the stress tensor (and the heat flux, not discussed above) in terms of the other dependent variables (density, velocity, pressure) and their gradients. Fluid closure relations are usually local; i.e., they relate the higher-order moments at a point in space to other variables at the same point. However, the long collision length in fusion plasmas suggests the inclusion of non-local closure effects for the directions parallel to the magnetic field. The inclusion of kinetic physics, especially electron kinetic physics, on MHD time scales is an extremely challenging task, but significant progress has been made. CEMM will support research and development under which several models for these closures can be tested and validated.

### 3.2.3 Local closure relations in the general case

We will consider new improved general expressions for the closure parts that can be determined by local conditions. Specifically, the ion gyroviscous tensor in the general model should include the terms associated with the pressure anisotropy and the anisotropic heat flux gradients, in addition to the conventional Braginskii term. These have been recently derived [56] for arbitrary magnetic geometry. The corresponding diamagnetic part of the perpendicular heat fluxes was also derived.

For the parallel closure terms, namely the  $\Pi_{\parallel}$  tensor and the parallel heat fluxes  $\mathbf{q}_{\parallel}$ , one may try solving their local evolution equations. These are available in the literature in the zero-Larmor-radius limit [57, 58,68], and their finite-Larmor-radius versions have also been obtained [56]. The difficulty with this approach is that it increases the order of the system introducing new waves (ion and electron acoustic), and that it involves higher fluid moments that must eventually be determined by non-local kinetic relations. However it may be a worthwhile effort, since the results should be less sensitive to approximations made in the kinetically evaluated terms than those obtained with lower moment kinetic closures. This will be explored further.

### 3.2.4 Drift ordering approximations

The generalized drift model (last row of Table 3.2.1), a nonlinear generalization of the drift ordering, was based on simplified forms of the ion gyroviscous stress tensor [59-61] on a slower-than-MHD time scale. The resulting momentum equations were derived to emphasize favorable numerical characteristics as well. Work with M3D has shown that the model gives a good approximation to linear two-fluid mode stabilization and clearly shows the mechanism of the ion  $\omega_{*i}$  stabilization (for the 1/1 mode [55]). The 'parallel vorticity' part of the ion gyro-viscous stress was found to have relatively little effect on the linear or nonlinear mode in many cases. An important task will be to test the approximation made in the model against the more complete models being developed here. These tests will also be significant to evaluate analytical theories of instabilities in two-species systems, many of which are based on variants of the drift ordering.

### 3.2.5 Parallel integral kinetic closures

Non-local expressions for the dominant parallel closures, derived by balancing the parallel free streaming and pitch angle scattering terms in the drift kinetic equation, are integrals of the fluid variables along parallel particle trajectories. [62, 63] For example, the non-local form of the parallel component of the conductive heat flow is  $\mathbf{q}_{\parallel\alpha} = \int_{-\infty}^{\infty} dL' [T(L) - T(L')] K(L, L')$  where the non-local dependence on  $T$  is explicit and  $K(L, L')$  contains collisional and trapped particle information [64]. At low temperatures, where collision lengths are short,  $\mathbf{q}_{\parallel\alpha}$  reduces to the local, Braginskii-like form, while at high temperatures where the plasma is nearly collisionless,  $\mathbf{q}_{\parallel\alpha}$  captures Landau-damping and particle trapping physics. This kinetic closure has been successfully implemented and tested in the NIMROD code [11]

and is presently being applied in calculations of heat transport in neoclassical tearing mode and disruption simulations. A similar expression will be derived for the parallel stress tensor, but further analytic development, being pursued as part of this proposal, is needed to include the effects of particle trapping in toroidal geometry; i.e., the neoclassical effects.

### 3.2.6 Parallel local closures

Local forms for the neoclassical parallel stress tensors have been incorporated into both NIMROD [65] and M3D [3], i.e.  $\mathbf{B} \cdot \nabla \cdot \mathbf{\Pi}_i^{nc} = mn \langle B^2 \rangle \mu_i (V_{\theta i} / B_\theta)$ . The local forms are not rigorously derived, but are designed to reproduce in an MHD simulation the physics used in analytic derivations [66] which have successfully been used in explaining experimental observations [37-40]. M3D has also directly solved the anisotropic temperature equations for electrons and ions [67], for the average temperatures  $\bar{T}_j = \frac{1}{3} [T_{j\parallel} + 2T_{j\perp}]$  and  $\Delta T_j = [T_{j\parallel} - T_{j\perp}]$  using the collisionless MHD temperature evolution equations [68], adding a simple collision operator, and closing them with the anisotropic heat fluxes computed from the standard M3D models. These closures have the advantage of being easy to implement and are much less computationally intensive than any kinetic calculation. The evaluation of their validity is a big part of this proposal. Currently the simulation closures have only included poloidal flow damping. For large islands, a toroidal flow damping also occurs [69] which is important for large islands and resistive wall modes. Including and evaluating these effects will be important for the applications discussed in Sec. 3.1.

### 3.2.7 Hybrid kinetic closures

The energetic particle effects enter through the momentum equation via the energetic ion stress tensor:

$$mn \frac{d\mathbf{V}}{dt} = -\nabla p - \mathbf{J} \times \mathbf{B} - \nabla \cdot \mathbf{\Pi}_i - \nabla \cdot \mathbf{\Pi}_h$$

Here  $\mathbf{\Pi}_i$  and  $\mathbf{\Pi}_h$  are the stress tensors of the thermal ions and energetic ions respectively. In the present hybrid model implemented in M3D [3] (and now in NIMROD [62]) the thermal stress tensor is closed by the drift MHD or resistive MHD model and the energetic stress tensor is closed kinetically by using the drift-kinetic or gyrokinetic equation. In particular, the energetic particle stress tensor is represented in a CGL form  $\mathbf{\Pi}_h = P_\perp \mathbf{I} + (P_\parallel - P_\perp) \mathbf{b}\mathbf{b}$ , and is calculated from an ensemble of energetic particles. These simulation particles are followed in the self-consistent electromagnetic fields by using the drift-kinetic equations. Compared to other simplified models, this hybrid model is fully self-consistent. It takes into account both fluid nonlinearity and particle nonlinearity. It also treats full geometric effects.

In last CEMM proposal period, we have benchmarked the hybrid model of M3D against the kinetic-MHD stability code NOVA2 [43] and use the code to simulate beam ion-driven Alfvén modes in NSTX (see Sec. 2.1.7). We have also carried out initial applications of M3D to fast ion-driven modes in stellarators.

We plan to extend this model in several ways. First, the collision effects on alpha particles will be included by using a pitch angle scattering collision operator. The collisional effects are known to be important for nonlinear dynamics of alpha-driven Alfvén modes near their stability threshold. Second, we will include more complete FLR effects of energetic particles by retaining the off-diagonal terms in the energetic ion stress tensor. Third, we will include more complete FLR effects of thermal ions to second order in  $k_\perp \rho_i$ . This can be done by using a more general two fluid model or by using the gyrokinetic equation to calculate the thermal stress tensor. It is known that thermal ion FLR effects are essential for predicting the damping of TAEs. They are also important for the stability of the internal kink mode near the ideal stability threshold.

### 3.2.8 Approach to the development and validation of extended MHD models

We propose to perform the following tasks in order to develop, understand, validate, and implement extended MHD models for computational modeling of fusion plasmas:

- We will pursue the development of both drift-ordered and general models in our computational models, as discussed in Sec. 3.2.1. M3D already has implemented the drift model, and NIMROD is working toward implementation of a more general model (see Sec. 3.2.3) based on a complete Ohm's law and Braginskii gyro-viscosity. The output of the codes will be compared for test cases that are applicable to both tokamaks and other confinement concepts. In this way we will systematically evaluate the limitations of the drift model and the computational efficacy of the more general approach.
- We will evaluate various models for the neo-classical closure, as discussed in Sec. 3.2.6. This will involve the solution of model problems describing neo-classical island growth in slab geometry as well as the seeding and growth of neo-classical tearing modes in tokamak geometry. This latter will provide the ultimate validation by direct comparison with experimental data.
- We will continue the development of general parallel kinetic closures, as discussed in sections 3.2.5 and 3.2.7. The integral approach development will focus on implementing an analogous, non-local form for the parallel component of the viscous stresses,  $\Pi_{\parallel\alpha}$ . The previously implemented calculation of  $\mathbf{q}_{\parallel\alpha}$  (Sec. 3.2.5) will provide the coding framework for calculating  $\Pi_{\parallel\alpha}$ , which again entails integrating fluid quantities along parallel particle trajectories. Upon calculating  $\Pi_{\parallel e}$  throughout the plasma domain it is necessary to incorporate it into the fluid equations in an efficient, numerically stable fashion.

### 3.3 Proposed Code Development

Under previous SciDAC funding, both NIMROD and M3D have become mature as general-geometry simulation codes for resistive MHD with multiple time-scales. M3D treats the fast magneto-acoustic wave implicitly to avoid the most severe time step restrictions, and NIMROD uses a semi-implicit advance to also remove the constraints from sound and Alfvén waves—time steps remain limited by advection in both. While the advances made for MHD simulations have been significant, extended-MHD modeling can be far more challenging. The presence of dispersive waves in two-fluid numerical computations implies that information propagates faster as spatial resolution is increased. Developing an effective implicit (or semi-implicit) treatment of these modes requires constructing numerical operators that stabilize the normal modes described in Sec. 2.2.5 without affecting the accuracy of the higher-order responses. Alternatively, two-fluid computation can be accomplished efficiently using equations for the drift-order behavior [55], at the loss of some generality. During the next funding cycle, we will continue to develop algorithms for two-fluid simulation, using information provided by the modeling studies described in Sec. 3.2, and implement them in NIMROD and M3D, as needed. In this section, we describe the specific tasks required for this effort and other work aimed at improving spatial representations.

#### 3.3.1 Numerical Considerations for Two-fluid Models

The equations for general extended-MHD, along with several simpler models that are valid in certain parameter regimes, have been given in Section 3.2. With the exception of resistive MHD, the equations of these models contain wave-like phenomena that are characterized by dispersion relations of the form  $\omega \sim k^2$ . From numerical analysis and experience with semi-implicit methods for resistive MHD [71,72,1], we know that any implicit or semi-implicit methods developed for extended-MHD must not introduce artificial mode coupling. Propagation of fast waves is necessarily inaccurate when evolving stiff systems at large time-step, but this will not affect the accuracy of the important slow response if the

numerical algorithm respects the orthogonality of the normal modes. Using MHD as an example, the Laplacian operator can be used in a semi-implicit advance, because it slows the propagation of the fastest waves [73], but it strongly couples the normal modes and will affect accuracy if the time-step exceeds a small fraction of the global Alfvén time. In contrast, the ideal MHD force operator embodies the complete set of independent normal modes responses and when used as a semi-implicit operator, allows accurate computation at time steps that significantly exceed the global Alfvén time [1].

The dispersive modes described in Sec. 2.2.5 impose even more demanding requirements on implicit algorithms for extended-MHD. Ever-faster modes will be supported as spatial resolution is increased, so the global propagation time decreases. If the algorithm has artificial mode coupling, accuracy requirements will then likely require decreasing the time-step with increasing spatial resolution, so the promised gain from the implicit advance is effectively lost. On the other hand, if the implicit algorithm respects the orthogonality of all dispersive normal modes, the gain relative to that in resistive MHD is much more significant.

While the numerical simulation of two-fluid models in conditions with widely separated time-scales is in its infancy relative to computational MHD, it is a critical-path item for CEMM. We will therefore pursue different approaches to a point where they can be compared and evaluated with regard to what is most effective in production simulations. Among the different possibilities, the two-fluid M3D algorithm based on the drift ordering [55] is the most mature. The others are described in the following section.

### 3.3.2 Algorithm development for dispersive modes

In analogy to what has proven effective for MHD, we expect that the differential operators of the second-order (in time) wave equations for the dispersive modes will produce semi-implicit operators that avoid mode coupling. These considerations lead us to fourth-order spatial derivative operators, which have already proven some merit in this regard [74]. The three approaches that will be considered are:

- use an auxiliary variable to make a larger system with second-order spatial derivatives,
- formulate the operator as a filter on the drives, and
- use the fourth-order operator directly with finite elements that have  $C^1$  continuity.

The first approach has been implemented in NIMROD for the whistler wave during the first grant period of CEMM [75], and initial test results for waves in periodic homogeneous conditions indicate acceptable numerical dispersion and stability properties. The magnetic field is advanced in two sequential segments—one using the MHD electric fields and the other using the Hall electric fields, as recommended in Ref. [74]. Tests of accuracy in ever more realistic computations will continue through the rest of the first grant period. If the algorithm is successful for simulations with Hall physics, it will be applied for the other dispersive modes during the second grant period.

The time-split nature of the first approach leads to first-order temporal convergence [76] that may render application to high-performance fusion experiments impractical. In the second approach [77], the semi-implicit operator is recast to filter the source terms appearing in the energy and induction equations instead. Here, the exact energy integral is preserved by the semi-discrete (no time differencing) equations and the fourth-order differential operator appear through a sequence of steps that use symmetric second-order operators. The net result is an algorithm that stabilizes the whistler wave and the KAW and is second-order accurate in time. The implementation of this approach in NIMROD has begun under the first grant period. Developments for nonlinear effects will be implemented during the second grant period, and tests on real applications will be performed.

A third approach is based on the representation by  $C^1$  finite elements [24] which possess enough continuity to handle fourth order operators directly. This approach has been applied to the stream-function/potential representation of the velocity field used in M3D and has shown to be effective in



allowing large time steps without polluting the spectrum in model 2D problems. This is being currently evaluated for suitability in the full M3D code. This approach is discussed below in Sec. 3.3.4.

### 3.3.3 Linear solver development for the implicit two-fluid algorithms in NIMROD

While the matrices for the MHD part of the NIMROD advance are Hermitian, the two-fluid advances require the solution of non-Hermitian matrices. Initial development has focused on the semi-implicit advance for the dominant part of the stiffness arising from linear terms, and the resulting matrices are solved with the SuperLU sparse parallel solver library [78] implemented in collaboration with TOPS. However, stiffness arising from nonlinear two-fluid terms will lead to non-Hermitian matrices that couple toroidal harmonics, and it is not practical to generate the elements of the convolution matrices. Thus, matrix-free methods are required. A matrix-free conjugate gradient (CG) implementation has been successful for the nonlinear resistive MHD system when using global preconditioning that applies SuperLU solves of approximate 2D linear systems. We therefore plan to apply matrix-free generalized minimum residual (GMRES) software, suited for non-Hermitian matrices, with global preconditioning via SuperLU for the nonlinear two-fluid advance. Because the solution of these algebraic systems dominates the computational effort, optimization is critical. Accordingly, we will also investigate alternative preconditioners, such as multigrid approaches [79] for the matrix-free GMRES solve. These developments will also be applied for the semi-implicit treatment of non-local  $\Pi_{||e}$  discussed in Sec.

3.2.5.

### 3.3.4 Higher-order-of-continuity elements in M3D

The finite elements presently being used by both NIMROD and M3D are classified as  $C^0$  elements, meaning that the functions being solved for are continuous from element to element, but their first derivatives are not forced to be continuous. We have begun a study of a  $C^1$  element, known as the reduced quintic triangular finite element, and have found some significant advantages. The expansion used in the element will represent a complete quartic polynomial in two dimensions, and thus the error will be of order  $h^5$  if the solution is sufficiently smooth. The quintic terms are constrained to enforce  $C^1$  continuity across element boundaries, allowing their use with partial differential equations involving derivatives up to fourth order. There are only three unknowns per triangular element in the global problem, which leads to lower rank matrices when compared with other high-order methods with similar accuracy but lower order continuity. The preliminary study showed that the element can be applied effectively to anisotropic diffusion and the time-dependent MHD and extended MHD equations. [24]

The compact representation associated with this element as well as the fact that its  $C^1$  continuity allows equations up to 4<sup>th</sup> order to be represented without introducing auxiliary variables leads to a very efficient implicit system for the extended-MHD equations. A semi-implicit method based on the 2D compressible two-fluid MHD equations using the M3D variables has now been formulated and is being tested. The 2D matrices are being solved using SuperLU. This system will be implemented for the full 3D M3D equations, but it still remains an issue how to handle the implicit derivatives in the toroidal direction. The present plan is to use a GMRES iteration, with the 2D SuperLU serving as a pre-conditioner, but alternative techniques will be discussed with our SciDAC partners in TOPS.

### 3.3.5 Straight field line coordinates

As discussed in Sec.3.1.4, we will investigate high-n TAE/EPM modes in a fusion plasma. Since the wavelength of these modes is much longer parallel to the magnetic field than perpendicular to it, we plan to implement a field aligned mesh in the M3D code in order to more efficiently represent them. Field-aligned meshes in a general toroidal system are complicated by the periodicity requirements, but techniques for dealing with this for a triangular unstructured mesh as used in M3D have emerged. [80] We also expect that this new mesh will have better numerical stability properties since it will do a better

job in resolving the shear Alfvén wave in a single dimension. When this is implemented in the M3D partially implicit time advance, it should lead to a time step restriction several times larger than the current value.

### 3.4 Integration Activities

We plan to collaborate with another fusion SciDAC activity, the Electromagnetic Wave-Plasma Interaction proposal (D. Batchelor, PI), on the beginning of an integrated calculation of the effect of external wave heating and current drive on MHD instabilities. This activity is prototypical of that which would occur in one of the Focused Integration Initiatives (FIIs) called out by the Fusion Simulation Project report [81].

The integration of these two activities is conceptually straightforward. The externally driven electromagnetic waves are much higher frequency than the MHD activity, and so the extended-MHD codes NIMROD and M3D will provide a sequence of static 3D “equilibrium geometry files” to the wave propagation codes. These files will contain an accurate description of the instantaneous plasma properties and background electric and magnetic field structure. The wave propagation codes will use these geometry files to perform the wave propagation studies and will calculate local 3D momentum and energy source terms that will be fed back into the electron and ion equations in the extended-MHD codes. This process will repeat as time proceeds.

Though conceptually simple, there are a number of computational and physics modeling issues that need to be resolved by the two teams in order to make such an integrated calculation feasible and practical: How is the perturbed plasma distribution function calculated and shared by the two codes? How does the massive data transfer occur? Can we achieve concurrency with both the extended-MHD and wave-propagation codes running simultaneously on large numbers of parallel processors? We are currently investigating several software packages that can assist in addressing these and other integration issues, among them are: the Model Coupling Toolkit (MCT), the Distributed Data Broker (DDB), and the Common Component Architecture (CCA). We expect to partner with the appropriate computer science group to implement one or more of these in our integration demonstration.

Since these issues, and others like them, will need to be addressed by a large-scale integrated simulation eventually, we see this activity as a prototype of those that will be encountered in a full integrated simulation of a burning plasma. These integrated simulations will be used to provide more quantitative answers to the sawtooth destabilization and NTM stabilization simulations discussed above in sections 3.1.1 and 3.1.2. The “integration” questions we expect to answer in the initial phases of this activity are:

- How best do we calculate the RF modifications to the electron and ion distribution functions for use in the extended-MHD codes?
- What computational framework is best suited for this coupling activity?

Ultimately, the “bottom line” physics questions we are after are:

- What power level is required to stabilize the neoclassical tearing mode in ITER with ECH?
- What power level and frequencies are required for ICRH destabilization of the sawtooth in ITER to avoid “giant sawteeth”

### 3.5 Visualization and Data Management (SAPP Program)

The most popular form of simulation and analysis of M3D/NIMROD data is centered around a single user running the simulation and the same user visualizing and analyzing the results. We have been involved in two projects to aid in this analysis. Our first visualization project was to create a tool for the M3D team for common visualization/data analysis. The HDF5 format of data was chosen as the M3D output because it is binary, platform independent, has the concept of parallel IO, hyperslaving, etc. We are now in the process of creating a similar look-and-feel visualization package for the NIMROD visualization. In order to simplify the coding and to facilitate cross-code comparisons, we are using a single code base for both the M3D and NIMROD analysis and visualization packages. This then allows us to create a comparative visualization package for these codes, without greatly increasing the complexity of our project.

In our collaborative studies, we have found that data movement becomes very important. We have begun looking at various methods for real-time data streaming of MHD simulation data to collaborators. Our approach is based on the method described in [82], where we actually reduced the overhead of the simulations running on the supercomputer by threading and buffering the I/O layer. In order to enhance the collaborative nature of the CEMM team, we are currently working with the Logistical Networking SciDAC Team [83]. Our vision is to perform the simulations that produce the data on a supercomputer (such as NERSC or the ORNL X1) and have the output stream to the collaborators. As in [82], we will construct this such that the MHD codes will not have any additional overhead using the streaming routines. The flexibility in these routines, allows us to change the file format if necessary, and it allows us to send different portions of the simulation to different researchers in the CEMM team. This becomes very valuable when simulations start to generate 10's of GB's / simulation. The logistic network allows us to use the concept of depots to store this temporary data on various depots throughout the country.

To further enhance the collaborative nature of our project, we propose to build collaborative tools inside of our package. This involves transferring the "minimum" amount of data necessary to meet the needs of the collaborators. We propose to use the logistic network method of reading x-nodes to transfer data to the visualization package, and process information locally. Using low-level socket routines for communication, we can transmit the minimal information, such as rotation angles, or GUI interaction, to other collaborators.

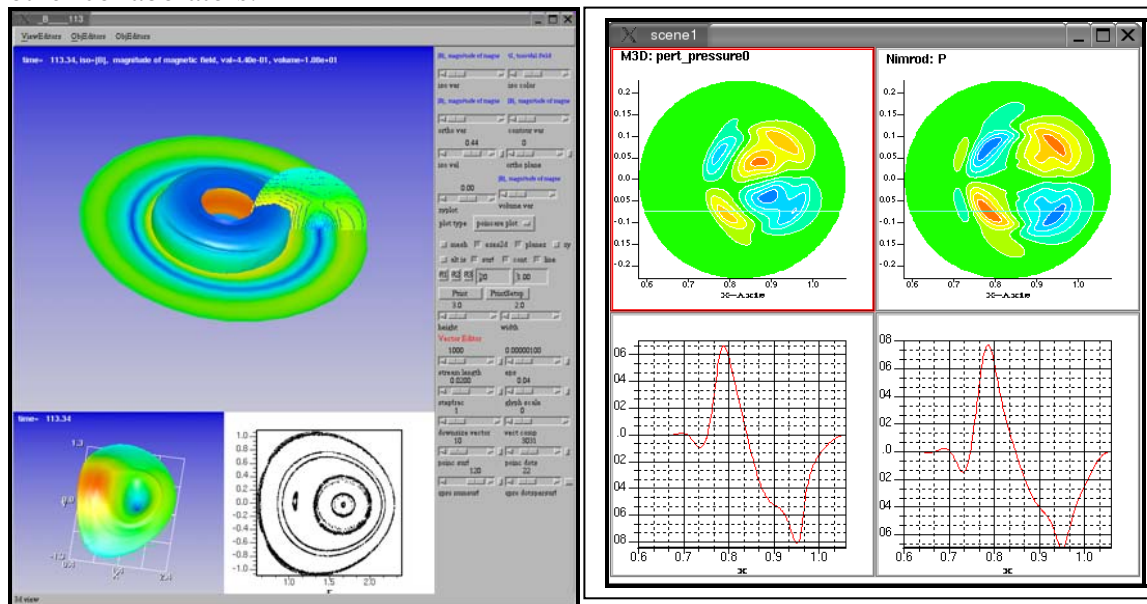


**Fig 3.5: Left shows sample screen dump of GUI for visually exploring data. Right shows application comparing results of NIMROD and M3D simulations.**

Our current visualization/analysis package is based on AVS/Express. Express was chosen because it is very stable, it runs on a wide range of platforms, and it is easy to develop code for users with a limited

amount of support. In order to support real-time-interactive visualization, we have integrated several of our analysis packages, such as a Poincare plot routine, into our visualization package. A sample screen dump is shown in the figure on the left, where we see that users are presented with a custom interface, and have the capability to print publication quality plots. Users can open many viewing windows of different functions from different simulations in one session. In a collaboration with NERSC, we are examining 3D MHD data visualization using Enight/Gold and using Paraview. Both of these systems allow for parallel processing of data. We feel that if the M3D/NIMROD data grows about two orders of magnitude larger, we will then require parallel data analysis and visualization, which these tools are equipped with.

In order to further investigate the data from the two codes, we have started to prepare an application which allows us to directly compare M3D and NIMROD data. Several new modules, including: coordinate transformations from M3D coordinates to NIMROD coordinates and phase shifting results will be created in the next phase of the proposal. The figure on the right shows a comparison between a M3D and NIMROD simulation. Here the user can analyze the data together to try to understand the differences between these two codes. For this proposal, we will improve and extend these systems as described in Sec. 3.7:

Visualizing magnetic and velocity data requires the visualization of 3D vector fields. Visualization of these fields is a difficult and time consuming task because of the large amounts of data and the computational expense of calculating streamlines, the most common visualization technique. To effectively visualize vector fields, key features must be detected. The points at which the vector field changes topologically are known as critical points (in three dimensions, there are critical points, lines and surfaces, but all are referred to here as critical points). Thus, effective visualization of vector fields lies in the effective visualization of critical points and nearby regions. We propose to investigate methods for detection, classification, tracking and visualizing critical points and the streamlines associated with them. New research in this area may be of value in visualizing vector phenomena in other disciplines.

### **3.6 Planning, management, and collaboration with other SciDAC projects**

The CEMM is a union and extension of two pre-existing teams built around the NIMROD and M3D codes. The internal management of these teams, involving group meetings and conference calls, has proven to be effective, and is preserved in the CEMM management. What we add through the union and extension is (1) 2-3 joint technical meetings per year held before the APS and Sherwood meetings, and (as called for) a special topical summer meeting, (2) the joint AMRMHD, Visualization, and model development activities, and (3) the code comparison activities. These later two categories have been jointly planned as part of the proposal process, and are monitored by the lead-PI. All deviations from the baseline plan are approved by the team members via an email and/or conference call discussion. The technical meetings and follow-up communications are the main form of information exchange.

In addition to our internal meetings, we will continue to reach out to the other SciDAC groups for collaborative activities. In particular: *TOPS* will continue to interact with us in improving the performance and parallel scaling of our linear solvers. *TSTT* will continue to interact with us and provide assistance in advanced meshing tools and in implementation of the high order  $C^I$  elements. *APDEC* will continue to collaborate with us on the further development and application of the Princeton/LBL AMRMHD code, with applications focusing on the simulation of pellet injection into burning plasmas. *Logistical Network* will work with us to set up data depots to facilitate collaborative graphics as described in Sec. 3.5. The *Wave-Particle Interaction SciDAC*, if renewed, will work with us to prototype a focused integration initiative (FII) as described in Sec. 3.2. The *Fusion Collaboratory* has expressed an interest in incorporating NIMROD and M3D into the fusion grid. In addition, *PERC* has chosen NIMROD as one of codes that they analyze in depth with regard to performance analysis, modeling, and optimization.

### 3.7: Timetable and Milestones

	Year 1	Year 2	Year 3
<b>Model development</b>	<ul style="list-style-type: none"> <li>Compare IGV stress in general ordering with drift 2-fluid model</li> </ul>	<ul style="list-style-type: none"> <li>Clarify 2-fluid effects in reconnection: islands and 1/1 mode</li> </ul>	<ul style="list-style-type: none"> <li>Compare two-fluid and non-local parallel closure for tokamak tearing-mode</li> </ul>
<b>M3D Code Development</b>	<ul style="list-style-type: none"> <li>Implement <math>C^1</math> elements in 2-fluid 2D form</li> <li>Add collision effects to fast ions</li> </ul>	<ul style="list-style-type: none"> <li>Extend <math>C^1</math> elements to full 2-fluid linear 3D simulation</li> <li>Field-aligned mesh and 2<sup>nd</sup> order FLR for thermal ions</li> </ul>	<ul style="list-style-type: none"> <li>Extend <math>C^1</math> elements to full 2-fluid non-linear 3D simulation</li> <li>Optimize matrix solves and time advance</li> </ul>
<b>NIMROD Code Development</b>	<ul style="list-style-type: none"> <li>Implement anisotropic ion stress (local operators)</li> <li>Semi-implicit algorithm for Hall term</li> <li>Upgrade hybrid option to high-order elements</li> </ul>	<ul style="list-style-type: none"> <li>Implement and test nonlocal stress closures and compare with local models</li> <li>Evaluate semi-implicit algorithms for full 2-fluid equations</li> </ul>	<ul style="list-style-type: none"> <li>Optimize semi-implicit algorithms for two-fluid terms</li> </ul>
<b>AMRMHD Code Development<sup>1</sup></b>	<ul style="list-style-type: none"> <li>Complete flux-surface grid AMR code for ideal MHD in tokamaks, including requisite mapped-grid versions of AMR hyperbolic solver</li> <li>Design and test 4<sup>th</sup>-order finite-volume solver for anisotropic diffusion</li> </ul>	<ul style="list-style-type: none"> <li>Complete initial implementation of 4<sup>th</sup> order anisotropic diffusion solver for AMR</li> <li>Complete flux-surface grid AMR code for resistive MHD</li> </ul>	<ul style="list-style-type: none"> <li>Design and test flux-tube coordinate version of 4<sup>th</sup> order solver for anisotropic diffusion</li> </ul>
<b>Visualization<sup>2</sup></b>	<ul style="list-style-type: none"> <li>Enhance the joint AVS-plotting package to allow viewing of all variables relevant to extended-MHD</li> <li>Develop comparative utilities to focus on differences for use in code-comparison studies</li> </ul>	<ul style="list-style-type: none"> <li>Develop streaming utilities to depots to facilitate rapid real time data transfer</li> <li>Integrate the Logistical Runtime System (Logistical networking software) into the visualization routines.</li> </ul>	<ul style="list-style-type: none"> <li>Integrate the magnetic island and other advanced viz tools into the visualization package.</li> <li>Develop AVS collaborative viz using Logistic network technology, and client-server based minimum information methods</li> </ul>
<b>Applications</b>	<ul style="list-style-type: none"> <li>Calculate 3D halo currents for a ITER disruption (M3D)</li> <li>Apply non-local parallel heat flow to NTMs and disruptions</li> <li>Sawtooth with 2-fluid model</li> <li>Investigate fundamental physics issues in instabilities induced by pellet injection with AMR code<sup>1</sup></li> <li>Begin discussions to integrate RF code with MHD code if applicable</li> </ul>	<ul style="list-style-type: none"> <li>Study toroidal flow damping due to error field</li> <li>Perform a burning-plasma sawtooth simulation with 2-fluid and energetic particle effects.</li> <li>High-n alpha-driven TAEs: linear stability</li> <li>Compare inside and outside pellet simulations with JET data (AMR)<sup>1</sup></li> </ul>	<ul style="list-style-type: none"> <li>Nonlinear resistive wall modes with flow damping in DIII-D and NSTX</li> <li>Tokamak tearing and NTM mode simulations</li> <li>ELM simulations</li> <li>High-n alpha-driven TAEs: nonlinear saturation and alpha particle transport</li> <li>Project pellet injection simulations to ITER(AMR)<sup>1</sup></li> </ul>

<sup>1</sup>AMR work is described in APDEC proposal; <sup>2</sup>Visualization work is to be funded by SAPP Program

### 3.8 Computing resource requirements

Essentially all the applications listed in Sec. 3.1 will be resource limited. The resources available determine the allowed resolution, which in turn determines what range of physical parameters can be realistically modeled. The CEMM projects used over 6,000,000 node-hours in FY2003, mostly at NERSC. These were in accounts (mp288, mp21, mp94, mp290, mp200, m127, and m275). In this and future years, we expect to use similar amounts and more at NERSC, as available. We are also beginning to work at ORNL, and look forward to production time on both the IBM-SP and the CRAY-X1 there. In addition, we are planning on contributing to the financing and making use of a 16 processor SGI Altix 350 which will be located at PPPL and will be used mainly for small jobs and for fast-turnaround debugging and model testing runs.

### 3.9 Summary

The work described here is aimed at developing powerful macroscopic simulation codes and using these on the most advanced computers available to contribute to the science base underlying proposed burning plasma tokamak experiments such as ITER. Many of the developments will also have more general applications beyond confined plasmas. The work scope also includes further developing and testing of the underlying extended-MHD model, formulating this in a way that can be used to perform practical computations, and applying this to the most critical burning plasma global stability problems. The proposal also includes an essential visualization component, an exploratory component with APDEC using the AMR technique, and a prototyping component involving code integration.

## IV. Subcontract or Consortium Arrangements

*The Princeton Plasma Physics Laboratory (PPPL)* is the lead institution for CEMM. The PPPL-specific work will concentrate on the M3D applications involving sawtooth and energetic particle modes, on M3D code improvements involving the higher order  $C^1$  elements, on the integration work with the Wave-Plasma SciDAC Center, on the Adaptive Mesh Refinement work (together with APDEC), and on developing advanced data transfer and graphics for all the codes.

*SAIC* will provide management for the NIMROD team, and will assist with management of CEMM.

They will derive and implement an implicit algorithm in NIMROD for the ion gyro-viscous stress, will contribute to simulations of major disruptions in advanced tokamaks, sawtooth driven islands and NTMs in ITER, linear and nonlinear studies of ELMs, and sawtooth dynamics in CDX-U and other tokamaks.

*University of Wisconsin* work-scope includes developments for the NIMROD code, application of new physical modeling capabilities to high-performance tokamak simulation, and collaboration that will help other CEMM groups be successful in their development and modeling efforts.

*Utah State University* will derive, apply, and evaluate non-local forms for the parallel heat flow and neoclassical parallel nonlocal stress in the NIMROD code.

*The University of Utah* will develop advanced tools for visualizing vector field topology of unique value to fusion extended-MHD simulations.

*TechX Corporation* will work with Eric Held of Utah State to compare local and nonlocal closures and use the results for local closure development, and will apply NIMROD to simulations of plasmas disruptions and the growth of tearing modes.

*The University of Colorado* will develop improved implicit algorithms for integrating the extended-MHD equations with the two-fluid dispersive terms present.

*The Massachusetts Institute of Technology* will be responsible for development and testing of the various extended-MHD models, proposing test problems to elucidate the physical effects included and missing in these models, and in carrying out the M3D tearing and neoclassical tearing mode calculations.

*New York University* will be responsible for the application of the M3D code to disruption modeling, resistive wall modes, and edge localized modes.

## Literature Cited:

- [1] C. R. Sovinec, A. H. Glasser, T. A. Gianakon, et al. "Nonlinear magnetohydrodynamics simulation using high-order finite elements", *J. Comp. Phys.*, **195**, 355 (2004)
- [2] C. R. Sovinec, T. A. Gianakon, E. D. Held, et al, "NIMROD: a computational laboratory for studying nonlinear fusion magnetohydrodynamics", *Phys. Plasmas*, **10**, 1727 (2003)
- [3] Park, W., Belova, E.V., Fu, G.Y., et al." Plasma simulation studies using multilevel physics models", *Phys. Plasmas*, **6**, 1796 (1999)
- [4] R. Samtaney, S.C. Jardin, P. Colella, and D. F. Martin, "3D Adaptive Mesh Refinement Simulations of Pellet Injection in Tokamaks", PPPL 3891 (to appear in *Comp. Phys. Comm.* 2004)
- [5] "National Energy Research Scientific Computing Center 2003 Annual Report", LBNL-54267, January 2004 , Lawrence Berkeley National Laboratory
- [6] B. C. Stratton, J. A. Breslau, R. V. Budny, et al, "The Role of Axisymmetric Reconnection Events in JET Discharges with Extreme Shear Reversal", *Plasma Phys. Control. Fusion*, **44**, 1127 (2002)
- [7] J. A. Breslau, S.C. Jardin, and W. Park, "Simulation Studies of the Role of Reconnection in the 'Current Hole' experiments in JET", *Phys. Plasmas*, **10**, 1665 (2003)
- [8] W. Park, J.A. Breslau, J. Chen, et al, "Current hole and snake in tokamaks and ST's, *Bull. Am. Phys. Soc.*, **48**, 283 (2003)
- [9] S. E. Kruger, D. D. Schnack, D. P. Brennan, T. A. Gianakon, and C. R. Sovinec, "Nonlinear MHD dynamics of tokamak plasmas on multiple time scales", submitted to *Nuclear Fusion*;
- [10] R. Samtaney, "Suppression of the Richtmyer-Meshkov Instability in the Presence of a Magnetic field", *Phys. Fluids*, **15**, L53-L56 (2003)
- [11] E.D. Held, J.D. Callen, C. C. Hegna, et al, "Nonlocal Closures for Plasma Fluid Simulations", to appear in *Physics of Plasmas*, May 2004
- [12] H. Strauss, G. Fu, W. Park, et al, "Nonlinear MHD and Energetic Particle Modes in Stellarators", IAEA-CN-94/TH/P2-12(19th IAEA Fusion Energy Conf. Lyon, France)
- [13] L.E. Sugiyama, H.R. Strauss, W. Park, G.Y. Fu, et al., "Two-fluid limits on stellarator performance: Explanation of three stellarator puzzles and comparison to axisymmetric plasmas," to be submitted to IAEA FEC 2004.
- [14] W. Park, J. Breslau, J. Chen, et al, "Nonlinear Simulation Studies of Tokamaks and STs", *Nuclear Fusion*, **43**, 483 (2003)



- [15] R. H. Cohen, H. L. Berk, B. I. Cohen, et al, “Theoretical investigation of field-line quality in a driven spheromak”, *Nuclear Fusion*, **43**, 1220 (2002)
- [16] G. A. Cone and C. R. Sovinec, “Controlled ramp-down of decaying spheromak plasmas,” *Bull. Am. Phys. Soc.* **48**, 152 (2003)
- [17] J. Breslau, W. Park, S. Jardin, et al.,” Resistive modes in CDX-U”, *Bul. Am. Phys. Soc.*, **48**, 281 (2003)
- [18] see <http://seesar.lbl.gov/anag/chombo>
- [19] P. Colella, “Multidimensional upwind methods for hyperbolic conservation laws”, *J. Comput. Phys.*, **87**,171 (1990)
- [20] R. Crockett, P. Colella, R. Fisher et al, “An unsplit cell-centered Godunov method for ideal MHD. Technical report, Physics Department, University of California, 2003, submitted to *Journal of Computational Physics*
- [21] S. K. Godunov. “A symmetric form for the equations of magnetohydrodynamics”, *Numerical Methods for the Mechanics of Continuous Media*, **3**, 26, (1995)
- [22] K. G. Powell, P.L. Roe, T. J. Linde, et al, “A solution-adaptive upwind scheme for ideal magnetohydrodynamics”, *J. Comput. Phys.*, **154**, 284 (1999)
- [23] M. Minion. “On the stability of Godunov-projection methods for incompressible flow”, *J. Comput Phys*, **123**, 435 (1996)
- [24] S. C. Jardin, “A triangular Finite Element with First-Derivative Continuity Applied to Fusion MHD Applications”, PPPL-3921 Princeton Plasma Physics Laboratory, Submitted to *J. Comp. Phys.* (2004) (also available on the CEMM web site <http://w3.pppl.gov/CEMM> on the “project page”.
- [25] T. H. Stix, *Waves in Plasmas*, AIP Press, New York, (1992)
- [26] S.I. Braginskii, “Transport processes in a plasma,” in *Reviews of Plasma Physics*, M.A. Leontovich (ed.), (Consultants Bureau, New York). (1965)
- [27] <http://w3.pppl.gov/rib/repositories/NTCC/catalog/Asset/grin.html>; Also H.R. Strauss, A. Pletzer, W. Park, et al., “MHD simulations with resistive wall and magnetic separatrix”, available on the <http://w3.pppl.gov/CEMM> web site on the “project page”
- [28] J. A. Breslau and S. C. Jardin, “A parallel algorithm for global magnetic reconnection studies”, *Comp. Phys. Comm.*, **151**, 8 (2003);

- [29] J. A. Breslau and S. C. Jardin, "Global Extended MHD Studies of Fast Magnetic Reconnection", *Phys. Plasmas*, **10**, 1291 (2003)
- [30] J. Birn, J.F. Drake, M.A. Shay, et al, "Geospace Environmental Modeling (GEM) Magnetic reconnection challenge, *Geophys. Res. Space*, **106**, 3715 (2001).
- [31] N. Sauthoff, G. Navratil, R. Bangerter, "Snowmass 2002: The fusion Energy Sciences Summer Study", PPPL-3665 (July 2002)
- [32] D.J. Campbell, D.F. Start, J.A. Wesson, et al, "Stabilization of sawteeth with additional heating in the JET tokamak", *Phys. Rev. Lett.*, **60**, 2148 (1988)
- [33] L-G. Ericsson, M. Mantsinen, D. Borba, et al, "Evidence for a wave-induced particle pinch in the presence of toroidally asymmetric ICRF waves"., *Phys. Rev. Lett.*, **81**, 1231 (1998)
- [34] C. Angioni, A. Pochelon, N Gorelenkov, et al., "Neutral beam stabilization of sawtooth oscillations in JET", *Plasma Phys. and Control. Fusion*, **44**, 205 (2002)
- [35] F. Porcelli, "Fast particle stabilization", *Plasma Phys. and Control. Fusion*, **33**, 1601 (1991).
- [36] J.W. Van Dam, M.N. Rosenbluth, Y.C. Lee, et al., "A generalized kinetic-energy principle" *Phys. Fluids*, **25**, 1349 (1982).
- [37] R.J. LaHaye, L.L. Lao, E. J. Strait, et.al. "High beta tokamak operation in DIII-D limited at low density collisionality by resistive tearing modes", *Nuclear Fusion*, **37**, 397 (1997)
- [38] Z. Chang, J.D. Callen, et al. "Observation on nonlinear neoclassical pressure-gradient-driven tearing modes in TFTR", *Phys. Rev. Lett.*, **74** 4663 (1995)
- [39] D.A. Gates, B. Loyd, A. Morris, et al, "Neoclassical islands on COMPASS-D" , *Nucl. Fusion*, **37**, 1593 (1997)
- [40] H. Zohm G. Gantenbein, A. Gude, et.al. "Neoclassical tearing modes and their stabilization by electron cyclotron current drive in ASDEX Upgrade" *Phys. Plasmas*, **8**, 2009 (2001)
- [41] D. P. Brennan, et al, "A Mechanism for Tearing Mode Onset Near Ideal Stability Boundaries", *Phys. Plasmas*, **10**, 1643 (2003);
- [42] A. M. Garofalo, T. H. Jensen, and E. J. Strait, " Analysis of stable resistive wall modes in a rotating plasma", *Phys. Plasmas*, **10**, 4776 (2003).
- [43] N.N. Gorelenkov, private communications, 2003.
- [44] P.B. Snyder, H.R. Wilson, et al., "Edge Localized Modes and the Pedestal: A Model Based on Peeling-Ballooning Modes," *Phys. Plasmas* **9** (2002) 2037

- [45] P.B. Snyder, H.R. Wilson et al., "ELMs and Constraints on the H-Mode Pedestal: Peeling-Ballooning Stability Calculation and Comparison to Experiment," Nucl. Fusion, **44**, 320 (2004)
- [46] H.R. Wilson, P.B. Snyder, R.L. Miller, and G.T.A. Huysmans, "Numerical Studies of Edge Localized Instabilities in Tokamaks," Phys. Plasmas, **9**, 1277 (2002)
- [47] A. Pankin, G. Bateman, A. Kritz, "Alcator C-mod predictive modeling", Phys. Plasmas, **8**, 4403 (2001)
- [48] Pomphrey, N., Bialek, J., Park, W., "Modelling of the toroidal asymmetry of poloidal halo currents in conducting structures", Nuclear Fusion, **38**, 449 (1998).
- [49] W. Park, E. Fredrickson, A. Janos, et al, "High-beta Disruption in Tokamaks", Phys. Rev. Lett., **75**, 1763 (1995)
- [50] S.C. Jardin, G.L. Schmidt, E.D. Fredrickson, et al, "A fast shutdown technique for large tokamaks", Nucl. Fusion, **40**, 923 (2000)
- [51] K. V. Roberts and J. B. Taylor, "Magnetohydrodynamic equations for finite larmor radius", Phys. Rev. Lett., **8**, 197 (1962).
- [52] M. N. Rosenbluth and A. Simon, "Finite Larmor radius equations with nonuniform electric fields and velocities", Phys. Fluids, **8**, 1300 (1965)
- [53] R. D. Hazeltine and J. D. Meiss, *Plasma Confinement*, Addison-Wesley, Redwood City, CA, 1992.
- [54] J. D. Callen, "Moment Approach to Collisional Plasma Transport", unpublished notes, 1986.
- [55] L. Sugiyama and W. Park, "A nonlinear two-fluid model for toroidal plasmas", Phys. Plasmas, **7**, 4644 (2000)
- [56] J. J. Ramos, "General fluid theory of collisionless magnetized plasmas", Bull. Am Phys Soc, **48**, 130 (2003)
- [57] G.L. Chew, M.L. Goldberger, and F.E. Low, "The Boltzmann equation and the one-fluid hydromagnetic equations in the absence of particle collisions," Proc. R. Soc. Lond. A, **236**, 112 (1956)
- [58] J. Ramos, "Dynamic evolution of the heat fluxes in a collisionless magnetized plasma" Phys. Plasmas, **10**, 3601 (2003)

- [59] R.D. Hazeltine and J.D. Meiss, “‘Shear’ Alfvén dynamics of toroidally confined plasmas,” Phys. Rep., **121**, 1 (1985)
- [60] Z. Chang and J.D. Callen, “Generalized gyroviscous force and its effect on the momentum balance equation”, Phys Fluids B, **4**, 1766 (1992)
- [61] E.V. Belova, “Nonlinear gyroviscous force in a collisionless plasma”, Phys. Plasmas, **8**, 3936 (2001).
- [62] E. D. Held, J. D. Callen, C. C. Hegna, “Conductive electron heat flow along an inhomogeneous magnetic field”, Phys. Plasmas, **10**, 3933 (2003).
- [63] E. D. Held, “Unified form for parallel ion viscous stress in magnetized plasmas”, Phys. Plasmas, **10**, 4708 (2003).
- [64] E.D. Held, J.D. Callen, C.C. Hegna, and C.R. Sovinec, “Conductive electron heat flow along magnetic field lines”, Physics of Plasmas, **8**, 1171 (2001)
- [65] T. A. Gianakon, S. E. Kruger, and C. C. Hegna, “Heuristic closures for numerical simulations of neoclassical tearing modes”, Phys. Plasmas, **9**, 536 (2002);
- [66] C.C. Hegna, “Nonlinear dynamics of pressure driven magnetic islands in low aspect ratio tokamaks”, Phys. Plasmas, **6**, 3980 (1999)
- [67] L.E. Sugiyama, W. Park, H.R. Strauss, S.R. Hudson, D. Stutman, and X-Z. Tang, “Studies of spherical tori, stellarators and anisotropic pressure with the M3D code,” Nucl. Fusion, **41**, 739 (2001).
- [68] P.B. Snyder, G.H. Hammett, W. Dorland, “Landau fluid models of collisionless magnetohydrodynamics”, Phys. Plasmas, **4**, 3974 (1997).
- [69] K.C. Shaing, “Plasma flow and confinement in the vicinity of a rotating island in collisional tokamak plasma”. Phys. Plasmas, **11**, 625 (2004)
- [70] C. C. Kim, C. R. Sovinec, S. E. Parker, and the NIMROD Team, “Hybrid Kinetic-MHD Simulations in General Geometry,” Comput. Phys. Commun., in press.
- [71] D.S. Harned and D.D. Schnack, “Semiimplicit method for long-time scale magnetohydrodynamic computations in 3 dimensions” J. Comp. Phys., **65**, 57 (1986)
- [72] K. Lerbinger and J. F. Luciani, “A new semiimplicit method for MHD computations,” J. Comput. Phys, **97**, 444 (1991)
- [73] D. D. Schnack, D. C. Barnes, Z. Mikić, D. S. Harned, and E. J. Caramana, “Semiimplicit magnetohydrodynamic calculations” J. Comput. Phys., **70**, 330 (1987)
- [74] D. S. Harned and Z. Mikić, “Accurate semi-implicit treatment of the hall-effect in magnetohydrodynamic computations”, J. Comput. Phys., **83**, 1 (1989)

- [75] H. Tian and C. R. Sovinec, “Semi-implicit treatment of the Hall effect in NIMROD simulations,” *Bull. Am Phys Soc.*, **48** p. 115 (2003)
- [76] D. A. Knoll, L. Chacon, L.G. Margolin, “On balanced approximations for time integration of multiple time scale systems”, *J. Comput. Phys.*, **185** 583 (2003)
- [77] D. C. Barnes, private communication (2003)
- [78] J. W. Demmel, J. R. Gilbert, Y.S. Li, “SuperLU Users Guide”, U.C. Berkeley, October 2003
- [79] J. Xu and J. Qin, “Some remarks on a multigrid preconditioner”, *SIAM J. Sci. Comput.*, **15**, 172 (1994)
- [80] Z. Lin, Private communication
- [81] J. Dahlburg, J. Coronas, D. Batchelor, et al, “Fusion Simulation Project: Integrated simulation and optimization of magnetic fusion systems”, *J. Fusion. Energy*, **20**., 135 (2001)
- [82] S. Klasky, S. Ethier, D. McCune et. al. , “Grid-Based Parallel Data Streaming implemented for the Gyrokinetic Toroidal Code”, *Proceedings of the ACM/IEEE SC2003 Conference*, (2003).
- [83] Beck, et al., “Algorithms for High Performance, Wide-area Distributed File Downloads”, *Parallel Processing Letters*, 207(2003)
- [84] W. Park, D. Monticello, H. Strauss, et al., “3-dimensional stellarator equilibrium as an ohmic steady-state”, *Phys. Fluids*, **29**, 1171 (1986)

**Budgets and Budget Explanation:**

(per year, in \$1000)

**Scientific Application:**

SAIC	\$155	(Schnack, Pankin)
UW	\$140	(Sovinec, Kim, Student)
USU	\$ 60	(Held, student)
TechX	\$ 60	(Kruger)
CU	\$ 60	(Barnes)
PPPL	\$205	year 1, \$255 years 2/3 ( Park, Breslau, Fu, Jardin, Chen)
NYU	\$140	(Strauss + postdoc)
MIT	\$130	(Sugiyama(\$70) and Ramos (\$60))
Computer	\$ 50	year 1 only (part of an SGI Altix 350)
<hr/>		
TOTAL	\$1000k	

**Scientific Application Partnership Program:**

PPPL	\$160k	Partnership with APDEC on AMR:	\$90k (Samtaney)
		Advanced Visualization and Data Transfer	\$70k (Klasky)
Univ. Utah	\$ 40k	Advanced MHD Visualization	\$ 40k (Sanderson)
<hr/>			
TOTAL	\$200k		

## Biographical Sketches:

**Dan Barnes** received a Ph. D. in Applied Mathematics in 1975 from Purdue University. He has held a number of positions at LANL, IFS, and SAIC, including Group Leader of the Magnetic Fusion Theory Group at LANL from 1989 to 1993. He is presently Principal Scientist at Coronado Consulting in Santa Fe, NM, and Senior Research Scientist at the Center for Integrated Plasma Studies at the University of Colorado. He is an internationally recognized expert in the fields of plasma physics and computational physics. He has over 23 years experience in the solution of complex, nonlinear problems involving both fluid and kinetic descriptions of plasmas and other physical systems. He has authored or co-authored over 75 refereed papers in this field, and has given numerous invited papers on this and related subjects. His present research interests include kinetic and fluid simulations of magnetically-confined plasmas, compact fusion systems based on electrostatic confinement of charge neutral and non-neutral plasmas, and reduced models for laser-plasma interaction modeling.

**James D. Callen** is Donald W. Kerst Professor Emeritus (as of July 2003) of Engineering Physics and Physics at the University of Wisconsin. He founded (in 1988) and directed the university's Center for Plasma Theory and Computation. He is a co-author of two books and over 160 refereed publications, and has served on a number of Department of Energy review panels and fusion plasma physics journal editorial boards. He chaired the APS Division of Plasma Physics in 1996. His current plasma research includes: developing fluid/kinetic hybrid descriptions of magnetically confined plasmas; studying the macroscopic phenomenology caused by MHD tearing-type modes and their effects on plasma behavior and confinement in tokamaks; and attempts to correlate the theory of collective macroscopic instabilities with experimental results from tokamaks, stellarators, and reversed-field pinches. He received his PhD in 1968 in Nuclear Engineering (applied plasma physics) from the Massachusetts Institute of Technology, held an NSF postdoctoral fellowship at the Institute for Advanced Study (Princeton) in 1968-69, taught at MIT from 1969-1972, was a research staff member and Theory Section Leader at ORNL 1972-1979, and has been at UW-Madison since 1979. He is a fellow of the American Physical Society and the American Nuclear Society, has been awarded a Guggenheim Fellowship and is a member of the National Academy of Engineering.

**Guo-yong Fu** is a Principal Research Physicist at the Princeton University Plasma Physics Laboratory. His main research area includes energetic particle physics and MHD stability of toroidal plasmas. He has authored over 60 refereed publications in plasma physics. He received a Ph.D in physics from The University of Texas at Austin in 1988. After a one year postdoctoral fellowship at the Institute of Fusion Studies in Austin, Texas, He worked on MHD stability in stellarators at the center for plasma physics research (CRPP) in Lausanne, Switzerland from 1989 to 1991. He joined PPPL in 1992. He is currently active in area of MHD stability in compact stellarators and nonlinear dynamics of energetic particle-driven fishbone and TAE. He won the Kaul Foundation Prize for excellence in plasma physics research in 1998.

**Chris C. Hegna** is an Associate Professor of Engineering Physics at the University of Wisconsin. His primary field of research is theoretical plasma physics with an emphasis on the area of plasma confinement using magnetic fields. He is the acting director of the University's Center for Plasma Theory and Computation. He is the author or co-author of over 70 refereed publications. Hegna's current research includes; the role of macroscopic instabilities in high temperature plasmas; nonideal and nonlinear magnetohydrodynamic instabilities; kinetic theory modifications to fluid-like descriptions of plasmas; plasma dynamics in non-symmetric magnetic systems; the role of magnetic geometry, symmetry and topology on plasma instabilities, turbulence and transport properties; self-organization properties of plasmas; anomalous current and momentum transport; magnetic reconnection in laboratory and astrophysical plasmas and dynamo processes. He received his PhD in Applied Physics from Columbia



University in 1989 and has been employed at the National Institute for Fusion Science (Nagoya, Japan), UKAEA Technologies, Culham Laboratory (Abingdon, England) and Columbia University working at the Princeton Plasma Physics Laboratory. He is a fellow of the American Physical Society.

**Eric D. Held** is an assistant professor of physics at Utah State University (USU), where he leads a fusion theory group which is contributing to the U. S. fusion effort both from an analytical and a numerical perspective. Dr. Held is an expert on the analytical derivation and numerical implementation of general closure relations for nearly collisionless plasmas. He has extensive experience developing and applying the plasma fluid code NIMROD in studies of parallel transport in high-performance fusion plasmas. Dr. Held was the recipient of the DOE Computational Science Graduate Fellowship as well as a DOE Fusion Energy Postdoctoral Fellowship. More recently, Dr. Held has been supported by the DOE Junior Faculty in Plasma Physics Award along with various other fusion theory grants.

**Stephen C. Jardin** is a Principal Research Physicist at the Princeton University Plasma Physics Laboratory. He is presently Co-Head of the Computational Plasma Physics Group at PPPL, Head of the Next Step Options Physics, and Theory Department MHD Coordinator. He has been Lecturer with Rank of Professor in the Princeton University Astrophysics Department since 1986. He holds a BS in Engineering Physics from the University of California, a MS (Physics) and MS (Nuclear Engineering) from MIT, and a PhD in Astrophysics from Princeton University (1976). He was the primary developer of several widely used MHD equilibrium, stability, and transport codes including the Tokamak Simulation Code (TSC). He holds 4 US patents, has had over 150 refereed publications in plasma physics, and has supervised 6 Princeton University PhD students. He is a member of Phi Beta Kappa and a Fellow of the American Physical Society. He has held key positions in several fusion device design teams including those for S-1, PBX-M, CIT, BPX, and TPX. He was the ARIES Physics leader from 1992-2000 and is presently a U.S. representative on the International Tokamak Physics Activity (ITPA) group on MHD, Plasma Control, and Disruptions. He is presently a member of the NERSC Executive Committee Users Group and is Chair of the NERSC Program Advisory Committee and was chair of the National Transport Code Collaboration (NTCC) Program Advisory Committee. He has served on recent FESAC subcommittees on the Integrated Simulation and Modeling of Fusion Systems and to review the Inertial Fusion Energy program.

**Christopher R. Johnson** is a Distinguished Professor and Director School of Computing as well as the Director of the Scientific Computing and Imaging Institute at the University of Utah. He has been active in research in the area of scientific computing, particularly in computational steering, inverse and imaging problems, problem solving environments, and scientific visualization. He has authored or coauthored over 100 refereed publications in these areas.

**Scott A. Klasky** is part of the Computational Plasma Physics Group at the Princeton University Plasma Physics Laboratory. He is currently head of the visualization subgroup of CPPG. He holds a BS in Physics from Drexel University, and a PhD in Physics from the University of Texas at Austin (1994). After one year of a postdoctoral fellowship at the center of relativity at Austin, Texas, he became a senior research computational scientist at the Northeast Parallel Architecture Center at Syracuse University. At NPAC, he developed a fully collaborative visualization system (SciVis), which later evolved into the National Fusion Collaboratory, Elvis, system. He was the lead designer of two display walls used at PPPL, and develops novel visualization software for researchers at PPPL. More recently he has been working with high speed data streaming, and grid computing.

**Scott Kruger** received his doctorate at the University of Wisconsin-Madison in 1999 under the supervision of Prof. J.D. Callen and C.C. Hegna. After his doctorate, he joined Science Applications

International Corporation. In January 2004, he joined Tech-X Corporation in Boulder, Colorado. Dr. Kruger is a computational plasma physicist with extensive experience in analytic development of fluid models, and the application of those models in numerical simulations, especially application of massively-parallel initial-value simulations of tokamak plasmas at the DIII-D National Fusion Facility. As a lead developer of the NIMROD code, Dr. Kruger has extensive experience in software design and development. His current research interests include simulations of disruption events in tokamak plasmas, improved fluid modeling, and topological feature extraction from large datasets for visualization.

**Wonchull Park** is a Principal Research Physicist at the Princeton University Plasma Physics Laboratory. He has a Ph. D from Columbia University, and is a Fellow of American Physical Society. His primary field of research is 3D numerical simulation studies of plasmas, using multilevel physics models, MHD, Two-fluids, and various Particle/Fluid hybrid models. He has authored or coauthored over 100 refereed publications in plasma physics

**Scott E. Parker** is an Associate Professor in the Department of Physics at the University of Colorado, Boulder. His research interests are in large-scale kinetic simulation of low-frequency plasma physics with 24 refereed publications in this area. He received his B.S. in Nuclear Engineering and Mathematics from the University of Wisconsin, Madison in 1985 and his Ph.D. in Engineering Science from the University of California, Berkeley in 1990. From 1990-1996 he was a Staff Research Physicist in the Theoretical Division at the Princeton Plasma Physics Laboratory. He received the DOE Junior Faculty Development Award in 1997, a DOE Fusion Postdoctoral Fellowship in 1990, a Kaiser Engineers Quadrex Fellowship and a University of California Regents Fellowship in 1985. In 1997 he was leader of the Cyclone Team, a DOE initiative to study the physics basis of transport predictions for ITER.

**Jesus Ramos** a Principal Research Scientist at the Plasma Science and Fusion Center of the Massachusetts Institute of Technology. He has a Ph.D. in Physics from the "Universidad Complutense" of Madrid, Spain. He has made extensive contributions to the magnetohydrodynamic theory of fusion plasmas and has participated in the design teams of Alcator C-Mod, CIT, ARIES, TPX and ITER. He has authored or co-authored 56 refereed publications.

**Allen R. Sanderson** is a senior staff scientist at the Scientific Computing and Imaging Institute, the University of Utah. He has been in the computer graphics and visualization field in both academia and industry since 1981, and received his Ph.D. in Computer Science from the University of Utah in 1996. His recent industrial work included co-leading the development of software known as RapidSite for modeling visualization of land development. During his first stay in academia he conducted and published research in the field of medical image analysis. Since his return to academia he has been part executive committee guiding the scientific computation and visualization package SCIRun. Currently he is conducting research on visualizing error and uncertainty.

**Ravi Samtaney** is a Computational Scientist in the Computational Plasma Physics Group at Princeton Plasma Physics Laboratory, Princeton University. He received a PhD in Mechanical and Aerospace Engineering from Rutgers University in 1994 following which he was a post-doc at Caltech in applied mathematics and aeronautics. His professional experience includes working at NASA Ames as a research scientist, and at Caltech as a research faculty. His expertise includes numerical analysis, and high performance computing. At PPPL, he is working on adaptive mesh refinement methods for MHD relevant to fusion.

**Dalton Schnack** is a computational physicist with over 30 years experience in the analytic and numerical solution of nonlinear, multidimensional problems in hydrodynamics and magnetohydrodynamics (MHD). He has authored or co-authored many papers in the fields of linear and nonlinear resistive MHD, and

computational methods related to such problems. He has extensive experience in the supercomputing environment. He is actively involved in studying the nonlinear MHD properties magnetic fusion experiments and the solar corona, and in the highly nonlinear (turbulent) properties of the Navier-Stokes and MHD equations. After receiving his B.S., Dr. Schnack worked for over seven years (1967-1973) for the Pratt and Whitney Division of United Technologies Corporation as a Senior Scientific Programmer/Analyst. There he worked on computational problems of steady flow in nozzles and supersonic exhaust jets, and the performance of axisymmetric compressors. During this time he completed work on an M.S. in physics, which included a thesis on ultrashort optical pulse propagation. Dr. Schnack did his doctoral research at Lawrence Livermore Laboratory under Prof. John Killeen where he began his interest in nonlinear MHD processes in fusion plasmas. After graduation he served as a staff physicist in the computational physics group at the National Magnetic Fusion Energy (MFE) Computer Center, a supercomputer network funded by the Department of Energy. In 1980 he joined the fusion theory group at Los Alamos National Laboratory where he worked on problems relevant to the reversed-field pinch and compact torus experiments. In July 1982 Dr. Schnack joined the Applied Plasma Physics and Technology Division of SAIC, and in 1996 was appointed Director of the Center for Energy and Space Science. He is presently Principal Investigator for two grants with the U. S. Department of Energy. He is actively involved in research related to the nonlinear fluid dynamics of advanced magnetic fusion devices, and the nonlinear properties of the MHD equations. Dr. Schnack is a member of Phi Kappa Phi, national scholastic honor society, and is a Fellow of the American Physical Society. He is also a member of the American Geophysical Union and the Solar Physics Division of the American Astronomical Society. He has been an active participant in the functions of the international fusion program for many years. Dr. Schnack has co-authored over 70 refereed publications, and 1 book.

**Carl R. Sovinec** has been an Assistant Professor of Engineering Physics at the University of Wisconsin-Madison since June, 2001. His research interests lie in computational plasma physics and magnetohydrodynamics and in numerical methods for solving partial differential equations. He received his BS from the United States Air Force Academy in 1985, an MS in Nuclear Engineering from the University of Washington in 1987, and a PhD in Plasma Physics from the University of Wisconsin-Madison in 1995. He served as a commissioned officer in the regular Air Force from 1985-1991, including four years as a research officer at the Phillips Laboratory in Albuquerque, NM. As a postdoctoral research associate and staff scientist at Los Alamos National Laboratory over the period of 1995-2001, he authored a large fraction of the NIMROD physics kernel.

**Hank Strauss** is a Research Professor in the Magnetofluid Dynamics Division of the Courant Institute of Mathematical Sciences, New York University. He has a PhD from the University of Texas. He is a fellow of the American Physical Society. He has worked in many areas of theoretical and computational plasma physics, particularly in magnetohydrodynamics. For the last several years, he has been highly involved in the M3D project.

**Linda E. Sugiyama** is a principal research scientist in the Research Laboratory of Electronics at the Massachusetts Institute of Technology. She has worked in many areas of the theory and numerical simulation of magnetically confined plasmas, including equilibrium, stability, transport, auxiliary heating, and nonlinear simulation. She first proposed and, with W. Park, developed the two-fluid MH3D-T code for axisymmetric confined plasmas, based on the existing MH3D MHD nonlinear code developed at PPPL. These codes formed the basis of the M3D project. She received a B.S. from the University of Wisconsin in 1975 and a Ph.D in Applied Mathematics from the Massachusetts Institute of Technology in 1980. Since then, she has worked at MIT, with brief sojourns at other institutions.

## **Description of Facilities and Resources**

Princeton Plasma Physics Laboratory (PPPL) is situated on the Forrestal Campus of Princeton University. The PPPL Theory and Computational Plasma Physics Divisions are a national resource for the plasma physics community. The laboratory maintains an open UNIX computer system, including a tiled display wall for high resolution visualization, and a suite of fully-equipped visitor offices.

The PPPL UNIX cluster contains within it a 128 processor 1.7 GHz 2 Gbyte RAM cluster with fast interconnects. PPPL is connected via an OC3 ESNET connection to NERSC and the other fusion facilities.

The CEMM is a fully distributed Center, and all participants have access to the PPPL computer facilities, to NERSC, to the ORNL computers, and to their own local computer facilities.

## Appendix 1: Description of NIMROD, M3D, and the Princeton/LBL AMRMHD code

The NIMROD code solves the nonlinear time-dependent extended-MHD equations with numerical methods that excel for extremely stiff and anisotropic systems. To address the multiple time-scales of nearly dissipation-free high-temperature plasmas, fluid moments and electromagnetic fields are advanced in time with a semi-implicit approach.[71] The complete linear ideal-MHD energy integral is used as the semi-implicit operator[72] to preclude artificial coupling of normal modes at large time-step,[73] and integration is based on the symplectic leap-frog scheme to avoid numerical dissipation. The spatial domain is represented with two-dimensional finite elements for the arbitrarily shaped poloidal plane and finite Fourier series for the toroidal direction. Lagrange polynomials of arbitrary degree serve as the basis functions for the finite elements, and production simulations are typically run with bicubic or biquartic elements (fourth- or fifth-order accurate, respectively) to resolve the extreme anisotropies in magnetized plasmas.[1] For parallel computations, the three-dimensional domain is divided into blocks of finite elements and layers of Fourier components. All communication (both point-to-point and collective) is accomplished with routines in the MPI library [<http://www.mpi-forum.org>]. The non-local effects of free-streaming plasma particles are modeled by accumulating kinetic contributions to fluid-closure terms along characteristics of the drift-kinetic equation, which is solved in the basis of the pitch-angle scattering operator.[62,63] For modeling fast-particle effects on macroscopic modes, a simulation-particle-based approach is being adapted from M3D for NIMROD's high-order finite elements.[70] The NIMROD code runs on a variety of hardware platforms from laptops with Linux or the Mac OSX operating system to massively parallel architectures with distributed memory. The source code for NIMROD has been publicly available for more than five years, and information for its use and modification is provided on the website <http://nimrodteam.org>.

The M3D code [3] (or multilevel 3D) is a massively parallel nonlinear 3D extended MHD code that makes no assumptions regarding the axisymmetry of the boundaries so that it is equally applicable to stellarators and to tokamaks. M3D consists of two parts, a mesh module and a physics module. The mesh module contains the grid, implementation of differential and integral operators, I/O, and inter-processor communication. The physics module includes resistive MHD, two-fluid, hybrid, and fully kinetic particles. M3D uses a stream function/potential representation for the magnetic vector potential and velocity that has been designed to minimize spectral pollution and lead to well-conditioned sparse matrix inversions. Parallel thermal conduction is simulated with the “artificial sound” method. [84] The solution algorithm is partially implicit in that only the most time-step limiting terms including the compressional Alfvén wave and field diffusion terms are implemented implicitly. The three dimensional mesh in M3D facilitates the resolution of multi-scale spatial structures, such as reconnection layers and the representation of fully three-dimensional boundaries that occur in evolving the free boundary of a tokamak or in a stellarator. The mesh uses unstructured triangular finite elements in the

poloidal section that can be of arbitrary order. A fully 3D parallel domain decomposition is used with a bias to minimizing the inter-processor communication during the elliptic solves. The PETSc library is used to provide high-performance portable sparse-matrix solvers.

The Princeton/LBL AMRMHD code is an adaptive mesh refinement 3D MHD code built within the Chambo [18] framework. The hyperbolic terms are evaluated using an unsplit second-order Godunov method [19,20] based on the symmetrized 8-wave formulation of the equations [21,22]. All variables are cell-centered with the solenoidal property of the magnetic field enforced by the application of a Hodge projection on the face-centered magnetic fields used in the flux calculation. The parabolic terms are treated with a semi-implicit method [23] that leads to variable coefficient Helmholtz equations which are solved using a multi-grid method. The method is designed to faithfully follow the multiple characteristics of the problem, yielding a faithful representation of highly anisotropic multiple-scalelength phenomena. Speed-up of computations due to AMR range up to more than 100 for some applications. A pellet mass source has been added that allows us to follow the pellet ablation process as it is injected into the tokamak.

## CEMM Simulation Codes:

	NIMROD	M3D	AMRMHD*
Poloidal discretization	High order quadrilateral finite elements	Triangular linear finite elements	Structured adaptive grid
Toroidal discretization	pseudospectral	Finite difference	Structured adaptive grid
Time integration	Semi-implicit	Partially implicit	Partially implicit and time adaptive
Enforcement of $\nabla \cdot \mathbf{B} = 0$	Error Diffusion	Vector Potential	Projection Method
Libraries	SuperLU (LBL)	PETSc (ANL)	CHOMBO (LBL)
Sparse Matrix Solver	Direct and Conjugate Gradient	GMRES and ICCG	Conjugate Gradient
Pre-conditioner	Direct solve of approximate matrices	Incomplete LU	Multigrid

\*Exploratory project

## Appendix II: Glossary of Acronyms

2D- Two spatial dimensions (assume symmetry in the third dimension)

3D- Three spatial dimensions

ANL- Argonne National Laboratory

AMRMHD- Adaptive Mesh Refinement magnetohydrodynamics code. This was developed in conjunction with Lawrence Berkeley Laboratory during our first proposal period

APDEC- Applied Partial Differential Equations Center. This was the name of the applied mathematics group at Lawrence Berkeley Laboratory that we collaborated with during the first proposal period to produce the AMRMHD code.

APS- American Physical Society. There is an annual meeting of the Division of Plasma Physics of the American Physical Society where we present much of our work.

AVS- Advanced Visualization System. This is a commercial software package for viewing complex three-dimensional structures.

$C^0$ - The class of functions that are continuous across cell boundaries, but do not necessarily have continuous derivatives.

$C^1$ - The class of functions that are continuous and have continuous first derivatives across cell boundaries, but do not necessarily have continuous higher derivatives.

CCA- Common Component Architecture: A DOE funded activity to provide tools to standardize interfaces between different software packages (programs)

CEL- Chapmann-Enskog-like approach. An iterative technique for solving for the plasma distribution function along magnetic field lines.

CEMM-Center for Extended Magnetohydrodynamic Modeling

CG-Conjugate Gradient. An iterative method for solving sparse matrix equations.

CGL- Chew-Goldberger-Low A fluid model described in Ref. [57]

CSET-Computer Science Enabling Technologies

CDX-U-Current Drive Experiment-upgrade. A small tokamak experiment at Princeton Plasma Physics Laboratory

Chombo-software framework for implementing finite difference methods for the solution of partial differential equations on block-structured adaptively refined rectangular grids. (see [seesar.lbl.gov/anag/chombo](http://seesar.lbl.gov/anag/chombo))

CUBIT-Sandia National Laboratory software for generating meshes. See [endo.sandia.gov/cubit](http://endo.sandia.gov/cubit)

DIII-D-Doublet-III tokamak in San Diego

DDB-Distributed Data broker. Software for coupling together applications codes.

DOE-Department of Energy

DT-deuterium/tritium. Mixture of hydrogen isotopes used in fusion experiments.

ECH-Electron Cyclotron Heating

ELITE-linear ideal MHD eigenvalue code developed specially to examine high mode number instabilities such as what occur at the plasma edge

ELM-Edge Localized Modes.

EPM-Energetic Particle Modes

FLR-Finite Larmor Radius

FY-Fiscal Year

GATO-ideal MHD eigenvalue code for low mode number stability

GB-giga-byte.  $10^9$  bytes

GUI-graphical user interface

GMRES-minimum residual method for solving sparse matrix equations iteratively

HDF5-file format for writing self-describing portable files

HYPRE-parallel mathematical library developed at Lawrence Livermore National Laboratory

IAEA-International Atomic Energy Authority. Every two years, a large international fusion meeting is held

ICCG-Incomplete Cholesky Conjugate Gradient method for iteratively solving sparse matrix equations.

ICRF-ion cyclotron resonant frequency



ICRH-ion cyclotron resonant heating

IGV-Ion gyro-viscous. One contribution to the ion stress tensor.

I/O-input and output

ISIC-Integrated software infrastructure centers. Part of the SciDAC organization. [see [http://www.osti.gov/scidac/computing/research\\_areas.html](http://www.osti.gov/scidac/computing/research_areas.html)]

ITER-International Thermonuclear Experimental Reactor

ITPA-International Toroidal Physics Activity

JET-Joint European Torus

KAW-Kinetic Alfvén Wave

LBL- Lawrence Berkeley Laboratory

LLNL-Lawrence Livermore National Laboratory

m- normally used to indicate the poloidal mode number (number of wavelengths the short way around the torus)

M3D-the multilevel 3D MHD code

MARS –a linear resistive MHD stability code developed in Europe

MCT-model coupling toolkit (Argonne)

MHD-Magnetohydrodynamic

n -normally used to indicate the toroidal mode number (number of wavelengths the long way around the torus)

NBI-Neutral Beam Injection

NERSC-National Energy Research Supercomputing Center

NIMROD-National Implicit MHD code with Resistivity-open discussion

NOVA2- a linear kinetic-MHD code based on a non-variational approach

NMA-Normal Mode Analysis. A GA/PPPL linear code for determining the unstable resistive wall modes using the eigenfunction method

NSTX-National Spherical Torus Experiment

NTM-Neoclassical Tearing Mode

OFES-Office of Fusion Energy Science

PERC-Performance evaluation research center. One of the SciDAC ISICs

PETSc-Portable Extendable Toolkit for Scientific programming

PPPL-Princeton Plasma Physics Laboratory

RF-Radio Frequency

RWM-Resistive Wall Mode. A tokamak MHD instability caused by the resistivity in the surrounding conducting wall

SAPP-Science Application Partnership Program

SciDAC-Scientific Discovery through Advanced Computing

SuperLU-a software package to directly solve a sparse matrix equation by first performing a lower-upper “LU” factorization

SSPX-spheromak experiment

ST – spherical torus

TAE-toroidal alfvén eigenmode

TFTR-Tokamak fusion test reactor

TOPS-Terascale Optimal Partial Differential Equation Simulation. One of the SciDAC ISIC centers (see [www.tops-scidac.org](http://www.tops-scidac.org))

TSC-Tokamak Simulation Code

TSTT-Terascale Simulation Tools and Technology Center. One of the SciDAC ISIC centers (see [www.tstt-scidac.org](http://www.tstt-scidac.org))

VALEN-a linear 3D finite element magnetics code for calculating aspects related to the active feedback control of the resistive wall mode (Columbia University)

VDE-Vertical Displacement Event



Center for Plasma Theory and Computation  
University of Wisconsin

1500 Engineering Drive, 503 ERB  
Madison, WI 53706-1609 USA  
Office (608) 263-8142  
FAX (608) 265-2438

March 5, 2004

Dr. Stephen C. Jardin  
Lead PI, CEMM Project  
Princeton Plasma Physics Laboratory  
PO Box 451  
Princeton, NJ 08543

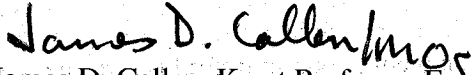
Dear Steve,

With this letter we would like to explicitly state and confirm our interest in and expectation of continuing collaboration with the Center for Extended Magnetohydrodynamic Modeling (CEMM) project. As you know, we have participated significantly in the NIMROD project since its beginning in the mid 1990s and in the CEMM project since its initiation a couple of years ago. The main form of our collaboration has been our: vigorous participation in virtually all of the various NIMROD and CEMM workshops over the years, provision of theoretical impetus for a number of problems team members are working on, and provision of theoretical support for adding some of the new physics to the codes.

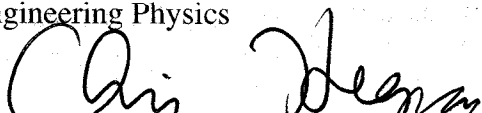
As evidence of our expected continuing involvement in the NIMROD and CEMM projects, we note that the proposal for our current DoE grant (on "Nonlinear and Nonideal MHD Theory," PI: C.C. Hegna, Co-PI: J.D. Callen, January 1, 2004 through December 31, 2006, about \$310k/yr) specifically identified collaborative support for the NIMROD project and the CEMM project as one of the four key areas of proposed research. The specific objectives for this research area identified in the Summary of the proposal were: "Collaborative participation in the NIMROD project; derivation of vector field equations and closure relations for use in numerical simulations of nonideal MHD physics." Also, many parts of the other three areas of the proposed research are likely to be germane to the CEMM project: emerging issues in magnetic island physics, the linear and nonlinear evolution properties of macroscopic ideal MHD instabilities, and kinetic-based closures for use in studies of macroscopic phenomena.

In summary, we have been heavily involved in the NIMROD and CEMM projects from their beginnings and are currently funded to continue to be vigorously involved. We very much look forward to participating in the next stage of the CEMM project which will hopefully garner more financial support commensurate with its great promise and importance to the fusion program.

Sincerely,

  
James D. Callen, Kerst Professor Emeritus  
of Engineering Physics and Physics

Chris C. Hegna, Associate Professor of  
Engineering Physics





COMPUTATIONAL RESEARCH DIVISION

March 15, 2004

Dr. Stephen Jardin  
MS27 C-Site A132  
Plasma Physics Laboratory  
PO Box 451  
Princeton, New Jersey 08543-0451

Dear Dr. Jardin,

This letter is in support of the SciDAC CEMM renewal proposal. Over the last three years, APDEC has been collaborating with CEMM to develop adaptive mesh refinement (AMR) algorithms and software for magnetic fusion applications. This work has been conducted primarily by Dr. Ravi Samtaney of PPPL, with support from the APDEC software development team at LBNL. During this time, Dr. Samtaney has been funded by a combination of APDEC funds and SciDAC SAPP funds. This work has served to demonstrate the potential usefulness of AMR to problems arising in magnetic fusion such as magnetic reconnection and tokamak fueling. In the APDEC renewal proposal submitted to DOE in January, we proposed developing over the next two years a more complete AMR simulation capability for tokomaks, including the representation of toroidal geometries using flux-surface mapped grids in logically rectangular coordinates, higher-order implicit discretizations for anisotropic conduction, and extensions to two-fluid models. This will entail a significant expansion of our activities in this area. We have budgeted \$165K/year for the next two years from APDEC funds to support Dr. Samtaney at PPPL, which we expect will be combined with \$90K/year of SAPP funding being proposed under CEMM for that purpose. We have also budgeted full-time support from APDEC to a member of the Applied Numerical Algorithms Group at LBNL, Dr. Terry Ligoeki, to work with Dr. Samtaney to develop these new capabilities. In addition, members of the APDEC software development team will be available as needed to make the required modifications to our AMR software framework.

We view the collaboration between CEMM and APDEC as having been both scientifically productive and intellectually challenging. We look forward to its continuance and expansion over the next two years.

Sincerely,

Phillip Colella  
Senior Mathematician  
Project Leader, APDEC

---

THE UNIVERSITY OF TENNESSEE

---



March 18, 2004

Stephen C. Jardin  
Princeton Plasma Physics Laboratory, MS 27  
P.O. 451  
Princeton, NJ 08543

College of Arts and Science  
Department of Computer Science  
203 Claxton Complex  
1122 Volunteer Boulevard  
Knoxville, TN 37996-3441  
(865) 974-5044  
FAX (865) 974-4444  
e-mail: info@cs.utk.edu  
<http://www.cs.utk.edu>

Dear Dr. Jardin:

As Director of the Logistical Computing and Internetworking (LoCI) Laboratory, which is part of the Department of Computer Science at the University of Tennessee, I am writing to express my support for this project and my enthusiasm at the opportunity to collaborate in it.

Working with my colleagues here at LoCI Laboratory, we have been collaborating with the SciDAC research community for more than two years now. This work has focused on the development and deployment of Logistical Networking infrastructure and middleware that serves the needs of advanced SciDAC applications, concentrating initially on the area of Astrophysics under the Terascale Supernova Initiative, more recently with Fusion Energy research as well. As you know, Logistical Networking integrates storage and processor resources into the shared network infrastructure in a highly scalable way in order to address the problems of distributed data management for collaborative, data intensive science.

Given the size and distribution of the CEMM community and its resources, and the major escalation in the volume of data that is anticipated under the project proposed here, we expect that our collaboration in this work will be of strong, mutual benefit to all concerned. The software and distributed storage infrastructure we already have deployed — 8TB in a private DOE/SciDAC testbed, 37TB in our public testbed — can start providing enhanced data management capabilities to CEMM researchers immediately. Moreover, by working with CEMM researchers and applications developers in areas such as efficient point to multi-point distribution, support for HDF5 and parallel I/O, and enhanced QoS between supercomputer simulation and visualization cluster, we believe our technology can provide CEMM applications with unparalleled capabilities, while at the same time driving our own research agenda in ways that will have a powerful, positive impact on the SciDAC and DOE Science community as whole.

Since your proposal, if executed, will have such potent impact both within the field, and across the research community as a whole, I urge that it be fully funded.

Sincerely,

Micah Beck  
Director/Associate Professor  
LoCI Lab

Terry Moore, Associate Director, LoCI

# OAK RIDGE NATIONAL LABORATORY

MANAGED BY UT-BATTELLE FOR THE DEPARTMENT OF ENERGY

D. B. Batchelor  
Batchelorbd@ornl.gov  
P.O. Box 2008  
Oak Ridge, TN 37831-6169  
Phone: (865) 574-1288  
Fax: (865) 576-7926

March 17, 2004

Stephen C. Jardin  
Director, SciDAC Center for Extended Magnetohydrodynamic Modeling  
Plasma Physics Laboratory  
James Forrestal Campus  
P.O. Box 451  
Princeton, New Jersey 08543

Dear Steve:

This letter is to confirm the intention of the SciDAC Center for Simulation of Wave-Plasma Interactions to collaborate with the SciDAC Extended Magnetohydrodynamic Modeling (CEMM) on the beginning of an integrated calculation of the effect of external wave heating and current drive on MHD instabilities. This activity is prototypical of that which will occur in one of the Focused Integration Initiatives (FIIs) called out by the Fusion Simulation Project report.

As we have discussed, the extended-MHD codes MINROD and M3D will provide a sequence of static 3D "equilibrium geometry files" to the wave propagation codes. These files will contain an accurate description of the instantaneous plasma properties and background electric and magnetic field structure. The wave propagation codes AORSA and TORIC coupled with a Fokker-Planck solver, either CQL3D or a Monte-Carlo solver, will use these geometry files to perform the wave propagation studies and will calculate local 3D momentum and energy source terms that will be fed back into the electron and ion equations in the extended-MHD codes. Other codes may also be involved as appropriate.

We agree that there are a number of computational and physics modeling issues that need to be resolved by our two teams in order to make such an integrated calculation feasible and practical: How is the perturbed plasma distribution function calculated and shared by the two codes? How does the massive data transfer occur? Can we achieve concurrency with both the extended-MHD and wave-propagation codes running simultaneously on large numbers of parallel processors? Since these issues, and other like them, will need to be addressed by a large-scale integrated simulation eventually, we see this activity as a prototype of those that will be encountered in a fully-integrated simulation of a burning plasma.

We wish you the best of luck in getting your project renewed, and we look forward to this exciting collaboration.

Sincerely,



Donald B. Batchelor  
Lead PI: Center for Simulation of Wave-Plasma Interactions

DBB:mrf

# Finite Element with First-Derivative Continuity Applied to Fusion MHD Applications

S. C. Jardin

Princeton University  
Plasma Physics Laboratory  
P. O. Box 451  
Princeton, NJ 08543  
E-mail: [jardin@princeton.edu](mailto:jardin@princeton.edu)

## Abstract

We describe properties of the reduced quintic triangular finite element. The expansion used in the element will represent a complete quartic polynomial in two dimensions, and thus the error will be of order  $h^5$  if the solution is sufficiently smooth. The quintic terms are constrained to enforce  $C^1$  continuity across element boundaries, allowing their use with partial differential equations involving derivatives up to fourth order. There are only three unknowns per node in the global problem, which leads to lower rank matrices when compared with other high-order methods with similar accuracy but lower order continuity. The integrations to form the matrix elements are all done in closed form, even for the nonlinear terms. The element is shown to be well suited for elliptic problems, anisotropic diffusion, the Grad-Shafranov-Schlüter equation, and the time-dependent MHD or extended MHD equations. The element is also well suited for 3D calculations when the third (angular) dimension is represented as a Fourier series.

# I. Introduction

Two dimensional (2D) finite elements are being used in a wide variety of fusion applications. Even in fully 3D calculations in toroidal geometry, it is common to use 2D elements in the poloidal plane, and to use either finite differences or a Fourier spectral representation in the toroidal angle.

While early work used primarily linear elements[1,2], it is now recognized that higher order elements offer significant advantages, and are essential to adequately represent highly anisotropic heat transport and other anisotropic processes[3,4,6]. However, the application of high-order elements to fusion problems has so far been restricted to the class of elements known as  $C^0$  elements, which includes both the spectral and the Lagrange basis. These are constructed so as to have the unknown function continuous between elements, but none of its derivatives are forced to be continuous. The rationale for this is that it is less complex to construct such elements and if the minimizing solution has high-order continuity, this solution will emerge from the Galerkin process without having to be specifically imposed.

However, there are clearly some advantages in using elements with higher order intrinsic continuity. We can expect that for a problem whose solution has continuous first-derivatives everywhere, i.e. satisfies  $C^1$  continuity, fewer basis functions will be required per element to approximate the true solution if the  $C^1$  constraint is imposed in the construction of the basis functions, i.e. if the degrees of freedom that are not compatible with global  $C^1$  continuity have been discarded from the outset. We can further expect that this will lead to smaller matrix sizes with similar sparseness patterns to the matrices that arise with the  $C^0$  elements, and thus a more efficient solution procedure should result.

Also, many problems in extended MHD involve operators higher than second order in space. Examples of these are the viscosity operator in the vorticity equation, and the hyper-resistivity operator in the magnetic flux equation. The  $C^1$  elements allow the treatment of fourth order operators by using the standard Galerkin technique of shifting two of the derivatives to the trial function, whereas this is not possible with the  $C^0$  elements, which need to introduce auxiliary variables and expand them in finite elements. Thus, the  $C^1$  elements can expect to have an additional efficiency and resultant smaller matrices since they do not need to introduce these auxiliary variables when third or fourth order derivatives are present. Conversely, in some cases several low order equations can be combined to produce a smaller number of higher order equations that can be approximated directly with these elements that possess higher order continuity.

We consider only triangular finite elements in this paper, in fact, only a particular triangular finite element known as the reduced quintic [6] (also called the Bell triangle [7,8] and the TUBA 3 element [9]). This reflects a bias that triangular elements are more flexible for representing complex geometry, and can be easily refined as needed simply by dividing one triangle into three or more. It is especially efficient and convenient when the different triangles connect only via the vertices, and that is where all the unknowns are defined. With these constraints, and that of  $C^1$  continuity, the reduced quintic element emerges. While this element has been used in



structural engineering studies since the late 1960s [10], it has apparently been overlooked by the extended MHD community. Here we show that it has some real advantages, and should be seriously considered as a basis for contemporary computational models of extended MHD in magnetized plasmas.

## II. The Reduced Quintic Finite Element

### A. The Elements

Consider the reduced quintic 2D triangular finite element in the  $x$ - $y$  plane as depicted in Fig. 1. In each triangular element, the unknown function  $\phi(x, y)$  is written as a general polynomial of 5<sup>th</sup> degree in the local Cartesian coordinates  $\xi$  and  $\eta$ :  $\phi(\xi, \eta) = \sum_{i=1}^{20} a_i \xi^{m_i} \eta^{n_i}$  (where the exponents  $m_i, n_i$  are given in Table 1) which would have 21 coefficients were there not additional constraints. Eighteen of the coefficients are determined from specifying the values  $\phi, \phi_x, \phi_y, \phi_{xx}, \phi_{xy}, \phi_{yy}$  at each of the 3 vertices, thus guaranteeing that globally all first and second derivatives will be continuous at each vertex. Since the one-dimensional quintic polynomial along each edge is completely determined by these values specified at the endpoints, it is guaranteed that the expansion is continuous between elements.

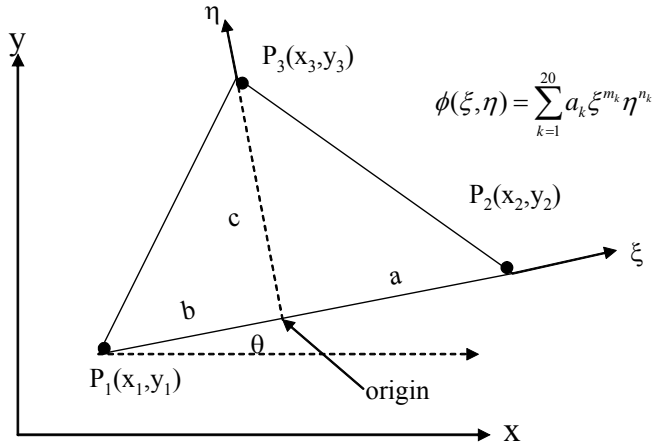


**Figure 1: Reduced quintic finite element is defined by the 4 geometric parameters  $a, b, c, \theta$ . A local  $(\xi, \eta)$  Cartesian system is used. The function and first 2 derivatives are constrained at the 3 points, and  $C^1$  continuity is imposed at the edges. Exponents  $m_i$  and  $n_i$  are given in table 1.**

The remaining three constraints come from the requirement that the normal derivative of  $\phi$  at each edge,  $\phi_n$ , reduce to a one-dimensional cubic polynomial along that edge. This implies that the two sets of nodal values completely determine  $\phi_n$  everywhere on each edge, guaranteeing its continuity from one triangle to the next so that the element is  $C^1$ . One of these three constraints is trivial and has been used to reduce the number of terms from 21 to 20 in the sum.

Note that in imposing these continuity constraints, the

expansion is no longer a complete quintic, but it does contain a complete quartic with additional constrained quintic coefficients to enforce  $C^1$  continuity between elements. Thus the name, “reduced quintic”. If the characteristic size of the element is  $h$ , then it follows from a local Taylor’s series analysis that the approximation error in the unknown function,  $\phi - \phi^h$ , will be of order  $h^5$ , which leads to global  $O(h^5)$  accuracy after integrating over the element.

k	$m_k$	$n_k$	k	$m_k$	$n_k$	k	$m_k$	$n_k$	k	$m_k$	$n_k$
---	-------	-------	---	-------	-------	---	-------	-------	---	-------	-------

1	0	0	6	0	2	11	4	0	16	5	0
2	1	0	7	3	0	12	3	1	17	3	2
3	0	1	8	2	1	13	2	2	18	2	3
4	2	0	9	1	2	14	1	3	19	1	4
5	1	1	10	0	3	15	0	4	20	0	5

**Table 1: Exponents of  $\xi$  and  $\eta$  for the reduced quintic expansion  $\phi(\xi, \eta) = \sum_{i=1}^{20} a_i \xi^{m_i} \eta^{n_i}$**

Suppose that we are approximating a square domain by partitioning it into  $n^2$  squares or  $2n^2$  triangles. The reduced quintic will asymptotically have  $N=6n^2$  unknowns, or three unknowns for each triangle. This scaling can be verified by the fact that if we introduce a new point into any triangle and connect it to the 3 nearby points; we will have generated 2 new triangles and introduced 6 new unknowns. We contrast this with linear elements that require only  $\phi$  at the nodes and thus have  $C^0$  continuity,  $\frac{1}{2}$  unknown per triangle, and an approximation error of order  $h^2$ .

Another popular class of higher order 2D finite elements, that has only  $C^0$  continuity enforced, is the Lagrangian elements. These use as a basis within each element a set of basis functions that are unity at a particular node and that vanish at all other nodes. Continuity requires that there be  $M+1$  nodes along each side for an  $M^{\text{th}}$  order polynomial element, with the remaining nodes being interior nodes (or “bubble nodes”). Thus for the Lagrangian elements, a quadratic element (6 coefficients per triangle) will have 3 nodes along each edge (2 vertex nodes and 1 edge node), a cubic element (10 coefficients per triangle) will have 4 nodes along each edge (2 vertex nodes and 2 edge nodes) and 1 interior node and a quartic element (15 coefficients per triangle) will have a total of 3 vertex nodes, 9 edge nodes, and 3 interior nodes. It is easily seen that these higher-order elements will asymptotically have 2,  $4\frac{1}{2}$ , and 8 unknowns per triangle (UK/T), respectively, (or 2,  $3\frac{1}{2}$  and 5 if you discount the interior nodes that can be efficiently eliminated by static condensation). We summarize these 2D triangular elements in Table 2.

	Vertex nodes	Line nodes	Interior nodes	accuracy order $h^p$	UK/T	UK/T <sup>#</sup>	continuity
linear element	3	0	0	2	$\frac{1}{2}$	$\frac{1}{2}$	$C^0$
Lagrange quadratic	3	3	0	3	2	2	$C^0$
Lagrange cubic	3	6	1	4	$4\frac{1}{2}$	$3\frac{1}{2}$	$C^0$
Lagrange quartic	3	9	3	5	8	5	$C^0$
reduced quintic	18	0	0	5	3	3	$C^1^*$

**Table 2: Summary of properties of the reduced quintic and the low-order Lagrange elements. UK/T is the number of unknowns per triangle. \* note  $C^2$  continuity at nodes. UK/T<sup>#</sup> is the number of unknowns per triangle, not counting interior nodes**

### B. Computations:

It is shown in Appendix A that if we locally number the unknowns  $\phi, \phi_x, \phi_y, \phi_{xx}, \phi_{xy}, \phi_{yy}$  at  $P_1$  as  $\Phi_1$ - $\Phi_6$ , at  $P_2$  as  $\Phi_7$ - $\Phi_{12}$ , and at  $P_3$  as  $\Phi_{13}$ - $\Phi_{18}$ , then the coefficients  $a_i$  for a given element are determined uniquely by the relation:

$$a_i = \sum_{j=1}^{18} g_{i,j} \Phi_j \quad (1.1)$$

where the  $20 \times 18$  matrix  $g_{i,j}$  depends only on the shape and orientation of the individual triangle. Thus, the general expression for the unknown function  $\phi$  in a given triangle is:

$$\phi(\xi, \eta) = \sum_{i=1}^{20} a_i \xi^{m_i} \eta^{n_i} = \sum_{i=1}^{20} \sum_{j=1}^{18} g_{i,j} \Phi_j \xi^{m_i} \eta^{n_i} \quad (1.2)$$

or,

$$\phi(\xi, \eta) = \sum_{j=1}^{18} v_j \Phi_j \quad (1.3)$$

We have defined the basis functions as

$$v_j \equiv \sum_{i=1}^{20} g_{i,j} \xi^{m_i} \eta^{n_i} \quad (1.4)$$

for  $j=1, 18$ . The 18 basis functions for each triangle, as defined in Eq. (1.4) have the property that they have a unit value for either the function or one of its first or second derivatives at one vertex and zero for the other quantities at this and the other nodes. They also have the  $C^1$  continuity property embedded. We illustrate the first six of these, associated with a particular vertex  $P_1$ , in Fig. 2. It is seen that unlike the Lagrange basis functions, these individual basis functions do not change sign within a triangle which might be an advantage in preserving positivity for physical quantities such as the density or pressure.

All of the integrals that need to be done to define the matrices that occur in the Galerkin method are of the form of 2D integrals of polynomials in  $\xi$  and  $\eta$  over the triangles. It is possible to convert these to sums of integrals that can each be done analytically by making use of the formula:

$$F(m, n) \equiv \iint_{triangle} \xi^m \eta^n d\xi d\eta = c^{n+1} \frac{[a^{m+1} - (-b)^{m+1}] m! n!}{(m+n+2)!} \quad (1.5)$$

Thus, all integrations are done in closed form to machine precision.

Consider a common integral (traditionally called the mass matrix) over the triangle that occurs when we apply the Galerkin method to applications that will be discussed in the next section:

$$\begin{aligned} \iint v_j(\xi, \eta) \phi(\xi, \eta) d\xi d\eta &= \sum_{k=1}^{18} \left[ \sum_{i=1}^{20} \sum_{l=1}^{20} g_{i,j} g_{l,k} F(m_i + m_l, n_i + n_l) \right] \Phi_k \\ &\equiv \sum_{k=1}^{18} M_{j,k} \Phi_k \end{aligned} \quad (1.6)$$

Other integrals needed for the applications presented, all of whose calculation is straightforward, are given in Appendix B.

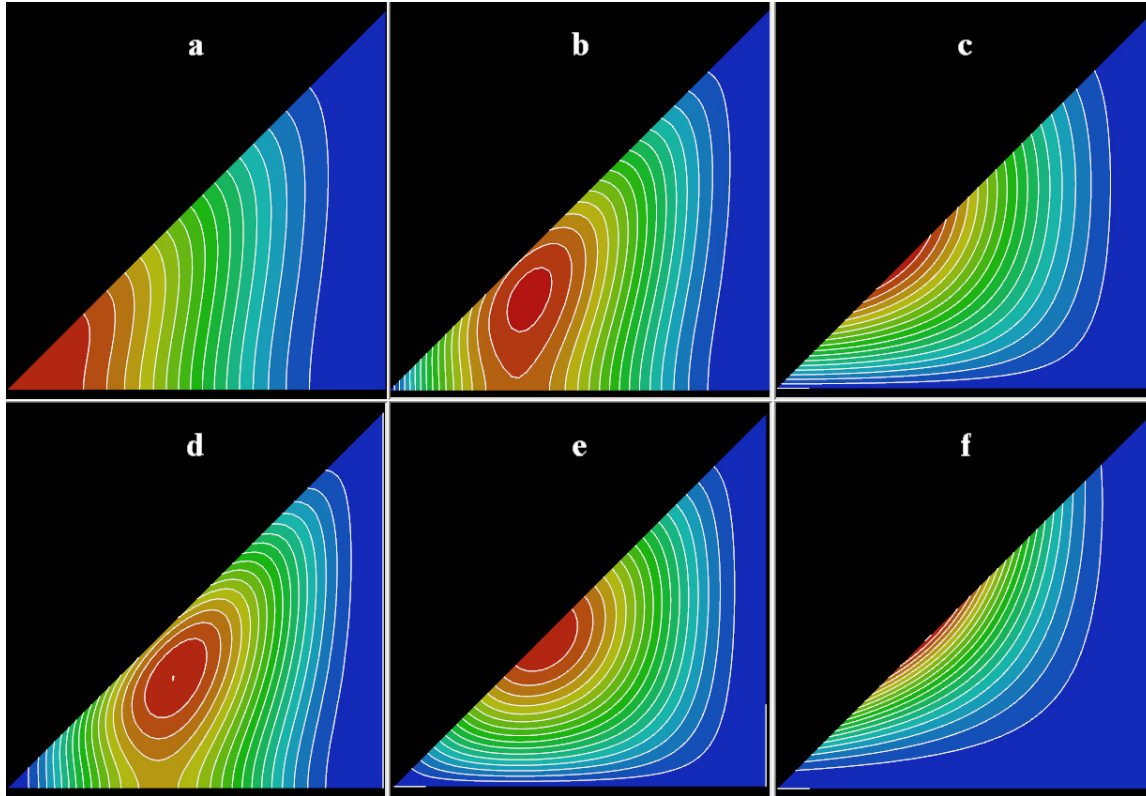
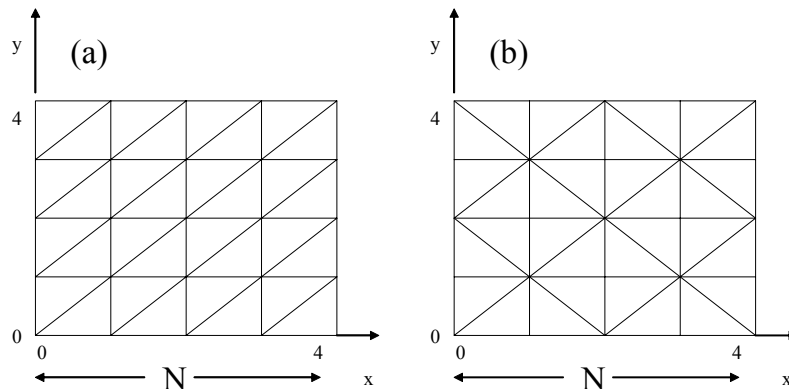


Figure 2: The 6 trial functions associated with the point  $P_1$  in the lower left corner. (a)  $\phi=1$ , (b)  $\phi_x=1$ , (c)  $\phi_y=1$ , (d)  $\phi_{xx}=1$ , (e)  $\phi_{xy}=1$ , (f)  $\phi_{yy}=1$ . None of the functions alternate sign. Red=1, Blue=0.

Essential boundary conditions are readily implemented by replacing the rows of the matrix  $M_{i,j}$  in Eq. (1.6) corresponding to the function value or derivative for which a boundary condition is to be applied by a row with zeros everywhere except for the diagonal, in which there is placed a one. Then the boundary value of the corresponding function or derivative is placed in the corresponding location in the RHS vector.

Figure 3: Region is divided into regular rectangles, each of which is divided into two right triangles. Mesh (a) has 6 sides per vertex; Mesh (b) alternates 4 and 8 sides per vertex.



### III. Applications

We present several examples that illustrate the accuracy and simplicity of this method. These applications are typical of those encountered in fusion MHD applications.

#### a. A Simple Elliptic Problem

Here we present a basic application of the method to a solution of Poisson's equation in a rectangular domain. Consider the equation:

$$\nabla^2 \Phi = f(x, y) \quad (1.7)$$

We wish to solve Eq. (1.7) on the domain  $0 < x < L_x$ ;  $0 < y < L_y$  with Dirichlet boundary conditions:  $\Phi(0, y) = \Phi(L_x, y) = \Phi(x, 0) = \Phi(x, L_y) = 0$ . Equation (1.7) is equivalent to finding the function  $\Phi(x, y)$  that minimizes the functional:

$$I(\Phi) = \iint_{\substack{0 < x < L_x \\ 0 < y < L_y}} \left[ \frac{1}{2} |\nabla \Phi|^2 + f \Phi \right] dx dy \quad (1.8)$$

For illustration, we choose the function  $f(x, y)$  obtained by differentiating the exact solution:  $\Phi(x, y) = x(x-L_x)y(y-L_y) \sin kx$ . For  $L_x=L_y=4$ , a square mesh is divided into  $N^2$  regular square subdivisions, each of which divided into two right triangles as shown in 3(a), so that there are a total of  $2N^2$  triangular elements with the linear dimension of each scaling like  $1/N$ .

The integrals in Eq. (1.8) are evaluated in Appendix B. Minimization gives the matrix equation

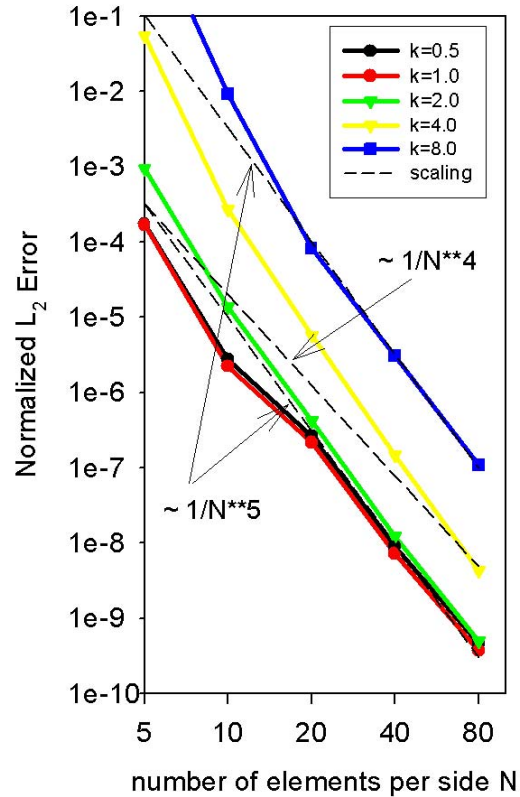
$$\mathbf{K}\Phi = \mathbf{F} \quad (1.9)$$

which is solved for the unknown vector  $\Phi$  using the sparse matrix direct solver routine SuperLU [11].

In Fig. 4 we plot the  $L_2$  norm of the error in solution for several values of  $N$  and  $k$ , verifying that we obtain the expected  $1/N^5$  scaling. Note that there is approximately one wavelength per cell when  $k = \pi N / 4$ .

#### b. Anisotropic Thermal Conduction

The second example is a demonstration of the accurate calculation of anisotropic thermal conduction. Let  $\mathbf{B}$  be a 2-dimensional magnetic field written in terms of a given flux function  $\psi(x, y)$ , i.e.,  $\mathbf{B} = \hat{z} \times \nabla \psi$  and suppose the source function  $S(x, y)$  is given, as are the two constants



is Fig.

the

Figure 4: Elliptic equation exhibits  $1/N^5$  scaling

denoting the isotropic thermal conductivity  $\kappa$ , and the parallel thermal conductivity  $\kappa_{\parallel}$ . Consider the functional

$$I = \iint \left[ \frac{1}{2} \kappa_{\parallel} |\mathbf{B} \cdot \nabla \Phi|^2 + \frac{1}{2} \kappa |\nabla \Phi|^2 + S(x, y) \Phi \right] \quad (1.10)$$

Minimizing this with respect to the unknown function  $\Phi$  gives the steady state anisotropic heat conduction equation:

$$\nabla \cdot \kappa_{\parallel} \mathbf{B} \mathbf{B} \cdot \nabla \Phi + \nabla \cdot \kappa \nabla \Phi = S(x, y) \quad (1.11)$$

The details of the evaluation of the matrix elements are given in Appendix B. For this application we let  $\psi(x, y) = \sin \frac{\pi x}{L_x} \sin \frac{\pi y}{L_y}$ ,

$$\text{and } S(x, y) = \frac{\sin(\pi x/L_x) \sin(\pi y/L_y)}{(\pi/L_x)^2 + (\pi/L_y)^2} \quad (1.11)$$

Since the magnetic field flux function is proportional to the source function, it is readily verified that the solution should be independent of the value of the parallel conductivity  $\kappa_{\parallel}$ , thus simplifying the error comparison.

The results are shown in Fig. 5. Again, we verify that at least  $N^{-5}$  scaling is obtained, that reasonable accuracy ( $10^{-5}$ ) can be obtained for values of  $\kappa_{\parallel}/\kappa$  as large as  $10^8$  values of  $N$  as low as 60. Note that the mesh shown in Fig. 3(a) was again used, so that there absolutely no attempt to align the element boundaries with the magnetic field direction for this demonstration.

### c. Ideal Tilting of an Incompressible Column

The incompressible MHD equations in 2D can be written in terms of a stream function  $\phi$  and a flux function  $\psi$  using the normal Poisson bracket notation (where subscripts denote differentiation), i.e.,  $[f, g] \equiv f_x g_y - f_y g_x = f_{\xi} g_{\eta} - f_{\eta} g_{\xi}$

$$\begin{aligned} \frac{\partial}{\partial t} \nabla^2 \phi + [\nabla^2 \phi, \phi] - [\nabla^2 \psi, \psi] &= \mu \nabla^4 \phi \\ \frac{\partial \psi}{\partial t} + [\psi, \phi] &= \eta \nabla^2 \psi \end{aligned} \quad (1.12)$$

Here  $\mu$  and  $\eta$  are constants denoting the plasma viscosity and resistivity, respectively.

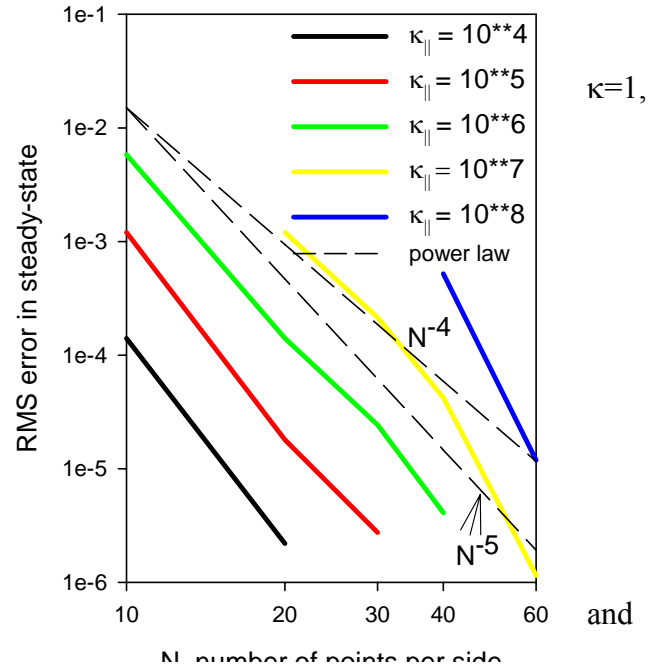


Figure 5: Convergence study shows  $N^{-5}$  convergence for anisotropic diffusion

and  
for  
was

Note that these equations obey an energy theorem:

$$\frac{\partial}{\partial t} \iint_{\text{domain}} \frac{1}{2} \left[ |\nabla \phi|^2 + |\nabla \psi|^2 \right] dx dy = - \left[ \eta |\nabla^2 \psi|^2 + \mu |\nabla^2 \phi|^2 \right] \quad (1.13)$$

subject to the vanishing of  $\partial\psi/\partial t$ ,  $\phi$ , and  $n \cdot \nabla \phi$  on the boundary.

Applying Galerkin's method to the set of equations (1.13), using the reduced quintic finite element, and applying  $\theta$ -weighted implicit finite differencing yields the following set of matrix equations to advance the solution from time  $n$  to  $n+1$ :

$$\begin{aligned} \begin{bmatrix} S_j^{11} & S_j^{12} \\ S_j^{21} & S_j^{22} \end{bmatrix} \begin{bmatrix} \Phi_j^{n+1} \\ \Psi_j^{n+1} \end{bmatrix} &= \begin{bmatrix} D_j^{11} & D_j^{12} \\ D_j^{21} & D_j^{22} \end{bmatrix} \begin{bmatrix} \Phi_j^n \\ \Psi_j^n \end{bmatrix} \\ \begin{bmatrix} S_j^{11} & S_j^{12} \\ S_j^{21} & S_j^{22} \end{bmatrix} &= \begin{bmatrix} A_{i,j} + \theta \delta t [\bar{G}_{i,j,k} \Phi_k^* + \mu B_{i,j}] & -\theta \delta t \bar{G}_{i,j,k} \Psi_k^* \\ \theta \delta t K_{i,j,k} \Psi_k^* & M_{i,j} + \theta \delta t [K_{i,k,j} \Phi_k^* - \eta A_{i,j}] \end{bmatrix} \\ \begin{bmatrix} D_j^{11} & D_j^{12} \\ D_j^{21} & D_j^{22} \end{bmatrix} &= \begin{bmatrix} \left\{ A_{i,j} - \delta t [G_{i,j,k} \Phi_k^n - \theta \bar{G}_{i,j,k} \Phi_k^*] \right. & \delta t (G_{i,j,k} \Psi_k^n - \theta \bar{G}_{i,j,k} \Psi_k^*) \\ \left. + (1-\theta) \mu B_{i,j} \right\} & \\ \delta t K_{i,j,k} (-\frac{1}{2} \Psi_k^n + \theta \Psi_k^*) & \left\{ M_{i,j} - \delta t [K_{i,k,j} (\frac{1}{2} \Phi_k^n - \theta \Phi_k^*)] \right. \\ & \left. -(1-\theta) \eta A_{i,j} \right\} \end{bmatrix} \end{aligned} \quad (1.14)$$

where  $\bar{G}_{i,j,k} \equiv G_{i,j,k} + G_{i,k,j}$ . The quantities occurring in the matrix are defined in the text and in Appendix B. Note that in the applications presented here, we set  $\Phi^* = \Phi^n$  and  $\Psi^* = \Psi^n$ , which

necessitated inverting the matrix on the left in Eq. (1.15) each time step. However, it may be possible in many applications to obtain stable and accurate calculations by keeping  $\Phi^*$  and  $\Psi^*$  fixed for a number of time steps, thus significantly reducing the solution time. This is always the case in a linear calculation.

Following [1,12] we define an initial bipolar vortex equilibrium state:

$$\psi = \begin{cases} [2/kJ_0(k)] J_1(kr) \cos \theta, & r < 1, \\ (r-1/r) \cos \theta, & r > 1, \end{cases} \quad (1.16)$$

$$J_1(k) = 0.$$

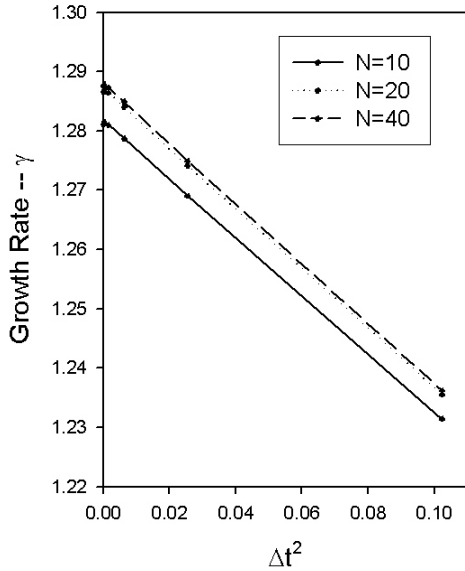


**Figure 6: Convergence study of linear growth rate for tilt mode problem**

When perturbed,

an instability occurs, growing exponentially as  $\exp \gamma t$ . The simulation box is again the square in Fig. 3(a) with sides of length 4 that is divided into  $N \times N$  rectangular regions, each with 2 triangles. Conducting, no slip boundary conditions are applied at the wall:  $\phi=0$ ,  $n \cdot \nabla \phi=0$ ,  $\partial\psi/\partial t=0$ . The first and second tangential derivatives of these quantities are also set to zero.

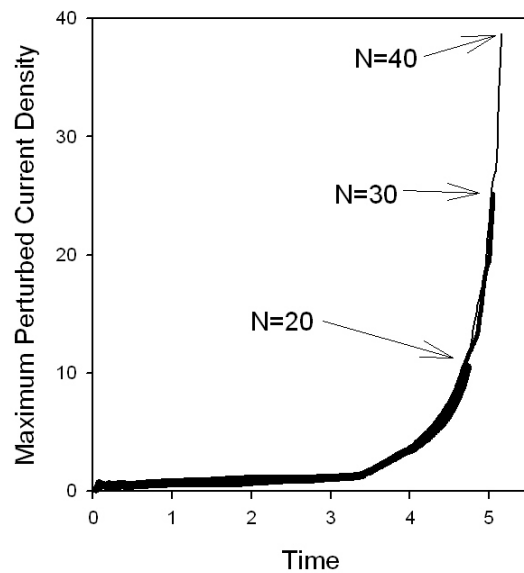
We show in Fig. 6 the dependence of the linear growth rate  $\gamma$  on the size of the time step  $\Delta t$  for a sequence of runs with  $\mu=0.005$ ,  $\eta=0.001$ ,  $\theta = 0.5$ , and varying number of rectangular regions per dimension  $N$ . For the smallest time step used,  $\delta t=0.01$ , the growth rate  $\gamma$  was 1.2876, changing only in the 6<sup>th</sup> decimal place when varying  $N$  from 30 to 40, making a further convergence study in  $N$  unnecessary.

In the nonlinear stages, near singular current sheets form and the resolution requirements become more demanding. We plot the maximum perturbed current density vs. time (as determined from taking the maximum value on a  $400 \times 400$  evaluation grid) for a run with  $(\mu, \eta) = (5 \times 10^{-3}, 10^{-4})$  in Fig. 7 for three different linear resolutions,  $N=20, 30, 40$ . We monitor energy conservation as to how accurately Eq. (1.14) is satisfied. The calculation used an initial time step of  $\delta t=0.02$ , which was reduced when the energy conservation was violated by more than 1%. When  $\delta t < 0.0002$ , the calculation was stopped.

We see from Fig. 7 that the calculations

**Figure 7: Maximum perturbed current in the tilt-mode calculation as a function of time for three resolutions**

$N=20, 30, 40$  give essentially the same results until the singularity begins its exponential growth, and that the  $N=40$  calculation can follow the singularity to about 4-times the height of the  $N=20$  calculation while still maintaining energy conservation to within 1%. If we relax this stringent energy conservation requirement, calculations would proceed much further without failing.



These calculations were repeated for  $N=40$  using the second mesh system shown in Fig. 3 as (b). We find essentially the same results, with the growth rate of the linear mode changing only beyond the 6<sup>th</sup> decimal place, and the eigenfunctions appearing identical.

Appendix C presents a form of the above equations that is especially convenient for looking at small deviations from an equilibrium configuration (linearized displacements). The linearized application is particularly efficient for a direct solver (SuperLU) as it requires only a single LU decomposition for a time dependent problem, and just a back substitution each time step.

Appendix D combines the two equations into a higher order equation for the stream function  $\phi$  that does not require the solution of the  $\psi$  equation. This leads to a very efficient implicit time advance that highlights the advantages of using  $C^1$  continuity elements.



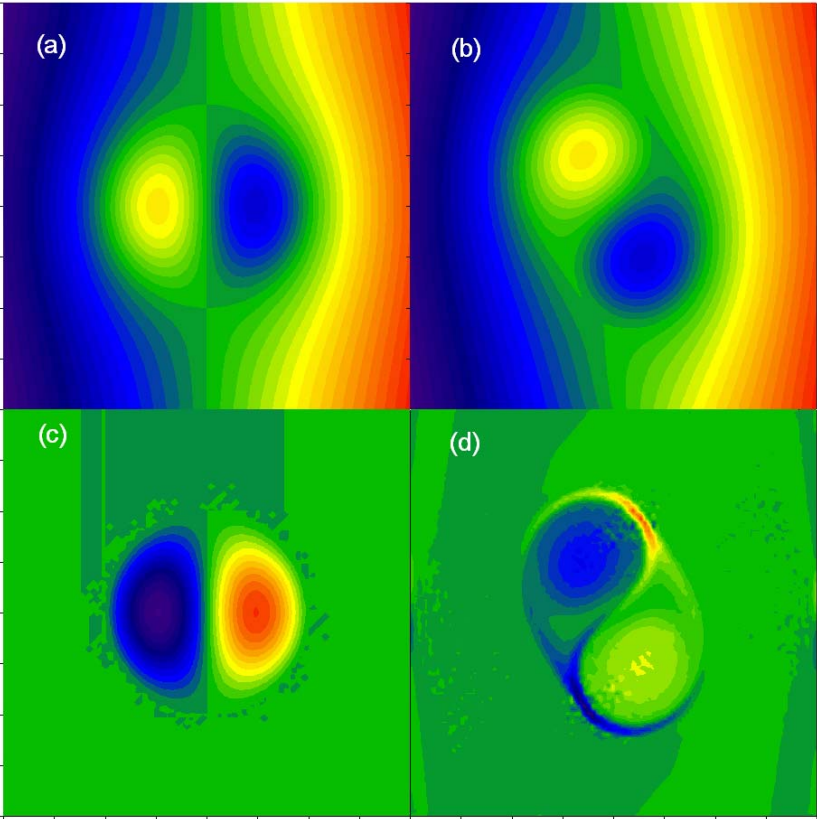


Figure 8: Poloidal flux at times  $t=0$  (a) and  $t=5$  (b) and plasma current at times  $t=0$  (c) and  $t=5$  (d) for the tilt mode problem with  $N=40$ . The singular currents can be seen developing in (d)

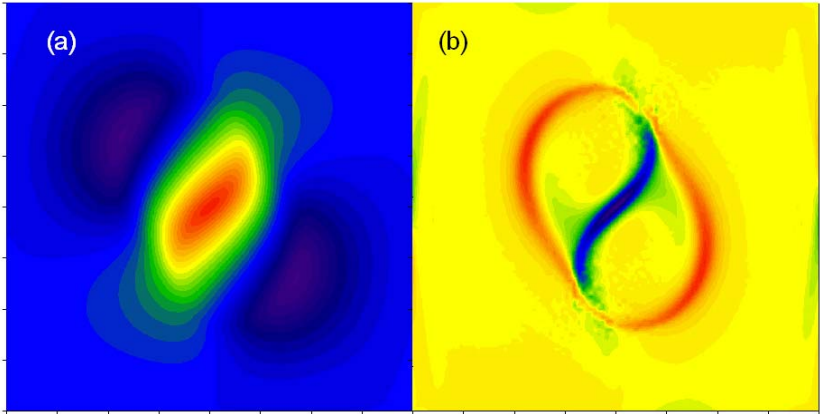


Figure 9: Stream function (a) and vorticity (b) for the tilt mode problem with  $N=40$  at time  $t=5$ .

**d. The Grad-Shafranov-Schlüter (GSS) Equation**

The equation that the poloidal magnetic flux function satisfies in force-balance for a 2D axisymmetric plasma equilibrium is well known to be:

$$\frac{\partial}{\partial x} \frac{1}{x} \frac{\partial \psi}{\partial x} + \frac{\partial}{\partial y} \frac{1}{x} \frac{\partial \psi}{\partial y} = - \left( xp'(\psi) + \frac{1}{x} gg'(\psi) \right) \quad (1.17)$$

Here,  $p(\psi)$  is the plasma pressure,  $g(\psi)$  is the toroidal field function so that  $g(\psi)/x$  is the toroidal field strength, and prime denotes a derivative with respect to  $\psi$ , the solution. To fully specify the problem, one must prescribe the two functions  $p'(\psi)$  and  $gg'(\psi)$  along with the boundary values for  $\psi$ . It is convenient to define the normalized flux function as  $\tilde{\psi} \equiv (\psi - \psi_0) / \Delta\psi$ , where we denote by  $\psi_0$  the value of the poloidal flux at the magnetic axis, and by  $\psi_L$  the value at the plasma-vacuum boundary, which is defined by the value of  $\psi$  at a specified limiter location  $(x_L, y_L)$ . We further define the flux depth of the plasma as  $\Delta\psi \equiv \psi_L - \psi_0$  so that values of  $0 \leq \tilde{\psi} < 1$  reside in the plasma, and values  $1 \leq \tilde{\psi}$  are in the surrounding vacuum region. For these studies, we define the pressure and toroidal field functions as functions of the normalized poloidal flux function,  $p = p(\tilde{\psi})$  and  $g^2 = g^2(\tilde{\psi})$ , with the functional form specified as follows:

$$p(s) = p_0 [1 + p_1 s + p_2 s^2 - (20 + 10p_1 + 4p_2)s^3 + (45 + 20p_1 + 6p_2)s^4 - (36 + 15p_1 + 4p_2)s^5 + (10 + 4p_1 + p_2)s^6] \quad (1.18)$$

and

$$g^2(s) = g_0^2(s) + \gamma_1 G_1(s) + \gamma_2 G_2(s) + \gamma_3 G_3(s) \quad (1.19)$$

where

$$\begin{aligned} G_1(s) &= s - 10s^3 + 20s^4 - 15s^5 + 4s^6 \\ G_2(s) &= s^2 - 4s^3 + 6s^4 - 4s^5 + s^6 \\ G_3(s) &= 1 - 20s^3 + 45s^4 - 36s^5 + 10s^6 \end{aligned} \quad (1.20)$$

These functional forms have been chosen so that the plasma current and pressure will go smoothly to zero at the plasma-vacuum boundary. The pressure function is then specified in terms of the three constants,  $p_0$ ,  $p_1$ , and  $p_2$ . The three constants appearing in the toroidal field function,  $\gamma_1$ ,  $\gamma_2$ , and  $\gamma_3$ , are used to prescribe the total plasma current  $I_p$ , the normalized reciprocal current density on axis  $q_0$ , and the slope of the current density near the axis  $J_\psi$ , respectively. The constant  $g_0$  is the value of the toroidal field function due to the external fields. Thus, the constants appearing in Eq. (1.19) are given by:

$$\begin{aligned} \gamma_1 &= -R_0 \left( R_0 p_0 p_1 + 2g_0 \Delta\psi / R_0^2 q_0 \right) \\ \gamma_2 &= - \left( J_\psi \Delta\psi / 2 + p_0 p_2 \right) \\ \gamma_3 &= - \left( I_p + \gamma_1 I_1 + \gamma_2 I_2 + I_0 \right) / I_3 \end{aligned} \quad (1.21)$$

The required integrals are obtained by first expressing the  $x$  and  $y$  derivatives of the functions  $xp'(\psi)$ ,  $\frac{1}{2x} G_1'(\psi)$ ,  $\frac{1}{2x} G_2'(\psi)$ ,  $\frac{1}{2x} G_3'(\psi)$  at each node in terms of the unknown vector

$\Psi \equiv \left[ \psi, \psi_x, \psi_y, \psi_{xx}, \psi_{xy}, \psi_{yy} \right]$  and then using the finite element expansion (1.3) to extend these over the triangles so that the integrals can be performed in closed form. Thus,

$$I_0 = \iint_{\text{plasma}} xp'(\psi) dx dy = \sum_{l=1}^N \sum_{j=1}^{18} C_j (xp')_j \quad (1.22)$$

$$I_k = \iint_{\text{plasma}} \frac{1}{2x} G'_k(\psi) dx dy = \sum_{l=1}^N \sum_{j=1}^{18} C_j \left( \frac{1}{2x} G'_k \right)_j, \quad k=1,3$$

where the first sum is over the  $N$  triangular elements, and we have denoted by  $(xp')_j$ , etc, the value of the function in brackets and it's derivatives through second order with respect to  $x$  and  $y$  at each of the three nodes defining each triangle. The integrating factor appearing in Eq. (1.22) is given by  $C_j = \sum_{p=1}^{20} g_{p,j} F(m_p, n_p)$ . These integrals and constants are recomputed each iteration as  $\psi$  changes.

The Galerkin method, together with a Picard iteration for the nonlinear equation (1.17) consists of multiplying by each test function, performing an integration by parts, integrating over the domain, and applying the iteration scheme:

$$\mathbf{A} \cdot \Psi^{n+1} = \mathbf{B}(\Psi^n) \quad (1.23)$$

where the matrix and vector elements are given in Appendix B. The boundary values are given using an analytic formula for the vector potential due to a filament source plus a uniform dipole field, which is required for equilibrium. Thus, at a boundary point of the domain  $(x_b, y_b)$ , the unknown  $\psi$  and its tangential derivatives are calculated from the formula:

$$\psi(x_b, y_b) = I_P \left[ G(x_b, y_b; x_0, y_0) + B_V (x_b^2 - x_0^2)/2 \right] \quad (1.24)$$

where

$$G(x_b, y_b; x_0, y_0) = \frac{\sqrt{x_b x_0}}{2\pi k} \left[ (2 - k^2) K(k^2) - 2E(k^2) \right]$$

$$k^2 = \frac{4x_b x_0}{(x_b + x_0)^2 + (y_b - y_0)^2} \quad (1.25)$$

$$B_V = \frac{1}{4\pi x_0} \left[ \ln \left( \frac{8x_0}{a} \right) - \frac{3}{2} + \left( \frac{\ell_i}{2} + \beta_P \right) \right]$$

with  $K(k^2)$  and  $E(k^2)$  being the complete elliptic integrals of the first and second kind,  $a$  is the plasma minor radius, defined by  $a^2 = (x_0 - x_L)^2 + (z_0 - z_L)^2$ , and  $\ell_i$  and  $\beta_P$  are the plasma internal inductance and poloidal beta. These are enforced by zeroing out the corresponding row of  $\mathbf{A}$  in Eq. (1.23), and inserting a one on the diagonal, and the boundary value in the appropriate location in  $\mathbf{B}$ . This is done for  $\psi$  and its first two tangential derivatives.

In the results presented here, we computed on the rectangular domain:  $10 < x < 14$ ,  $-2 < y < 2$ , that was divided into  $2N^2$  equally spaced triangular elements. Other parameters were  $(x_0, y_0) = (12.1, 0)$ ,  $(x_L, y_L) = (10.5, 0)$ ,  $p_0 = 0.01$ ,  $p_1 = -1$ ,  $p_2 = 0$ ,  $I_P = 1$ ,  $g_0 = 36.4$ ,  $q_0 = 1$ ,  $J_\psi = 0$ , and we set  $(\ell_i/2 + \beta_P) = 1.2$ .

This gives a value of  $\psi_0 = -6.165228$ , changing only in the 7<sup>th</sup> decimal place for  $N \geq 15$ . We plot in Fig. 10 the  $L_2$  error in Eq. (1.17) as a function of  $N$ . This is defined by directly evaluating each side of Eq. (1.17) at each node point in the plasma region, squaring the difference, summing these, and taking the square root of the sum divided by the number of node points summed. It is seen that the error converges approximately as  $N^{-3.5}$ . We postulate that this behavior is due to the fact that the functions in Eq. (1.17) only have continuous derivatives through second order at the plasma-vacuum interface, and thus the higher order terms in the expansion are not completely effective in reducing the error further.

#### IV. Summary and Discussion

We have shown that the reduced quintic 2D triangular finite element is well-suited for many problems arising in fusion MHD applications. It is to work with, and has excellent convergence properties if the actual solution is smooth enough.

We have demonstrated its applicability on a 2D elliptic problem, in the solution of the anisotropic conduction problem, in a time-dependent reduced-problem and for the 2D axisymmetric toroidal equilibrium problem.

The element requires only three unknowns per triangle, which is considerably less than other high-order elements of comparable accuracy (Table 2). The fact that it forces  $C^1$  continuity, and is thus suitable for problems involving derivatives up to fourth order in space makes it very efficient for systems of equations that can be combined into a smaller number of higher order equations.

This property to handle higher order equations was utilized in Appendix D to cast the reduced incompressible resistive MHD equations in a fully implicit form that consisted of two sequential sparse matrix linear solves, each of rank  $(3N)^2$  for a problem with  $N$  triangles. We can contrast this to  $C^0$  methods of comparable accuracy, which would have to solve the combined system together (more variables), and would also have more unknowns per triangle per variable, resulting in considerably larger matrices.

It has been recognized since the 1970s that the reduced quintic finite element has many advantageous properties. In [6] it is referred to as “one of the most interesting and ingenious of all finite elements” and it states that “a series of careful numerical experiments has given first prize to this remarkable element”, referring to the studies in reference [10]. The example problems presented in this paper support the notion that this element offers many advantages for extended MHD calculations. Future studies will focus on a more complete system of equations, and on the application of the element to irregular domains.

#### Acknowledgements

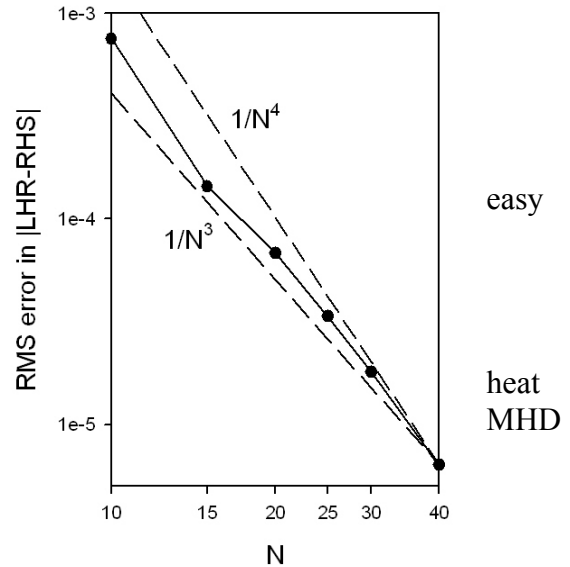


Figure 10: RMS error in GSS equation as a function of elements per side. Convergence is  $\sim N^{-3.5}$

This work was supported by US DoE contract DE-AC02-76CH03073. The author has benefited from discussions with his colleagues, in particular P. Fischer, A. Glasser, W. Park, G. Richter, R. Samtaney, C. Sovinec, and H. Strauss. S. Klasky has assisted in the preparation of the figures.

## References

1. H. R. Strauss and D. W. Longcope, *J. Comput. Phys.*, **147**, 318-336 (1998)
2. W. Park, E. V. Belova, G. Y. Fu, et al, *Phys Plasmas* **6** 1796-1803 Part 2 May 1999
3. C. R. Sovinec, A. H. Glasser, G. A. Gianakon, et al, "Nonlinear magnetohydrodynamics simulations using high-order finite elements", *J. Comput Phys.* To appear 2004
4. P. Fischer, "Spectral Element Solution of Anisotropic Diffusion in a Tokamak Model Geometry", in press
5. Glasser, A. H., "The SEL macroscopic modeling code", *Computer Physics Communications*, to appear 2004
6. G. Strang and G. Fix, "An Analysis of the Finite Element Method", Prentice-Hall Inc., 1973
7. D. Braess, "Finite Elements", Cambridge University Press, 2002
8. K. Bell, "Analysis of Thin Plates in Bending Using Triangular Finite Elements", Feb. 1968, Institutt for Statikk, Norges Tekniske Hogskole, Tronkheim
9. J.H. Argyris, J. Fried, and D. W. Sharpf, "The TUBA Family of Plate Elements for the Matrix Displacement Method", *The Aeronautical Journal*, **72**, 1968 pp. 701-709
10. G. R. Cowper, E. Kosko, G. M. Lindberg, and M. D. Olson, *AIAA Journal*, **7** 1957 (1969)
11. J.W. Demmel, J.R. Gilbert, Y. S. Li, "SuperLU Users Guide", U.C. Berkeley, October 2003.
12. R. Richard, R. D. Sydora, and M. Ashour-abdalla, *Phys. Fluids B* **2**, 488 (1990)

## Appendix A: The transformation matrix

To derive the transformation matrix  $g_{ij}$ , we first calculate the value of  $\phi$  and it's derivatives with respect to the local Cartesian coordinates  $\xi$  and  $\eta$  at the three vertex points, and combine this with the two constraint equations enforcing  $C^1$  continuity along the edges. (Note that the third constraint was automatically satisfied in removing the 21<sup>st</sup> coefficient in the sum). Using the expansion  $\phi(\xi, \eta) = \sum_{i=1}^{20} a_i \xi^{m_i} \eta^{n_i}$ , the two additional constraint equations become:

$$5b^4ca_{16} + (3b^2c^3 - 2b^4c) a_{17} + (2bc^4 - 3b^3c^2) a_{18} + (c^5 - 4b^2c^3) a_{19} - 5bc^4a_{20} = 0$$

$$5a^4ca_{16} + (3a^2c^3 - 2a^4c) a_{17} + (-2ac^4 - 3a^3c^2) a_{18} + (c^5 - 4a^2c^3) a_{19} - 5ac^4a_{20} = 0$$

and thus the transformation matrix  $\mathbf{T}$  in the local coordinates takes the form:

$$= \begin{bmatrix} 1 & -b & 0 & b^2 & 0 & 0 & -b^3 & 0 & 0 & 0 & b^4 & 0 & 0 & 0 & 0 & -b^5 & 0 & 0 & 0 & 0 & 0 \\ 0 & 1 & 0 & -2b & 0 & 0 & 3b^2 & 0 & 0 & 0 & -4b^3 & 0 & 0 & 0 & 0 & 5b^4 & 0 & 0 & 0 & 0 & 0 \\ 0 & 0 & 1 & 0 & -b & 0 & 0 & b^2 & 0 & 0 & 0 & -b^3 & 0 & 0 & 0 & 0 & 0 & 0 & 0 & 0 & 0 \\ 0 & 0 & 0 & 2 & 0 & 0 & -6b & 0 & 0 & 0 & 12b^2 & 0 & 0 & 0 & 0 & -20b^3 & 0 & 0 & 0 & 0 & 0 \\ 0 & 0 & 0 & 0 & 1 & 0 & 0 & -2b & 0 & 0 & 0 & 3b^2 & 0 & 0 & 0 & 0 & 0 & 0 & 0 & 0 & 0 \\ 0 & 0 & 0 & 0 & 0 & 2 & 0 & 0 & -2b & 0 & 0 & 0 & 2b^2 & 0 & 0 & 0 & -2b^3 & 0 & 0 & 0 & 0 \\ 1 & a & 0 & a^2 & 0 & 0 & a^3 & 0 & 0 & 0 & a^4 & 0 & 0 & 0 & 0 & a^5 & 0 & 0 & 0 & 0 & 0 \\ 0 & 1 & 0 & 2a & 0 & 0 & 3a^2 & 0 & 0 & 0 & 4a^3 & 0 & 0 & 0 & 0 & 5a^4 & 0 & 0 & 0 & 0 & 0 \\ 0 & 0 & 1 & 0 & a & 0 & 0 & a^2 & 0 & 0 & 0 & a^3 & 0 & 0 & 0 & 0 & 0 & 0 & 0 & 0 & 0 \\ 0 & 0 & 0 & 2 & 0 & 0 & 6a & 0 & 0 & 0 & 12a^2 & 0 & 0 & 0 & 0 & 20a^3 & 0 & 0 & 0 & 0 & 0 \\ 0 & 0 & 0 & 0 & 1 & 0 & 0 & 2a & 0 & 0 & 0 & 3a^2 & 0 & 0 & 0 & 0 & 0 & 0 & 0 & 0 & 0 \\ 0 & 0 & 0 & 0 & 0 & 2 & 0 & 0 & 2a & 0 & 0 & 0 & 2a^2 & 0 & 0 & 0 & 2a^3 & 0 & 0 & 0 & 0 \\ 1 & 0 & c & 0 & 0 & 0 & c^2 & 0 & 0 & 0 & c^3 & 0 & 0 & 0 & 0 & c^4 & 0 & 0 & 0 & 0 & c^5 \\ 0 & 1 & 0 & 0 & c & 0 & 0 & 0 & 0 & 0 & c^2 & 0 & 0 & 0 & 0 & c^3 & 0 & 0 & 0 & 0 & c^4 \\ 0 & 0 & 1 & 0 & 0 & 2c & 0 & 0 & 0 & 0 & 3c^2 & 0 & 0 & 0 & 0 & 4c^3 & 0 & 0 & 0 & 0 & 5c^4 \\ 0 & 0 & 0 & 2 & 0 & 0 & 0 & 2c & 0 & 0 & 0 & 0 & 2c^2 & 0 & 0 & 0 & 0 & 2c^3 & 0 & 0 & 0 \\ 0 & 0 & 0 & 0 & 1 & 0 & 0 & 0 & 2c & 0 & 0 & 0 & 0 & 3c^2 & 0 & 0 & 0 & 0 & 4c^3 & 0 & 0 \\ 0 & 0 & 0 & 0 & 0 & 2 & 0 & 0 & 0 & 6c & 0 & 0 & 0 & 0 & 12c^2 & 0 & 0 & 0 & 0 & 20c^3 & 0 \\ 0 & 0 & 0 & 0 & 0 & 0 & 0 & 0 & 0 & 0 & 0 & 0 & 0 & 0 & 0 & 5a^4c & 3a^2c^3 - 2ac^4 + c^5 - 2a^4c & 3a^3c^2 - 4a^2c^3 & 5ac^4 & 5ac^4 \\ 0 & 0 & 0 & 0 & 0 & 0 & 0 & 0 & 0 & 0 & 0 & 0 & 0 & 0 & 0 & 5b^4c & 3b^2c^3 - 2bc^4 - 2b^4c & 3b^3c^2 - 4b^2c^3 & 4b^2c^3 - 5bc^4 & -5bc^4 \end{bmatrix}$$

This satisfies  $\mathbf{\Phi}' = \mathbf{T} \mathbf{A}$ , where  $\mathbf{\Phi}'$  denotes the vector produced by stringing together the function and derivatives with respect to  $\xi$  and  $\eta$  [Cartesian coordinates that are rotated with respect to  $(x,y)$ .] at the three vertices, and with the final two elements zero: i.e.

$$\mathbf{\Phi}' = [\phi^1, \phi_{\xi}^1, \phi_{\eta}^1, \phi_{\xi\xi}^1, \phi_{\xi\eta}^1, \phi_{\eta\eta}^1, \phi^2, \dots, \phi^3, \dots, 0, 0]$$

This can be solved for the coefficient matrix by inverting  $\mathbf{T}$ , thus  $\mathbf{A} = \mathbf{T}^{-1} \mathbf{\Phi}'$ . A useful check is to verify that the numerically evaluated determinant of  $\mathbf{T}$  has the value  $-64(a+b)^{17}c^{20}(a^2+c^2)(b^2+c^2)$ . Note that since the final two elements of  $\mathbf{\Phi}'$  are zero, we can replace  $\mathbf{T}^{-1}$  by the  $20 \times 18$  matrix  $\mathbf{T}_2$  which consists of the first 18 columns of  $\mathbf{T}^{-1}$ .

To get the coefficient matrix  $\mathbf{A}$  in terms of the vector containing the actual derivatives with respect to  $(x,y)$ , we have to apply the rotation matrix  $\mathbf{R}$ . This is compactly defined in terms of the angle  $\theta$  appearing in Fig. 1 by:

$$\mathbf{R} = \begin{bmatrix} \mathbf{R}_1 & & \\ & \mathbf{R}_1 & \\ & & \mathbf{R}_1 \end{bmatrix} \quad (1.26)$$

where

$$\mathbf{R}_1 = \begin{bmatrix} 1 & 0 & 0 & 0 & 0 & 0 \\ 0 & \cos \theta & \sin \theta & 0 & 0 & 0 \\ 0 & -\sin \theta & \cos \theta & 0 & 0 & 0 \\ 0 & 0 & 0 & \cos^2 \theta & 2 \sin \theta \cos \theta & \sin^2 \theta \\ 0 & 0 & 0 & -\sin \theta \cos \theta & \cos^2 \theta - \sin^2 \theta & \sin \theta \cos \theta \\ 0 & 0 & 0 & \sin^2 \theta & -2 \sin \theta \cos \theta & \cos^2 \theta \end{bmatrix} \quad (1.27)$$

Thus, if we define the matrix  $\mathbf{G} = \mathbf{T}_2 \mathbf{R}$ , this relates the coefficient matrix directly to the unknown vector consisting of the function and derivatives with respect to  $(x,y)$ , thus:  $\mathbf{A} = \mathbf{G} \Phi$ , or in

component notation:  $a_i = \sum_{j=1}^{18} g_{i,j} \Phi_j$  for  $i=1,20$ .

## Appendix B: Matrix Elements

The most basic matrix element was given in Eq. (1.6). Here we give the remaining ones that occur in the example problems that have been presented. In obtaining these results, we perform integration by parts as required to equalize the number of derivatives operating on the test and trial functions.

$$\iint v_j(\xi, \eta) \nabla^2 \phi(\xi, \eta) d\xi d\eta = \sum_{k=1}^{18} A_{j,k} \Phi_k \quad (1.28)$$

$$A_{j,k} = \sum_{p=1}^{20} \sum_{q=1}^{20} g_{p,j} g_{q,k} \left[ m_p m_q F(m_p + m_q - 2, n_p + n_q) + n_p n_q F(m_p + m_q, n_p + n_q - 2) \right]$$

$$\iint v_j(\xi, \eta) \nabla^4 \phi(\xi, \eta) d\xi d\eta = \sum_{k=1}^{18} B_{j,k} \Phi_k \quad (1.29)$$

$$B_{j,k} = - \sum_{p=1}^{20} \sum_{q=1}^{20} g_{p,j} g_{q,k} \left\{ \begin{array}{l} m_p(m_p - 1)m_q(m_q - 1) \times F(m_p + m_q - 4, n_p + n_q) \\ + n_p(n_p - 1)n_q(n_q - 1) \times F(m_p + m_q, n_p + n_q - 4) \\ + [m_p(m_p - 1)n_q(n_q - 1) + m_q(m_q - 1)n_p(n_p - 1)] \\ \times F(m_p + m_q - 2, n_p + n_q - 2) \end{array} \right\}$$

In 2D, if the magnetic field is written as  $\mathbf{B} = \hat{z} \times \nabla \psi$ , and if  $\psi$  has the expansion as in Eq. (1.3), i.e.,  $\psi = \sum_{i=1}^{18} v_i \Psi_i$ , then we can compute the matrix element:

$$\iint v_j(\xi, \eta) \nabla \cdot \mathbf{B} \mathbf{B} \cdot \nabla \Phi d\xi d\eta = \iint [v_j, \psi] [\phi, \psi] d\xi d\eta$$

$$= \sum_{k=1}^{18} R_{j,k} \Phi_k$$

$$R_{j,k} \equiv \sum_{i=1}^{18} \sum_{l=1}^{18} \sum_{p=1}^{20} \sum_{q=1}^{20} \sum_{r=1}^{20} \sum_{s=1}^{20} g_{p,j} g_{q,i} g_{r,k} g_{s,l} (m_p n_q - m_q n_p) (m_r n_s - m_s n_r) \times$$

$$F(m_p + m_q + m_r + m_s - 2, n_p + n_q + n_r + n_s - 2) \Psi_i \Psi_l \quad (1.30)$$

$$\iint v_i(\xi, \eta) [\nabla^2 \psi, \psi] d\xi d\eta = \sum_{j=1}^{18} \sum_{k=1}^{18} G_{i,j,k} \Psi_j \Psi_k$$

$$G_{i,j,k} = \sum_{p=1}^{20} \sum_{q=1}^{20} \sum_{r=1}^{20} g_{p,i} g_{q,j} g_{r,k} (m_p n_r - m_r n_p) \left[ \begin{array}{l} m_q(m_q - 1) F(m_p + m_q + m_r - 3, n_p + n_q + n_r - 1) \\ + n_q(n_q - 1) F(m_p + m_q + m_r - 1, n_p + n_q + n_r - 3) \end{array} \right] \quad (1.31)$$



$$\iint v_i(\xi, \eta) [\psi, \phi] d\xi d\eta = \sum_{j=1}^{18} \sum_{k=1}^{18} K_{i,j,k} \Psi_j \Phi_k \quad (1.32)$$

$$K_{i,j,k} = \sum_{p=1}^{20} \sum_{q=1}^{20} \sum_{r=1}^{20} g_{p,i} g_{q,j} g_{r,k} (m_q n_r - m_r n_q) F(m_p + m_q + m_r - 1, n_p + n_q + n_r - 1)$$

Suppose  $f(x, z)$  is a function with a known Taylor's series expansion about the origin of each triangle:

$$f(x, z) = \sum_{k=0}^4 \sum_{l=0}^k \frac{1}{l!(k-l)!} \left[ \frac{\partial^k f}{\partial x^l \partial z^{k-l}} \right]_{x_0, z_0} (x-x_0)^l (z-z_0)^{k-l}$$

$$= \sum_{k=0}^4 \sum_{l=0}^k \left[ \frac{\partial^k f}{\partial x^l \partial z^{k-l}} \right]_{x_0, z_0} \sum_{p=0}^l \frac{(\cos \theta)^{l-p} (-\sin \theta)^p}{p!(l-p)!} \sum_{q=0}^{k-l} \frac{(\sin \theta)^{k-l-q} (\cos \theta)^q}{q!(k-l-q)!} \xi^{k-p-q} \eta^{p+q}$$

Then, we can compute:

$$\iint [v_j^i f] dx dz = \sum_{k=0}^4 \sum_{l=0}^k \sum_{p=0}^l \sum_{q=0}^{k-l} M_{klpq}^i F(k-p-q+m_j, p+q+n_j) \quad (1.33)$$

$$M_{klpq}^i = \left[ \frac{\partial^k f}{\partial x^l \partial z^{k-l}} \right]_{x_0, z_0} \frac{(\cos \theta_i)^{l-p} (-\sin \theta_i)^p}{p!(l-p)!} \frac{(\sin \theta_i)^{k-l-q} (\cos \theta_i)^q}{q!(k-l-q)!}$$

where the index  $i$  refers to the number of the triangle.

In order to evaluate the differential operator appearing in the GSS equation, we first expand the function  $(1/x)$  in terms of it's derivatives as in Eq. (1.3), i.e.  $1/x = \sum_{k=1}^{18} v_k (1/x)_k$ . Using this, we can calculate the matrix element

$$\iint_{\text{element}} v_j \left( \frac{\partial}{\partial x} \frac{1}{x} \frac{\partial \psi}{\partial x} + \frac{\partial}{\partial y} \frac{1}{x} \frac{\partial \psi}{\partial y} \right) dx dy = \sum_{k=1}^{18} I_{k,j} \Psi_j \quad (1.34)$$

$$I_{k,j} = \sum_{i=1}^{18} \sum_{p=1}^{20} \sum_{q=1}^{20} \sum_{r=1}^{20} g_{p,i} g_{q,k} g_{r,j} \left[ \begin{array}{l} m_q m_r F(m_p + m_q + m_r - 2, n_p + n_q + n_r) \\ + n_q n_r F(m_p + m_q + m_r, n_p + n_q + n_r - 2) \end{array} \right] \left( \frac{1}{x} \right)_i$$

The terms appearing on the right of Eq. (1.17) are readily calculated once terms like  $xp'(\psi)$  are expanded in terms of their derivatives, i.e.  $xp' = \sum_{j=1}^{18} v_j (xp')_j$ , thus

$$\iint_{\text{triangle}} v_j xp' dx dy = \sum_{k=1}^{18} \sum_{p=1}^{20} \sum_{q=1}^{20} g_{p,j} g_{q,k} F(m_p + m_q, n_p + n_q) (xp')_k \quad (1.35)$$

### Appendix C: Alternate form for incompressible MHD matrices:

The matrices in Eq. (1.15) can also be written in terms of the deviation of the solution from an initial equilibrium. Thus, if we define the vector:

$$\begin{bmatrix} \tilde{\Phi}_j^n \\ \tilde{\Psi}_j^n \end{bmatrix} \equiv \begin{bmatrix} \Phi_j^n \\ \Psi_j^n \end{bmatrix} - \begin{bmatrix} \Phi_j^0 \\ \Psi_j^0 \end{bmatrix} \quad (1.36)$$

The matrix equations can be written

$$\begin{bmatrix} S_j'^{11} & S_j'^{12} \\ S_j'^{21} & S_j'^{22} \end{bmatrix} \begin{bmatrix} \tilde{\Phi}_j^{n+1} \\ \tilde{\Psi}_j^{n+1} \end{bmatrix} = \begin{bmatrix} D_j'^{11} & D_j'^{12} \\ D_j'^{21} & D_j'^{22} \end{bmatrix} \begin{bmatrix} \tilde{\Phi}_j^n \\ \tilde{\Psi}_j^n \end{bmatrix} \quad (1.37)$$

$$\begin{bmatrix} S_j'^{11} & S_j'^{12} \\ S_j'^{21} & S_j'^{22} \end{bmatrix} = \begin{bmatrix} A_{i,j} + \theta\delta t[\bar{G}_{i,j,k}(\tilde{\Phi}_k^* + \Phi_k^0) + \mu B_{i,j}] & -\theta\delta t\bar{G}_{i,j,k}(\tilde{\Psi}_k^* + \Psi_k^0) \\ \theta\delta tK_{i,j,k}(\tilde{\Psi}_k^* + \Psi_k^0) & M_{i,j} + \theta\delta t[K_{i,k,j}(\tilde{\Phi}_k^* + \Phi_k^0) - \eta A_{i,j}] \end{bmatrix}$$

$$\begin{bmatrix} D_j'^{11} & D_j'^{12} \\ D_j'^{21} & D_j'^{22} \end{bmatrix} = \begin{bmatrix} A_{i,j} - \delta t\bar{G}_{i,j,k}[\frac{1}{2}\tilde{\Phi}_k^n + \Phi_k^0] & \delta t\bar{G}_{i,j,k}[\frac{1}{2}\tilde{\Psi}_k^n + \Psi_k^0] \\ -\theta(\tilde{\Phi}_k^* + \Phi_k^0) + (1-\theta)\mu B_{i,j}] & -\theta(\tilde{\Psi}_k^* + \Psi_k^0)] \\ -\delta tK_{i,j,k}[\frac{1}{2}\tilde{\Psi}_k^n + \Psi_k^0] & M_{i,j} - \delta t\{K_{i,j,k}[\frac{1}{2}\tilde{\Phi}_k^n + \Phi_k^0 - \theta(\tilde{\Phi}_k^* + \Phi_k^0)] \\ -\theta(\tilde{\Psi}_k^* + \Psi_k^0)] & -(1-\theta)\eta A_{i,j}\} \end{bmatrix} \quad (1.38)$$

This form allows the matrices to be evaluated only once per problem for a linear calculation. In this case, the LU decomposition is performed only once at the outset, and Eq. (1.37) is solved every timestep with a matrix multiplication and the LU back-substitution.

## Appendix D: A second alternative form for the reduced MHD equations matrices.

We note that it is possible to eliminate  $\dot{\psi}$  from the time advancement equation for  $\phi$  in Eq. (1.13). After applying the  $\theta$ -centered time differencing, this yields the set of time advance equations:

$$\left\{ \nabla^2 + \theta \delta t L_1 + (\theta \delta t)^2 L_2 \right\} \tilde{\Phi}^{n+1} = \left\{ \nabla^2 + \theta \delta t L_1 + \theta(\theta-1) \delta t^2 L_2 \right\} \tilde{\Phi}^n - \theta \delta t^2 L_2 \Phi^0 + \delta t R \quad (1.39)$$

$$S'^{22} \tilde{\Psi}^{n+1} = -S'^{21} \tilde{\Phi}^{n+1} + D'^{21} \tilde{\Phi}^n + D'^{22} \tilde{\Psi}^n \quad (1.40)$$

The feature of this formulation is that Eq. (1.39) does not involve  $\tilde{\Psi}^{n+1}$ , and so these two equations can be solved in series, resulting in a much faster solution time compared to the formulation given in Eq. (1.15).

We have defined the operators

$$\begin{aligned} L_1 \tilde{\Phi}^{n+1} &= [\nabla^2 \tilde{\Phi}^{n+1}, \tilde{\Phi}] + [\nabla^2 \tilde{\Phi}^{n+1}, \Phi^0] + [\nabla^2 \tilde{\Phi}, \tilde{\Phi}^{n+1}] + [\nabla^2 \Phi^0, \tilde{\Phi}^{n+1}] - \mu \nabla^4 \tilde{\Phi}^{n+1} \\ L_2 \tilde{\Phi}^{n+1} &= [\nabla^2 \tilde{\Psi} + \nabla^2 \Psi^0, \tilde{\Psi} + \Psi^0, \tilde{\Phi}^{n+1}] - [[\tilde{\Phi}^{n+1}, \nabla^2 \tilde{\Psi} + \nabla^2 \Psi^0], \tilde{\Psi} + \Psi^0] \\ &\quad - [[\nabla^2 \tilde{\Phi}^{n+1}, \tilde{\Psi} + \Psi^0], \tilde{\Psi} + \Psi^0] - 2 [[\tilde{\Phi}_x^{n+1}, \tilde{\Psi}_x + \Psi_x^0], \tilde{\Psi} + \Psi^0] \\ &\quad - 2 [[\tilde{\Phi}_y^{n+1}, \tilde{\Psi}_y + \Psi_y^0], \tilde{\Psi} + \Psi^0] \\ R &= -[\nabla^2 \tilde{\Phi}^n, \tilde{\Phi}] - [\nabla^2 \Phi^0, \tilde{\Phi}^n] - [\nabla^2 \tilde{\Phi}^n, \Phi^0] \\ &\quad + [\nabla^2 \tilde{\Psi}^n, \tilde{\Psi}^n] + [\nabla^2 \Psi^0, \tilde{\Psi}^n] + [\nabla^2 \tilde{\Psi}^n, \Psi^0] + \mu \nabla^4 \tilde{\Phi} \end{aligned}$$

Evaluation of the terms in Eq. (1.39) requires computation of the new integrals that appear in the matrix elements. For any functions  $\phi, \psi, \zeta$  with corresponding vectors  $\Psi, \Phi, Z$ :

$$\begin{aligned} \iint v_i(\xi, \eta) [[\phi, \nabla^2 \psi], \zeta] d\xi d\eta &= \iint \nabla^2 \psi [\phi, [v_i, \zeta]] d\xi d\eta \\ &= \sum_{j=1}^{18} \sum_{k=1}^{18} \sum_{l=1}^{18} P_{i,j,k,l} \Psi_j \Phi_k Z_l \end{aligned} \quad (1.41)$$

where

$$P_{i,j,k,l} = \sum_{p=1}^{20} \sum_{q=1}^{20} \sum_{r=1}^{20} \sum_{s=1}^{20} g_{p,i} g_{q,j} g_{r,k} g_{s,l} \left\{ \begin{aligned} & \left[ m_r(n_p + n_s - 1) - n_r(m_p + m_s - 1) \right] (m_p n_s - m_s n_p) \times \\ & \left\{ \begin{aligned} & m_q(m_q - 1) F(m_p + m_q + m_r + m_s - 4, n_p + n_q + n_r + n_s - 2) \\ & + n_q(n_q - 1) F(m_p + m_q + m_r + m_s - 2, n_p + n_q + n_r + n_s - 4) \end{aligned} \right\} \end{aligned} \right\} \quad (1.42)$$

similarly,

similarly,

$$\begin{aligned} \iint v_i(\xi, \eta) [\nabla^2 \psi, [\zeta, \phi]] d\xi d\eta &= \iint \nabla^2 \psi [v_i, [\phi, \zeta]] d\xi d\eta \\ &= \sum_{j=1}^{18} \sum_{k=1}^{18} \sum_{l=1}^{18} P_{k,j,i,l} \Psi_j \Phi_k Z_l, \end{aligned} \quad (1.43)$$

Other needed relations follow from the permutation symmetry of the Poisson bracket, thus

$$P_{i,j,k,l} = -P_{l,j,k,i} \quad (1.44)$$

We further define

$$\begin{aligned} \iint v_i(\xi, \eta) \left\{ [[\phi_x, \psi_x], \zeta] + [[\phi_y, \psi_y], \zeta] \right\} d\xi d\eta &= \iint \left\{ [\psi_x, \phi_x] + [\psi_y, \phi_y] \right\} [v_i, \zeta] d\xi d\eta \\ &= \sum_{j=1}^{18} \sum_{k=1}^{18} \sum_{l=1}^{18} R_{i,j,k,l} \Phi_j \Psi_k Z_l \end{aligned} \quad (1.45)$$

where

$$R_{i,j,k,l} = \sum_{p=1}^{20} \sum_{q=1}^{20} \sum_{r=1}^{20} \sum_{s=1}^{20} g_{p,i} g_{q,j} g_{r,k} g_{s,l} \left\{ \begin{array}{l} (m_p n_s - m_s n_p) \times \\ \left[ \begin{array}{l} m_q m_r [(m_r - 1)n_q - (m_q - 1)n_r] \times \\ F(m_p + m_q + m_r + m_s - 4, n_p + n_q + n_r + n_s - 2) \\ + n_q n_r [m_r(n_q - 1) - m_q(n_r - 1)] \times \\ F(m_p + m_q + m_r + m_s - 2, n_p + n_q + n_r + n_s - 4) \end{array} \right] \end{array} \right\} \quad (1.46)$$

Multiplying Eq. (1.39) by each test function, integrating over the triangles, and using these and previous definitions, we obtain:

$$\iint v_i \nabla^2 \tilde{\Phi} d\xi d\eta = \sum_{j=1}^{18} A_{i,j} \tilde{\Phi}_j \quad (1.47)$$

$$\iint v_i L_1 \{ \tilde{\Phi} \} d\xi d\eta = \sum_{j=1}^{18} \left[ -\mu B_{i,j} + \sum_{k=1}^{18} (G_{i,j,k} + G_{i,k,j}) (\tilde{\Phi}_k + \Phi_k^0) \right] \tilde{\Phi}_j$$

$$\begin{aligned} \iint v_i L_2 \{ \tilde{\Phi} \} d\xi d\eta &= \sum_{j=1}^{18} \sum_{k=1}^{18} \sum_{l=1}^{18} \left[ P_{j,k,i,l} + P_{j,l,i,k} + \left( \begin{array}{l} P_{i,j,k,l} + P_{i,j,l,k} - P_{i,k,j,l} - P_{i,l,j,k} \\ -2R_{i,j,k,l} - 2R_{i,j,l,k} \end{array} \right) \right] \times \\ &\quad \frac{1}{2} (\Psi_l^0 + \tilde{\Psi}_l) (\Psi_k^0 + \tilde{\Psi}_k) \tilde{\Phi}_j \end{aligned} \quad (1.48)$$

and finally

$$\iint v_i R d\xi d\eta = \sum_{j=1}^{18} \left[ \mu B_{i,j} \tilde{\Phi}_j^n + \sum_{k=1}^{18} (G_{i,j,k} + G_{i,k,j}) \left[ \left( \frac{1}{2} \tilde{\Psi}_k^n + \Psi_k^0 \right) \tilde{\Psi}_j^n - \left( \frac{1}{2} \tilde{\Phi}_k^n + \Phi_k^0 \right) \tilde{\Phi}_j^n \right] \right] \quad (1.49)$$

# MHD Simulations with Resistive Wall and Magnetic Separatrix

H.R. Strauss

*New York University, New York, New York*

A. Pletzer, W. Park, S. Jardin, J. Breslau, G. Y. Fu

*Princeton University Plasma Physics Laboratory, Princeton, New Jersey*

L. Sugiyama

*MIT, Cambridge, MA*

---

## Abstract

A number of problems in resistive MHD magnetic fusion simulations describe plasmas with three regions: the core, the halo region, and the resistive boundary. Treating these problems requires maintenance of an adequate resistivity contrast between the core and halo. This can be helped by the presence of a magnetic separatrix, which in any case is required for reasons of realistic modeling. An appropriate mesh generation capability is also needed to include the halo region when a separatrix is present. Finally a resistive wall boundary condition is required, to allow both two dimensional and three dimensional magnetic perturbations to penetrate the wall. Preliminary work is presented on halo current simulations in ITER. The first step is the study of VDE (vertical displacement event) instabilities. The growth rate is consistent with scaling inversely proportional to the resistive wall penetration time. The simulations have resistivity proportional to the  $-3/2$  power of the temperature. Simulations have been done with resistivity contrast between the plasma core and wall of 1000 times, to model the vacuum region between the core and resistive shell. Some 3D simulations are shown of disruptions competing with VDEs. Toroidal peaking factors are up to about 3.

*Key words:* MHD; Resistive Wall; Magnetic separatrix

---

<sup>1</sup> This work was supported by USDOE.

## 1 Introduction

In several resistive MHD simulational problems, the plasma model consists of three regions: the plasma core, the plasma halo region, and a resistive wall connecting the plasma to an external vacuum magnetic field.

Example problems having these regions are VDEs and halo current simulations in ITER, with the aim of determining maximum wall stresses caused by asymmetric forces during disruptions. Other problems with some of these features is the effect of error magnetic fields on toroidal rotation, and the evolution of resistive wall modes. Another related category of problem is the development of external kink modes, particularly in compact quasi axisymmetric stellarators.

Tackling these problems requires a resistive MHD code to have three numerical capabilities. First, a three dimensional time dependent resistivity is needed, with adequate contrast of maximum and minimum values. Second, mesh generation is required within a realistic boundary, which may contain a divertor. Third, a resistive wall boundary condition is needed, with a method of solving the external vacuum magnetic field.

These capabilities have been developed for the M3D code [1,2]. The resistivity is proportional to the  $-3/2$  power of the temperature. Simulations have been done with temperature contrast between the plasma core and wall of 100, to model the halo region between the core and resistive shell.

The M3D code includes resistive wall boundary conditions, which match the solution inside the resistive wall to the exterior vacuum solution. The exterior problem is solved with a Green's function method, using A. Pletzer's GRIN code [3].

As a computational example of a problem requiring these capabilities, preliminary work is presented on halo current simulations in ITER[4]. The first step is the study of VDE (vertical displacement event) instabilities[5]. The growth rate is consistent with scaling inversely proportional to the resistive wall penetration time. Some 3D simulations are shown of disruptions competing with VDEs. The toroidal peaking factor[6] can be as high as 3.

## 2 Resistivity Model

A main problem is to have a time dependent resistivity, which is nearly constant along magnetic field lines. In two dimensions, and in mildly three dimensional cases,

a magnetic separatrix can provide an adequate temperature contrast. Open field lines are in contact with the wall, which is held at a relatively low constant temperature. Inside the separatrix, if the cross field thermal conduction is small, the temperature can be maintained at much higher values.

In M3D, the temperature is evolved with the “artificial sound” [7] model, which resembles Landau fluid models [8]

$$\frac{\partial T}{\partial t} = -\mathbf{v} \cdot \nabla T - \gamma_0 T \nabla \cdot \mathbf{v} + \mathbf{B} \cdot \nabla q_{\parallel}$$

$$\frac{\partial q_{\parallel}}{\partial t} = -\frac{1}{\tau_a} q_{\parallel} - \mathbf{B} \cdot \nabla T q_{\parallel}$$

where  $\gamma_0 = 2/3$ ,  $T$  is the temperature,  $\mathbf{v}$  is the velocity,  $\mathbf{B}$  is the magnetic field,  $q_{\parallel}$  is the heat flux, and  $\tau_a$  is a constant. In Landau fluid models,  $\tau_a$  is a more complicated quantity, but it is difficult to generalize to realistic three dimensional magnetic fields.

In three dimensional disruption calculations, the magnetic field becomes stochastic and no longer can isolate the halo region from the core. The regions mix and the core is cooled, resulting in a thermal quench. In turn this causes a current quench, because of the high resistivity.

### 3 Mesh Generation

M3D combines a two dimensional unstructured mesh with finite element discretization in poloidal planes [9], with a pseudo spectral representation in the toroidal direction. An unstructured mesh similar to that used in the calculations is shown in Fig.2(a). The boundary geometry is realistic, for example the ITER - FEAT first wall[10]. The halo part of the mesh containing the open magnetic field lines was made using the ellipt2d package [11], which incorporates the Triangle [12] mesh generation code. The core part of the mesh is aligned with the equilibrium magnetic flux surfaces. It is possible to generate the mesh and initialize using EQDSK equilibrium files. These files contain data describing the curves of the outer wall and the last closed flux surface. These curves are filled in with an unstructured, but good quality mesh by Triangle, which carries out a Delauney triangulation of this region. Extra points are added to the boundaries to improve mesh quality and ensure the desired resolution. The region inside the last closed flux surface is triangulated by M3D. The EQDSK file contains the poloidal flux function  $\psi$  on a cartesian grid, and the coordinates of the magnetic axis. M3D uses this information to produce a mesh with sides aligned with contours of constant  $\psi$ , as well as rays connecting the magnetic axis to the mesh points on the last closed flux surface.

## 4 Resistive Wall Boundary Conditions

The plasma is bounded by a thin resistive wall. Surrounding this is an outer vacuum region, which can contain external current sources.

The vacuum field is represented as

$$\mathbf{B}_v = \nabla\psi_v \times \nabla\phi + \nabla\lambda + I_0\nabla\phi \quad (1)$$

where  $I_0$  is a constant which is equal to the constant part of  $I$  in the plasma. The reason for  $I_0$ , as well as  $\psi_v$ , is to be able to match the vacuum solution to a plasma equilibrium with a net current, and net toroidal magnetic field. The function  $\psi_v$  depends on the poloidal coordinates  $R, Z$  and is independent of toroidal angle  $\psi$ . It satisfies the vacuum Grad Shafranov equation  $\Delta^*\psi_v = 0$ .

To satisfy  $\nabla \cdot \mathbf{B}_v = 0$ ,  $\nabla^2\lambda = 0$ . On the resistive wall boundary, integrating  $\nabla \cdot \mathbf{B}$  across the thin shell gives the requirement that the normal component of magnetic field is continuous at the wall. This gives a boundary condition to determine the vacuum field.

The vacuum field is solved by the GRIN code. From Green's identity one has an integral equation relating  $\partial\psi_v/\partial n$  to given  $\psi_v$ , and  $\lambda_n$  to given  $\partial\lambda_n/\partial n$  on the boundary contour [13] When discretized, these integral equations become matrix equations which are set up and solved by GRIN. Given a set of boundary points,  $R_i, Z_i$

$$\left(\frac{\partial\psi_v}{\partial n}\right)_i = \sum_j K_{ij}^0 \psi_{pj} + S_i, \quad (2)$$

$$\lambda_i^n = \sum_j K_{ij}^n (\mathbf{B}^p \cdot \hat{n})_j \quad (3)$$

where  $K_{ij}^0, K_{ij}^n$  are matrices that can be precomputed given the set of boundary points. The source term  $S$  in (2) can be obtained from the applied external currents, or else using the ‘‘virtual casing’’ method. In this method we first perform an ideal equilibrium calculation, with  $\psi = 0$  on the boundary. Equating  $\partial\psi_v/\partial n = \partial\psi_p/\partial n$ , the source term required for equilibrium is found from  $S = \partial\psi_p/\partial n$  where the right side is obtained from the ideal equilibrium.

Now the magnetic field components in the plasma have to be matched using resistive evolution at the inner boundary, which is a thin resistive shell of thickness  $\delta$  and



resistivity  $\eta_w$ . Ohm's Law at the resistive wall is

$$\frac{\partial \mathbf{A}}{\partial t} = \nabla \Phi + \frac{\eta_w}{\delta} \hat{n} \times [[\mathbf{B}]].$$

In addition, a toroidal electric field is applied to balance resistive diffusion. An example of the temperature in an equilibrium, with “virtual casing” source terms in the boundary conditions, is shown in Fig.1(a).

## 5 VDE and Disruption Simulations

The VDE instability growth rate is proportional to the wall resistivity  $\eta_w$ . This scaling is consistent with simulations, as will be shown below. To get the scaling it seems necessary to be in a regime in which the core resistive decay time  $\tau_{core}$  is longer than the wall penetration time  $\tau_w$ , which in turn is longer than the halo resistive decay time  $\tau_{halo}$ ,  $\tau_{core} > \tau_w > \tau_{halo}$ . Here  $\tau_{core} = S\tau_A$ , and  $\tau_{halo} = (T_{halo}/T_{core})^{3/2}\tau_{core}$ , where  $\tau_A = R/v_A$  is the Alfvén time,  $R$  is the major radius,  $v_A$  is the Alfvén velocity,  $T_{halo}, T_{core}$  are temperatures in the halo and core respectively,  $S = a^2 v_A / (\eta R) = 10^4$  in the simulations, where  $a$  is the geometric half width in the midplane, and  $S$  is the initial value at the magnetic axis. For over two orders of magnitude variation in  $\eta_w/\delta_w$ , the growth rate of the VDE scales as  $\gamma = 4.0\eta_w/\delta_w$ . The growth rate  $\gamma$  as a function of  $\eta_w/\delta_w$  is shown in Fig.2(b).

The temperature in the nonlinear stage of the VDE is shown in Fig.1(b) at time  $t = 103\tau_A$ , as the plasma is pulled into the divertor.

The halo current is the poloidal current flowing into the resistive wall. The normal component of the poloidal current integrated over the wall,  $I_h$ , is  $I_h(\phi) = \frac{1}{2} \int |\hat{n} \cdot \mathbf{J}| R dl$ . Half the absolute value is taken in the integrand because  $\nabla \cdot \mathbf{J} = 0$  implies the total normal current is zero when integrated over the wall and the toroidal angle  $\phi$ . The toroidal peaking factor [6] is defined as the maximum of  $I_h(\phi)$  divided by its toroidal average  $\langle I_h \rangle = 1/(2\pi) \int I_h d\phi$ , that is,  $tpf = I_{h(max)}/\langle I_h \rangle$ . In the following simulation,  $tpf \approx 2$ .

It is useful to normalize halo current to total plasma current. The halo current fraction  $F_h$  will be defined as the ratio  $F_h = \langle I_h \rangle / \langle I_\phi \rangle$ , where the denominator is  $I_\phi = \int J_\phi dR dZ$ .

In three dimensional simulations, disruptions can occur. In one scenario, a disruption causes a thermal quench, which in turn causes a current quench. This is accompanied by a VDE.

The following calculation is an example of this scenario. The initial state has  $q = 0.6$  on axis, with a  $q = 1$  inversion radius including most of the core plasma. This is internal kink unstable. When the instability is sufficiently nonlinear, toroidal coupling to other modes causes a disruption. The plasma cools because of transport along stochastic field lines. This raises the resistivity and dissipates the current. This is accompanied by a VDE. The time history of the the normalized peak current and peak temperature in Fig.3(a). The temperature quench proceeds the current quench. The current, plotted with a dashed line, declines in value more slowly than the temperature, shown as a solid line. The time history of the toroidal peaking factor is shown in Fig.3(b), The toroidal peaking factor almost reaches 3, but most of the time oscillates around 2. The dashed curve in Fig.3(b) is the halo current fraction  $F_h$  multiplied by 10 to be easily read. The halo current peaks at 0.4 but then decays to about 0.1. It should be remarked that this is the instantaneous halo current fraction; both halo current and toroidal current are evolving in time. The temperature is shown at the time  $t = 113\tau_A$  in Fig.1(c). After the disruption and expansion to the wall, the plasma rapidly cools. This tends to quench halo current. The halo current in this case is small.

## 6 Summary and Conclusion

A number of problems in resistive MHD magnetic fusion simulations describe plasmas with three regions: the core, the halo region, and the resistive boundary. Treating these problems requires maintenance of an adequate resistivity contrast between the core and halo. This can be helped by the presence of a magnetic separatrix, which in any case is required for reasons of realistic modeling. An appropriate mesh generation capability is also needed to include the halo region when a separatrix is present. Finally a resistive wall boundary condition is required, to allow both two dimensional and three dimensional magnetic perturbations to penetrate the wall.

M3D simulations have been done of VDEs and halo currents produced by disruptions. A resistive wall boundary condition was applied on a boundary having the shape of the ITER - FEAT first wall. The spatially and temporally varying resistivity was computed proportional to the  $-3/2$  power of temperature. A temperature contrast of 100 between the plasma core and the edge was applied.

Two dimensional simulations of VDEs confirmed that the growth rate is proportional to the wall resistivity, over two orders of magnitude where the linear scaling assumptions are valid.

In three dimensional simulations, disruptions were initiated by a large inversion radius internal kink. Thermal transport along a stochastic magnetic field caused a thermal

quench, followed by a current quench and a VDE. The toroidal peaking factor could be as high as 3, and oscillated around 2.

## References

- [1] PARK, W., BELOVA, E.V., FU, G.Y., TANG, X.Z., STRAUSS, H.R., SUGIYAMA, L.E., "Plasma Simulation Studies using Multilevel Physics Models" *Phys. Plasmas* **6** 1796 (1999).
- [2] SUGIYAMA, L.E., PARK, W., STRAUSS, H.R., HUDSON, S.R, STUTMAN, D., TANG, X.Z., Studies of Spherical Tori, Stellarators and Anisotropic Pressure with M3D, *Nucl. Fusion* (2001).
- [3] <http://w3.pppl.gov/rib/repositories/NTCC/catalog/Asset/grin.html>
- [4] Perkins, F. W., Post, D. E., Uckan, N. A., Azumi, M., Campbell, D. J., Ivanov, N., Sauthoff, N. R., Wakatani, M., Nevins, W.M., Shimada, M., and Van Dam, J., editors, "ITER Physics Basis," *Nuclear Fusion* **39**, 2137 (1999).
- [5] Sayer, R.O., Peng, Y-K. M., Jardin, S. C., Kellman, A. G., Wesley, J. C., "TSC plasma halo simulation of a DIII-D vertical displacement event," *Nuclear Fusion* **33**, 969 (1993).
- [6] Pomphrey, N., Bialek, J., Park, W., "Modeling the toroidal asymmetry of poloidal halo currents," *Nuclear Fusion* **38**, 449 (1998).
- [7] PARK, W., MONTICELLO, D., STRAUSS, H., MANICKAM,
- [8] P. B. Snyder, G. W. Hammett, and W. Dorland, *Phys. Plasmas* **4**, 3974 (1997). *Phys. Fluids* **29** (1986) 1171.
- [9] STRAUSS, H.R. and LONGCOPE, W., An Adaptive Finite Element Method for Magnetohydrodynamics, *J. Comput. Phys.* **147**, 318 - 336 (1998).
- [10] Gribov, Y., private communication.
- [11] Pletzer, A., "Python & Finite Elements", *Dr. Dobb's Journal* #334, p. 36 (March 2002) <http://ellipt2d.sourceforge.net>
- [12] J. R. Shewchuk, *Computational Geometry: Theory and Applications* **22**, 21 - 74 (2002)
- [13] Chance, M., *Phys. Plasmas* **4**, 2161 (1997).

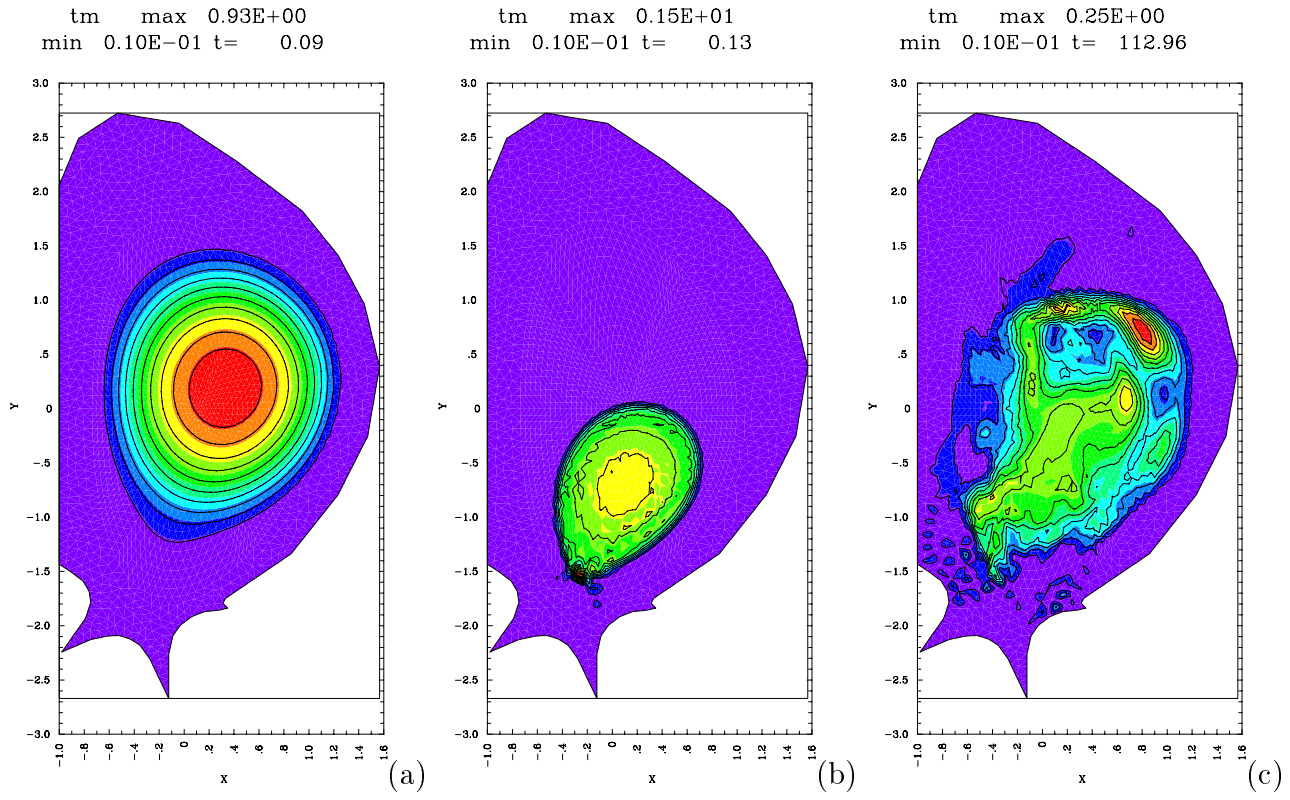


Fig. 1. (a) temperature at  $t = 0t_A$  (b) temperature at  $t = 103t_A$  in a 2D VDE (c) temperature at  $t = 113t_A$  in a 3D disruption

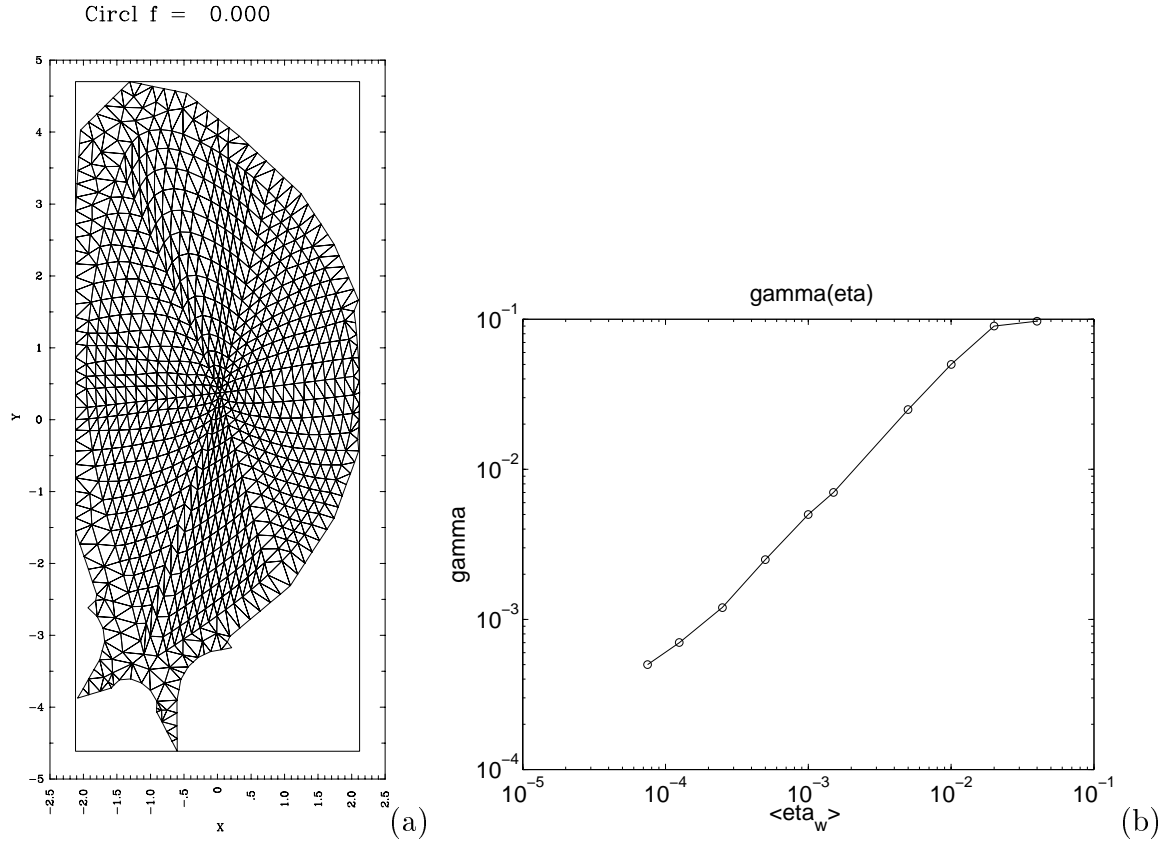


Fig. 2. (a) Mesh (b) Growth rate of VDEs vs.  $\eta_w/\delta_w$

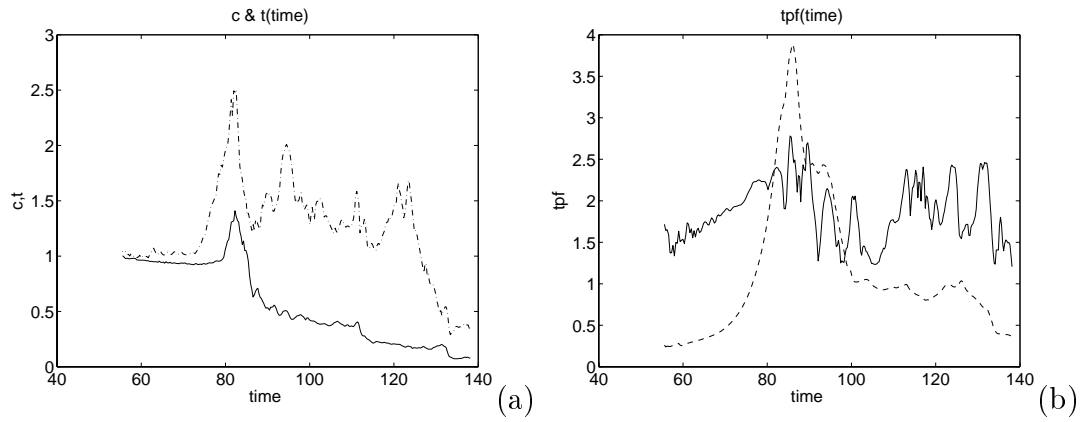


Fig. 3. (a) normalized peak toroidal current (dotted line) and peak temperature vs. time (b) toroidal peaking factor tpf (solid line) and halo current fraction times ten,  $10F_h$ , (dashed line) vs. time